Addis Ababa University
አዲስ አበባ ዩኒቨርሲቲ

SEEK WISDOM, ELEVATE YOUR INTELLECT AND SERVE HUMANITY !

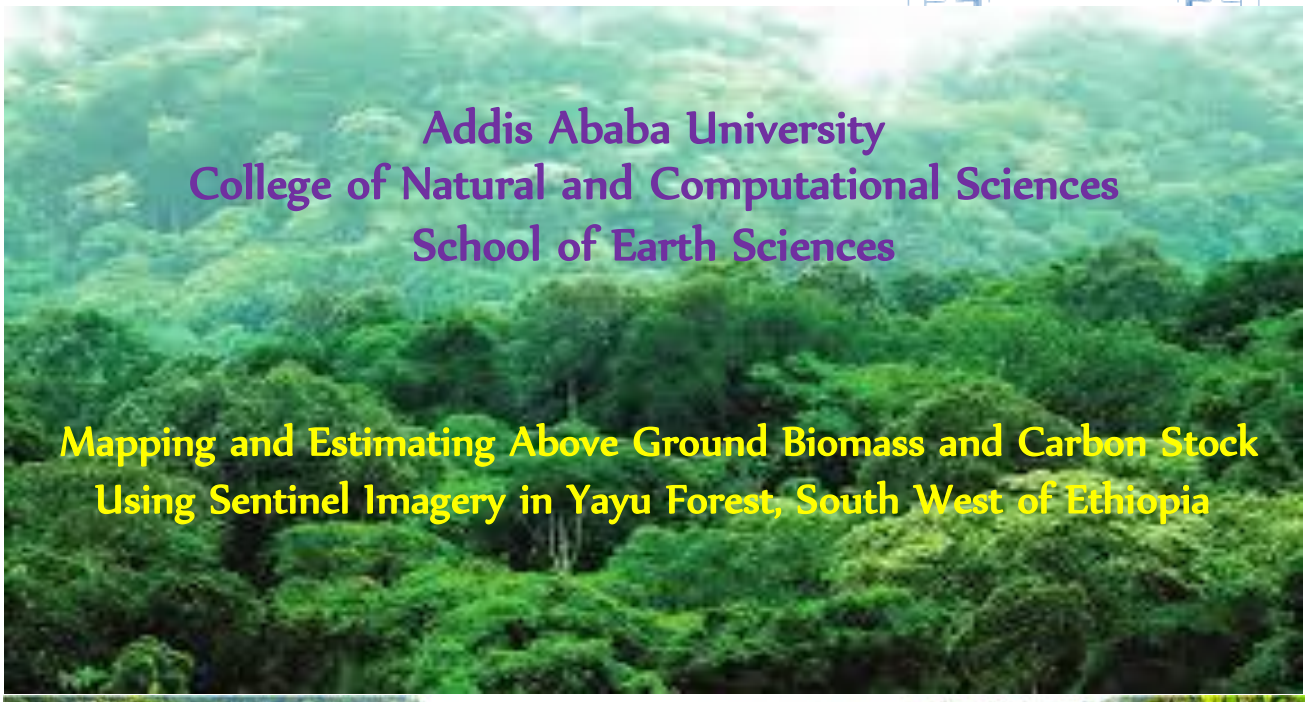

Addis Ababa University
College of Natural and Computational Sciences
School of Earth Sciences

Mapping and Estimating Above Ground Biomass and Carbon Stock Using Sentinel Imagery in Yayu Forest, South West of Ethiopia

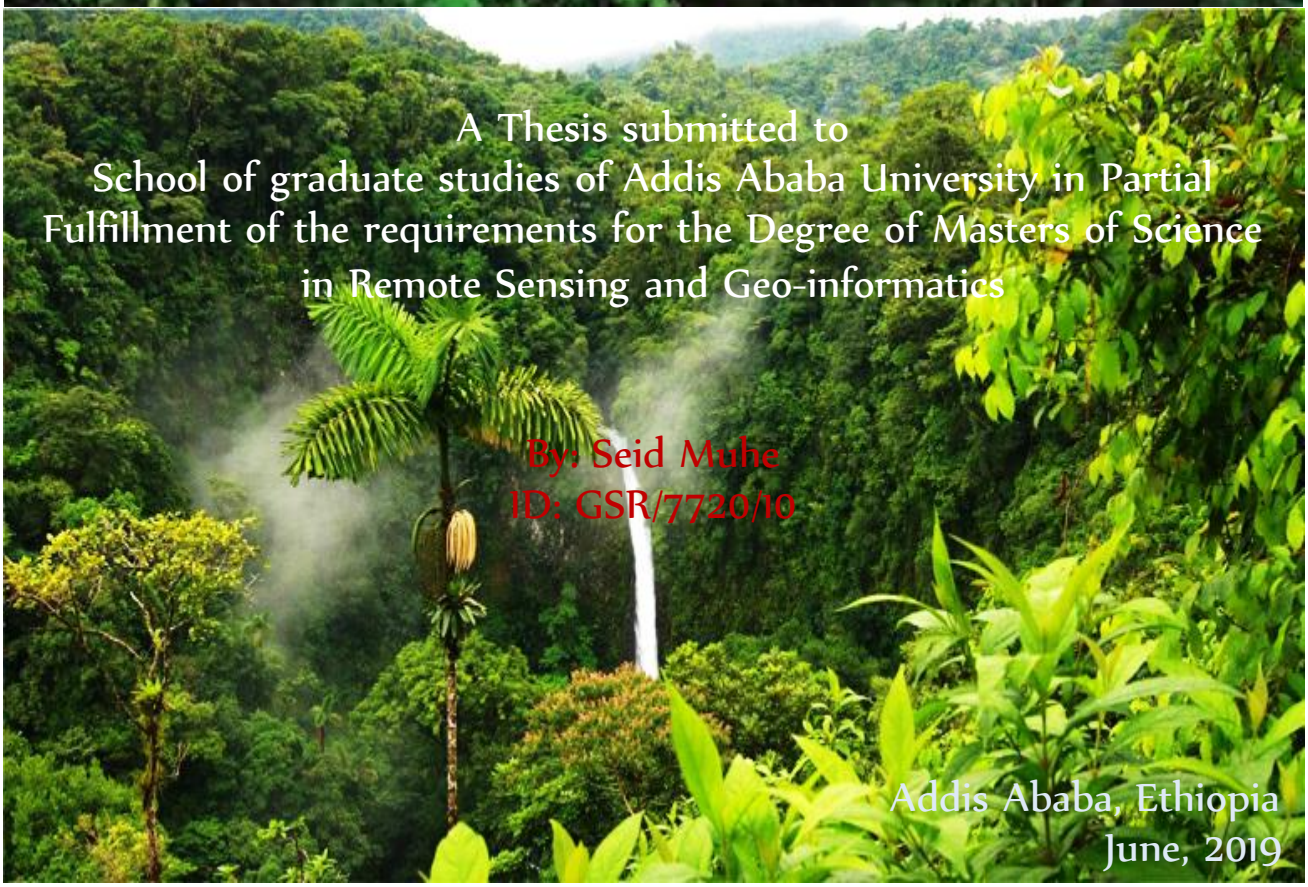

A Thesis submitted to
School of graduate studies of Addis Ababa University in Partial Fulfillment of the requirements for the Degree of Masters of Science in Remote Sensing and Geo-informatics

By: Seid Muhe
ID: GSR/7720/10

Addis Ababa, Ethiopia
June, 2019

Addis Ababa University
College of Natural and Computational Sciences
School of Earth Sciences

Mapping and Estimating Above Ground Biomass and Carbon Stock Using Sentinel Imagery in Yayu Forest, South West of Ethiopia

By: Seid Muhe
ID: GSR/7720/10

Advisor: Dr. Tesfaye Korme
Co-Advisor: Dr. Mekuria Argaw

A Thesis submitted to
School of graduate studies of Addis Ababa University in Partial Fulfillment of the requirements for the Degree of Masters of Science in Remote Sensing and Geo-informatics

Addis Ababa, Ethiopia
June, 2019

Addis Ababa University
School of Graduate Studies

Declaration

This is to certify that thesis prepared by ***Seid Muhe***, entitled: ″***Mapping and Estimating Above Ground Biomass and Carbon Stock Using Sentinel Imagery in Yayu Forest, South West of Ethiopia***" and submitted in partial fulfillment of the requirements for the degree of Masters of Science in Remote sensing and Geo-informatics complies with the regulations of the University and meets the accepted standards with respect to the originality and quality.

By:

Seid Muhe Signature_____ Date_____

Signed by the Examining committee:

Advisor:

Dr. Tesfaye Korme Signature_____ Date _____

Co-Advisor:

Dr. Mekuria Argaw Signature_____ Date _____

Examiner:

Prof. Dereje Ayalew Signature_____ Date _____

Dr. K.V. Suryabhagavan Signature_____ Date _____

Chairperson:

Prof. Dereje Ayalew Signature_____ Date _____

Acknowledgments

First and for most I would like to thank the almighty GOD "Allah" who helped me to accomplish this MSc thesis work.

A special thanks goes to my instructor and first advisor Dr. Tesfaye Korme, Associate professor, from College of Natural and Computational Sciences, School of Earth Sciences, Addis Ababa University, for his advice and continuous support, feedback and comments throughout my research period. Also, I am very grateful to my second supervisor Dr. Mekuria Argaw, Associate professor, from College of Natural and Computational Sciences, School of Enviromental Sciences, Addis Ababa University, for his dedication and assistance throughout my research period, especially on the forestry part.

I would also like to express my appreciation to all Earth Science Department staffs for their unreserved help directly or indirectly during my study at Addis Ababa University.

I give thanks to the office of Ethiopian Coffee Forest Forum for their support in the field forest parameter data. I am particularly grateful to Dr. Tadesse Woldemariam who played a huge role in organizing and providing plot based tree census data.

My sincere gratitude goes to my colleagues for their cooperation, as we exchanged ideas in some aspects of my research and their dedication as we worked together in the lab.

Lastly, my deepest gratitude goes to my parent, father and mother, providing me moral to achieve my dreams, I just can't thank them enough. Also, my heartfelt appreciation goes to, my brothers, sisters and friends and the rest of my family for putting me in their prayers.

Table of Contents

List of Figures

List of Tables

List of Appendices

List of Acronyms

AGB	Above Ground Biomass
ASM	Angular Second Moment
BPV	Biophysical Variable
Cab	Capability of chlorophyll content
CDM	Clean Development Mechanism
dB	Decibel
DBH	Diameter at Breast Height
DEM	Digital Elevation Model
EC	European Commission
ECFF	Ethiopian Coffee Forest Forum
EREC	Inverted Red-Edge Chlorophyll
ESA	European Space Agency
FAO	Food and Agricultural Organization
FAPAR	Fraction of Absorbed Photosynthetically Active Radiation
FCOVER	Fraction of Vegetation Cover
GCOS	Global Climate Observing System
GHG	Green House Gases
GLCM	Grey Level Co-occurrence Matrix
GPS	Global Positioning System
GRD	Ground Range Detected
LAI	Leaf Area Index
LU/LC	Land-use/Land cover

MSI	Multispectral Instrument
NDVI	Normalized Difference Vegetation Index
QGIS	Quantum GIS
RADAR	Radio Detection and Ranging
REDD+	Reducing Emissions from Deforestation and Forest Degradation
RS	Remote Sensing
SAR	Synthetic Aperture Radar
SAVI	Soil Adjusted Vegetation Indices
SNAP	Sentinel Application Platform
SPSS	Statistical Package for the Social Sciences
TNDVI	Transformed Normalized Difference Vegetation Index
UNFCCC	United Nations Framework Convention on Climate change
VH	Vertical transmission and Horizontal reception
VI	Vegetation Index
VV	Vertical transmission and Vertical reception

Abstract

Accurate forest above-ground biomass (AGB) and carbon stock estimation is crucial for sustaining forest management and mitigating climate change to support REDD+ (reducing emissions from deforestation and forest degradation, plus the sustainable management of forests, and the conservation and enhancement of forest carbon stocks) processes. However the major challenge for REDD+ is to find an accurate method for biomass estimation. Thus, the main objective of this study is to assess the potential of texture analysis using grey level co-occurrence matrix derived from sentinel 1 C band GRD image and, vegetation indices and vegetation biophysical variables derived from Sentinel-2 medium resolution images in estimating AGB and carbon stock in Yayu tropical forest, south west of Ethiopia. Both Sentinel 1 ground range detected and Sentinel 2 multispectral instrument used for this study were acquired in February, 2018. Twenty two variables from sentinel 1 including polarization (VV and VH) and twenty variables from sentinel 2 including selected bands were used in this study. Forest stand parameter data such as DBH and tree height collected in 2016 were taken from office of Ethiopian Coffee Forest Forum and converted to AGB using available allometric equation. The correlation of biomass value measured in each plot and the radar information extracted using texture analysis of radar images, as well as variables extracted from optical image were assessed by the Pearson correlation coefficients. Regression modelling was applied based on chosen variables to estimate AGB for the whole study area and the estimated result was validated by considering the coefficient of determination between observed and predicted AGB. The strongest correlation (r = 0.65 - 0.74) was identified between sentinel 2 biophysical variables and AGB in the study area. Relatively weak to moderate correlations (r = -0.24 to 0.47) were found between sentinel 1 extracted variables and AGB. Band 4, IRECI, LAI, FCOVER and FAPAR were selected based on their correlation coefficient to develop AGB predictive model. The model has a coefficient of determination value of 0.74 and root mean square error (RMSE) of 0.16 ton/pixel. Forest above ground biomass and carbon stock map were produced by the developed model. Overall Sentinel 2 variables performed better in estimating AGB and carbon stock compared to sentinel 1 GRD image in the study area. Integrating field data with remote sensing method increases the accuracy of estimating forest AGB and carbon stock.

Keywords: Above ground biomass, Sentinel imagery, Carbon stock, Texture analysis, Grey level grey level co-occurrence matrix, Vegetation indices, Biophysical variables.

Chapter 1 Introduction

1.1 Background of the study

Climate change is one of the major problems that the world is facing currently. The main contributor to this phenomenon is land use changes due to an increase in anthropogenic activities such as deforestation, burning of fossil fuel and industrial expansions. This leads to global warming because of high levels of carbon dioxide (CO_2) in the atmosphere along with other Green House Gases (GHG) that trap the thermal energy. This global warming phenomenon causes climate change and consequently results in natural disasters like earthquakes, floods, drought, high temperatures, wildfires and so on (NASA, 2016).

Forests have an important role in the reduction of CO_2 in the atmosphere (Alkama and Cescatti, 2016). Particularly tropical rainforests have high contribution to the global carbon cycle as they store about 40% of the world's terrestrial carbon (Mauya et al., 2015). However, they are being cleared at a fast rate, leading to 12-20% of the overall anthropogenic CO_2 emissions despite of their significance (Collins, 2015). Thus, an initiative was launched under the United Nations Framework Convention on Climate change (UNFCCC), where developing countries will be able to gain financially, if they reduce emissions from human activities under the Reduction of Emissions from Degradation and Deforestation program (REDD+). The main objective of REDD+ Measurement Reporting and Verification (MRV), is to monitor and asses the amount of above-ground biomass/carbon stock and subsequently the carbon that has been emitted (Mermoz et al., 2015).

Accurate forest above-ground biomass (AGB) is crucial information for sustaining forest management and mitigating climate change to support REDD+ (reducing emissions from deforestation and forest degradation), plus the sustainable management of forests, and the conservation and enhancement of forest carbon stocks processes. As a result, rapid and accurate estimation and monitoring of AGB over various scales of space and time are crucial for greatly reducing the uncertainty in carbon stock assessments, and for informing strategic forest management plans (Pan et al., 2011).

Forest type is classified as natural and plantation forest based on their origin. In Ethiopia context natural forest means a forest where any naturally grown trees, shrubs and other plants having woody and non-woody characters are found, whereas plantation forest or man-made forest means forest other than natural forest and which is developed by man planting of seedling or any other means. Forest structure can be characterized by several variables (attributes), including Diameter at Breast Height (DBH), volume, basal-area (BA), stems per hectare, mean tree height and Live above Ground Woody

Biomass (LAGWB). Among these stand volume is arguably the most important variable in plantation forestry and the ability to model and map the spatial distribution of merchantable timber volume using remote sensing technologies is a central goal of much research. Similar to volume, biomass plays an important role in understanding the function of forests in the environmental and ecosystem services. Ethiopia is a country rich in biodiversity with a wide range of ecological physiographic heterogeneity, having arid lowlands in the east to rainforest in the west and high-altitude afro-alpine vegetation in the central highlands (Bekele-Tessema et al., 1993). Ethiopia's flora is estimated to range from 6500 to 7000 species of higher plants of which 12% are endemic (Lemma, 2005).

Ethiopia has planned Remote Sensing data acquisition and analysis approach as alternative means for national forest management, monitoring, reporting and verification of forest stand volume and biomass. This is through case study (pilot project) and lesson learnt approach, for example in the adopted Clean Development Mechanism (CDM) and Reduced Emission from Deforestation and Degradation (REDD+) schemes. They are mentioned as climate change funding mechanisms available for financing forestry sector in the Woreda Climate Resilient Green Economy Investment Planning Guide (WCRGEIPG). This guide is aimed at generating internationally accepted, nationally adopted and Woreda specific data.

In the past three decades, Landsat images have been mostly used for forest AGB estimation (Dube et al, 2015) mainly because of the freely-accessible long archive images with medium spatial resolution. However, one common problem is data saturation in Landsat imagery; an increase in biomass has been found to result in spectral saturation problems and this normally leads to under-estimation of biomass.

The European Commission (EC) and European Space Agency (ESA) initiated the Sentinel-1 mission (launched on April 2014), which aims to provide information services for security and environmental application. Information is derived from earth observation satellites in conjunction with ground based data. Sentinel-1 mission uses a C-band frequency (8 – 4 GHz or 3.8−7.5 cm). It comprises of two satellites with the same orbital plane, namely, Sentinel-1A and Sentinel-1B with a revisit time of 12 days. Moreover, Sentinel-1 provides a much higher spatial and temporal resolution compared to its predecessors such as the ERS-1, ERS-2, JERS, SIR-C/X-SAR, RADARSAT, SRTM, EnviSAT-AShhAR, RADARSAR-II, LIGHTSAR, ALOS-PALSAR, TerraSAR-X (Attema et al., 2007).

Sentinel-2 is a polar orbiting satellite equipped with a multi-spectral instrument, MSI sensor, launched on 23 June 2015 by the European Space Agency (ESA), provides a significant improvement in spectral coverage, spatial resolution, and temporal frequency over the current generation of Landsat sensors

(Gómez, 2017). It presents high potential for applications in land management, agricultural industry (food security), forestry (AGB), disaster control, and humanitarian relief operations (Aschbacher, J, 2012). The spectral configuration of Sentinel-2 is comparable to some commercial satellite data, such as Worldview-2 and RapidEye, because of the presence of the red-edge band, but is further improved by incorporating shortwave infrared bands (SWIR). The unique characteristics of Sentinel-2 as compared to commercial satellites is the only inclusion of the red-edge band, which is important for vegetation assessment and monitoring (Ramoelo et al., 2015).

Sentinel-2 capture image with a swath width of 290-km in 13 spectral bands traversing from visible and near-infrared (NIR) wavelengths to shortwave infra-red wavelengths at refined (10, 20 m) and coarse (60 m) spatial resolution. Furthermore, the presence of four bands within the red-edge region, centered at 705 (band 5), 740 (band 6), 783 (band 7), and 865 nm (band 8a) gives the sensor high potential for mapping various vegetation characteristics (Shoko, 2017). For instance Ramoelo et al., (2015) successfully demonstrated the potential of Sentinel-2 MSI red-edge bands for e-estimating grass nutrients. Similarly, Forkuor et al. (2017) compared the use of Landsat 8 and Sentinel-2 data for mapping land use land cover (LULC) in rural Burkino Faso, where they concluded that the classification performance by Sentinel-2 red-edge bands alone produced better results than Landsat 8 and comparable results to other Sentinel-2 bands (i.e., visible, NIR, and SWIR).
The above-mentioned Sentinel satellite constellation series, including the Sentinel-1 C-band Synthetic Aperture Radar (SAR) and the Sentinel-2 multispectral instrument by the European Space Agency (ESA), provide new capabilities for AGB mapping with wide coverage, a short return cycle, and a long lifespan as the same data format (Powell et al., 2010).

The present thesis used correlation and regression algorithm to estimate AGB for Yayu natural forest, south west region of Ethiopia. The choice of this model is based on prior studies, which approach provides one of the best accuracies modeling AGB. Regression analysis is a common way to develop AGB estimation models (Lu, 2006). After analyzing the correlation of AGB and extracted variables, if it seems that single regression did not show a significant correlation, it is a must to use multi-linear regression for modelling AGB.

1.2 Problem Statement

Biomass estimation using the allometric equation is generally accepted as a non-destructive method to assess tree aboveground biomass and carbon stock. The most important tree parameter in the equation is DBH, unfortunately, the DBH cannot be seen with remote sensing techniques that capture data from above and it is a very challenging task to measure DBH due to forest accessibility complexities (Shrestha and Nandin-Erdene, 2011).

Nowadays, there is a growing demand for reliable information on forest and tree carbon stock at both country and global levels. This implies that monitoring the state and changes of forests carbon pools is an important element. Therefore, measuring and estimating carbon stocks and changes in carbon stocks in various pools are very important to carbon trading and marketing. This requires transparent and verifiable methods, quantification of uncertainties and appropriate monitoring systems for carbon stocks. The greatest carbon pool of a tree is the Above-Ground Biomass (AGB), but this is mainly affected by anthropogenic activities in the forest that cause degradation by decreasing the forest areas ultimately affecting the carbon stock and the sequestration of carbon dioxide from the atmosphere. Therefore, estimation of biomass/carbon is vital in monitoring the amount of carbon fluxes (Vashum and Jayakumar, 2012).

Combining remote sensing and sample plot data has become a popular method to generate spatially explicit estimations of forest AGB (McRoberts et al., 2013). Even though the traditional method of estimation forest above ground biomass is very accurate, it is time consuming, tedious and costly. To solve this problem it is necessary to use satellite imagery which is free of charge and easy to use and also provides a comparable result with the traditional or conventional approach.

1.3 Significance of the study

There are two basic approaches to forest biomass estimation: traditional field-based methods and Remote Sensing (RS) methods. The traditional methods are time consuming, laborious, difficult to implement in inaccessible areas (Pan et al., 2011), and destructive in nature. Hence, research has favored remote sensing techniques since their inception. Although biomass cannot be directly measured from space, the use of spectrally-derived parameters from sensor reflectance (bands) enables increased biomass prediction accuracy when combined with field-based measurements (Dong, 2003). This study will attempt to contribute to the development of remote sensing-based predictive mapping techniques for forest AGB using freely accessible multi-source remote sensing data with a relatively high spatial resolution. The main aim of this study is, therefore, to investigate the performance of

Sentinel 1 SAR backscatter information and Sentinel 2 multispectral indices and vegetation biophysical variables combined with field measurements for estimating AGB and carbon stock in Yayu forest, South West of Ethiopia.

1.4 Objective of the study

1.4.1 General Objective

- ✓ The main objective of this study is to map and estimate forest above ground biomass and carbon stock using sentinel imagery in Yayu forest, south west of Ethiopia.

1.4.2 Specific Objective

- ✓ To evaluate texture analysis using gray level co-occurrence matrix of Sentinel-1 Ground Range Detected (GRD) Synthetic Aperture Radar image for forest above ground biomass and carbon stock estimation.
- ✓ To investigate vegetation indices and biophysical variables derived from Sentinel-2 Multispectral Instrument (MSI) image for forest above ground biomass and carbon stock estimation.
- ✓ To identify best predictor variables by combining sentinel 1 GRD derived information and sentinel-2 MSI derived spectral band and vegetation indices using SPSS software.
- ✓ To develop AGB and carbon stock predictor model for the study area based on best estimator variables
- ✓ To produce forest above ground biomass and carbon stock map for the study area.

1.5 Scope of the study

This research focus on estimating forest above ground biomass of Yayu District by developing predictive model and it doesn't include below ground biomass. It also restricted to forest AGB excluding other land cover types. The developed equation was also used for only that area because of difference in information gained from satellite image of different land forms and forest types.

1.6 Limitation of the study

The present study used all possible option and efforts to come up with the best result, starting from acquiring primary and secondary data to analysis in different software. However, it has limitation regarding absence of high resolution and long wave length SAR imagery such as L band which has strong relationship with forest above ground biomass.

1.7 Organization of the Thesis

The thesis comprises five chapters as follows: Chapter 1 – *Introduction*: introduces the background, statement of the problem, objective of the study, describe significance of the study, conceptual framework of the research as well as scope and limitation of the study. Chapter 2 – *Literature review*: reviews the concept of forest, above ground biomass, methods to estimate AGB and application of remote sensing data for biomass estimation using optical and radar data. Chapter 3 – *Materials and methods*: describes the characteristics of study area, materials and methods used in this research to achieve the research objectives and intermediate result of analysis. Chapter 4 – *Results and discussion*: summarized the results obtained during the data analysis and discussed about the result. Chapter 5 – *Conclusion and recommendation*: derive conclusions from the discussion in the previous chapter and links to the research objectives and, recommend on issues related to this study.

Chapter 2 Literature Review

2.1 Forest

Forests sequester a large amount of carbon and play an important role in the global climate system (Pan et al., 2013). According to Nandy et al. (2019) quantification of forest biomass is, thus, vital for carbon budget accounting, carbon flux monitoring and for understanding the forest ecosystem response to climate change. However, reforestation, afforestation and avoiding deforestation are the mechanisms of decreasing climate change (Hunt, 2009; Luong et al., 2015). Therefore, estimation of the forest biomass/carbon stocks not only contributes in Reducing Emissions from Deforestation and forest Degradation (REDD) but also in the sustainable management of forest (Hussin et al., 2014). Deforestation in the tropics is of particular significance because of its rapid speed and the REDD (Reducing Emissions from Deforestation and Forest Degradation in Developing Countries) initiative aims at reducing the C losses through performance-based credits by comparison of performance against a business-as-usual reference emission level. In addition to deforestation, forest degradation and enhancement of carbon stock through forest growth are other components of the forest C changes which influence the REDD credits. In order to realize this payment-for ecosystem-service, the tropical countries need to document their annual changes in forest C stocks, and satellite remote sensing is likely to be a major data provider for this phenomena.

Remotely sensed data integrated with forest inventories has become an effective approach to estimate aboveground biomass (AGB) and ultimately carbon stocks. The United Nations collaborative programme on REDD (UN-REDD) has also suggested that national forest monitoring systems should include the use of remote sensing (RS) technology for conducting inventory to evaluate forest carbon reference, monitor forest cover, and to assess forest degradation. RS based studies relate image reflectance, spectral indices and image texture with in-situ measurements to estimate biomass (Kushwaha et al., 2014; Lu, 2005; Nelson et al., 2000; Sales et al., 2007; Yadav and Nandy, 2015).

With the development of new sensors, improved spatial, spectral, radiometric, and temporal resolutions, RS images can further contribute to fine-scale mapping and frequent monitoring of forest biomass/carbon. Better data integration approaches are also required for accurate and spatially explicit estimations of forest AGB (Nandy et al., 2019).

2.2 **Tropical Rainforest**

Tropical rainforests are located around the equator in humid areas between 10^0 N and 10^0 S latitude at an elevation below 3000 feet, they are grouped into three main types; Neotropical, African and the indo-Malaysian (CLOUDBRIGE nature reserve, 2016). The forest covers 6% of the world's land and provides habitat for plant species. A quarter of the world's medicine comes from the tropical forest. These forest ecosystem have a complex structure which is divided in to four layers (Fig 2.1: Tropical Rainforest Structure): the emergent top layer is the composed of trees that range from 100 to 240 feet (30–70 m) tall. These trees are usually very large and they are not closely packed. They are characterized by smooth trunks with few branches and they also lose their leaves during dry monsoon wind. The upper canopy trees are composed of trees with height ranging from 60 to 130 feet (20–40 m) tall. They reduce penetration of light into the lower canopy and it also provides habitat for many animal species, since food is abundant at this layer. The lower canopy layer comprises of trees which are 60 feet (20 m) height or lower and it's characterized by shrub, plants, and small trees. Lastly, the forest floor is the lowest layer in a tropical forest, most of the parts in this layer receive little light and its top soil is also very thin with poor soil (Michael, 2001).

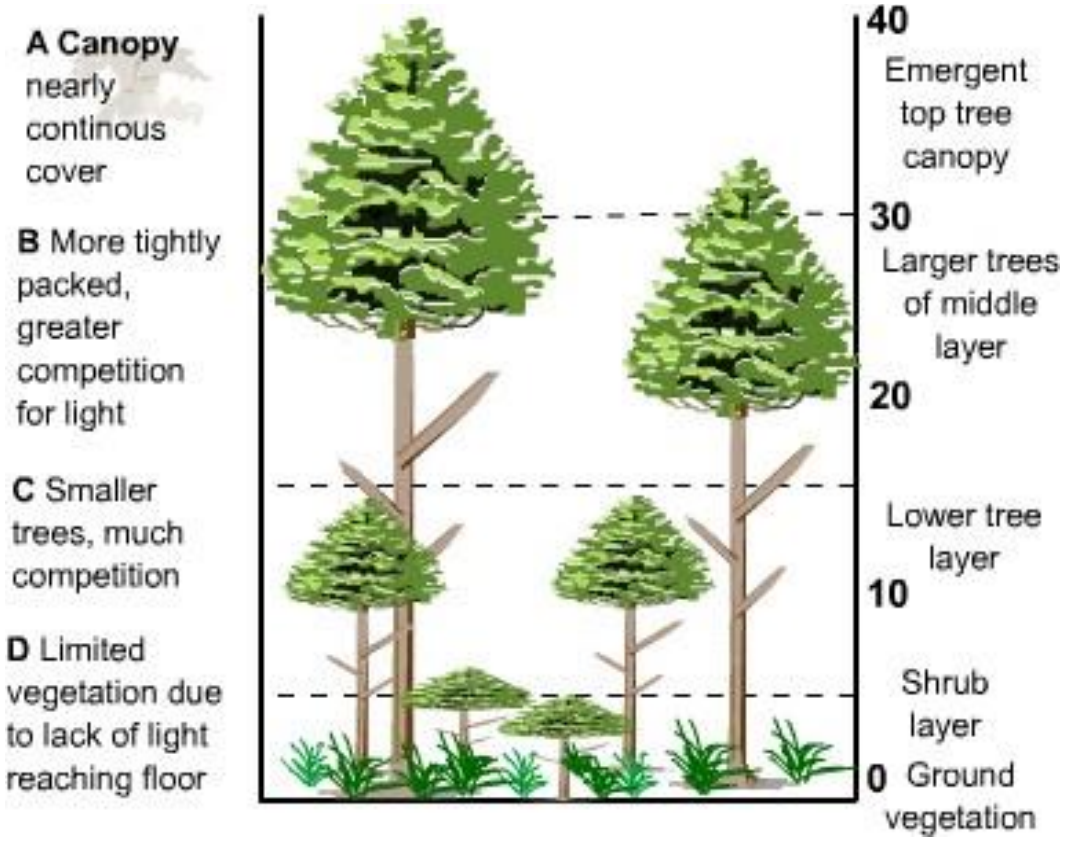

Figure 2.1: Tropical Rainforest Structure Source: (S-cool, 2016)

2.3 Global Carbon Cycles and Forest

According to Patenaude et al. (2005) the world's greatest concern is on CO2, therefore, an understanding of global carbon cycles is one of the fundamental steps in addressing greenhouse gases concerns. Forest plays a crucial role in the carbon cycle as they dominate the terrestrial vegetation, which exchanges CO2 with the atmosphere through photosynthesis and respiration (Dixon et al., 1994; Patenaude et al. (2005). The rate at which greenhouse gases are being released into the atmosphere has increased mainly due to the burning of fossil fuels for both domestic and industrial purposes, but also as a result of land clearance and deforestation. All plant materials contain carbon (normally around 50% of dry weight), and burning or decomposition of cleared vegetation releases it to the atmosphere, mainly in the form of CO_2 (Matthews and Broadmeadow, 2003).

According to Alexandro and Yamagata, (2002); Ahern et al. (1991) the amount of carbon stored in a forest ecosystem depends on the age of forest and forest site productivity. Terrestrial carbon sink may result from the global shift in forest age, when there is regional deforestation of old growth natural forests for the purpose of commercial plantation establishment. In this respect it seems that forest age is one of the points of intervention at which the future evolution of the carbon cycle might be influenced by age dependent forest management practices. Most temperate and boreal forests are actively managed, and forest age depends on the length of harvest cycles there. As biomass increases with stand age, postponing harvesting to the age of biological maturity may result in the formation of a large carbon sink.

2.4 Above Ground Biomass

Biomass, in general, includes the aboveground and below-ground living mass, such as trees, shrubs, vines, roots, and the dead mass of fine and coarse litter associated with the soil. Biomass is often defined in dry weight terms. Above-ground tree biomass, for example, refers to the weight of that portion of the tree found above the ground surface, when oven-dried until a constant weight is reached. Plot-level biomass estimates are typically expressed on a per-unit area basis (for example, Mg/ha or kg/m) and are made by summing the biomass values for the individual trees on a plot, then standardizing for the land area covered by that plot. Biomass control the potential carbon emission that could be released to the atmosphere due to deforestation, and regional biomass changes have been associated with important outcomes in ecosystem functional characteristics and climate change. The roles and impacts of biomass on carbon cycles, soil nutrient allocations, fuel accumulation, and habitat environments in terrestrial ecosystems have long been recognized. Accurate delineation of biomass

distribution at scales ranging from local and regional to global becomes important in reducing the uncertainty of carbon emission and sequestration, understanding their roles in influencing soil fertility and land degradation or restoration, and recognizing their roles in environmental processes and sustainability (Foody et al. 2003). According to Lu (2006) outlined methods for estimating AGB, including field measurements, remote-sensing, and GIS techniques. Remote-sensing techniques have many advantages in AGB estimation over traditional field measurement methods and provide the potential to estimate AGB at different scales.

A basic parameter for characterizing the spatial distribution of carbon in the biosphere, the so-called biomass – defined here as the amount (mass) of dry organic matter of plant origin – is about twice the mass of carbon in a forest. Biomass is in fact the basic unit for measuring carbon, and is the variable used in order to quantify the contribution of forests to the carbon cycle. Over 80% of the above-ground terrestrial biomass is contained in forests, it is therefore necessary to measure and follow this variable in time in order to reduce uncertainties in our knowledge of the climate system (Global Climate Observing System, or GCOS). Forest biomass is therefore identified as an essential climate variable by the GCOS. Also worth mentioning, carbon sequestration, e.g. into forest biomass, is the only climate change mitigation mechanism recognized by the Kyoto Protocol, other than the reduction of human-induced greenhouse gas emissions (GCOS, 2006).

2.5 **Forest Biomass and Carbon Sequestration Assessment**

The term biomass refers to plant biomass density per unit area. This is the mass of the plant matter in a dry state. The measurement units are g/m2 or, more commonly used by foresters, ton per hectare. In a forest, biomass is found in both above-ground and below-ground plant parts, as well as in the litter. Only the above-ground biomass is measurable. This is the biomass of tree elements including the trunk, branches, bark, foliage and fruit. Starting from a pragmatic basis, forest biomass can only be measured through the felling of the trees that compose it. As these destructive methods cannot be conducted on a large scale, non-destructive measurements are therefore used. The methods rely mainly on trunk volume measurements, performed to quantify forest resources using the diameter (DBH, or diameter at breast height), the height (H), and a shape factor taking into account the shape of the trunk. To obtain the trunk biomass, the volume is multiplied by the density of the dry wood. The total biomass of a tree is then derived from the biomass of the trunk, by means of a factor to account for the proportion of mass of the trunk relative to the total mass of the tree. Wood density and different factors are unique to each species. While this method is reasonably convenient for mono-specific forest stands (such as

plantations which are usually composed of a single species) or limited in the number of species (such as the case for most temperate and boreal forests), it is, however, much more complex to conduct in tropical forests, given the difficulties in the identification of often unknown species and the much higher number of species (often greater than 300 per hectare, compared with less than 50 species throughout the whole Europe), and also for reasons of accessibility.

Biomass is the total mass of all living organisms; most of it on the Earth is produced by green plants through photosynthesis. It is of fundamental significance in ecosystems, it provides the entire basis of energy flow and food chain. Biomass is also vital for human being the largest portion of our food supply is from plants (Hua *et al.*, 1996). IPCC. (1996) defines biomass as all living or dead organic matter. The vegetation biomass changes with time per unit area. The biomass of a terrestrial ecosystem is an important climate variable since it absorbs and releases carbon into the atmosphere. According to IPCC, (1996) biomass in a terrestrial ecosystem is divided into Above Ground Biomass (AGB) which defined as all living biomass above the soil including, stem, stump, branches, bark, seed and foliage and Below Ground Biomass (BGB) which are all living biomass of live roots.

According to Rosillo-Calle *et al.* (2007) Remote sensing techniques provide an alternative to traditional methods in estimating biomass production or carbon dynamic of forest and plantation. With the abilities of capturing spatially explicit information and repeatable monitoring even in remote area in a cost effective way, these have become popular for estimating growing stock of biomass or its productivity area.

2.6 Methods for Assessment of Forest Biomass and Forest Carbon Stock

Application of appropriate biomass estimation methods and transparent and consistent reporting of forest carbon inventories are needed in both scientific literature and the GHG inventory measures (Somogyi et al., 2006). A variety of approaches and data sources have been used to estimate forest biomass and forest carbon stocks in different pools. Such approaches are remote sensing-based estimates of AGB combined with field measurement of forest stand characters such as height, diameter and basal area measurements (Wulder et al., 2008).

2.6.1 **Field measurement**

Forest inventory measurements and direct estimation of aboveground biomass through destructive harvesting could greatly improve our quantification of forest carbon stocks. Measurements of diameter at breast height (DBH) and diameter at stump height (DSH) alone or in combination with tree height can be converted to estimates of forest carbon stocks using linear relationships derived from various allometric equation, volume tables and yield tables (Wulder et al., 2008). Measurements of diameter at breast height (DBH) alone or in combination with tree height can be converted to estimates of forest carbon stocks using linear relationships (Gibbs et al., 2007).

The linear and multiple linear regression equation approach require the selection of the regression equation that is best adapted to the conditions in the study area. Linear and multiple linear regression models have been fitted to data in various situations of variable site and ecological conditions globally (Ponce-Hernandez, 2004).

Stratification of systematic and random sampling schemes by broad forest types greatly increases survey efficiency by reducing unnecessary sampling and ensuring that major variation has been captured. It is important to assess how forest carbon stocks vary across an area before designing a stratified sampling scheme. This information is used to define sampling strata or broad forest categories with similar forest carbon stocks. Information on soil types, drainage class, elevation, topography and land-use history are likely universally important to understanding the spatial distribution of carbon stocks (Gibbs et al., 2007).

2.6.1.1 **Allometric Equation**

The basic principle of the allometric equations is that in many organisms, the growth rate of one part of the organism is proportional to that of another. For example, the trunk diameter of a tree is highly correlated with trunk weight. If a range of tree sizes is measured, a regression equation can be derived for predicting tree weight. Since tree diameter is easy to measure but tree weight is much more difficult to determine, this gives a relatively easy way to estimate the standing biomass of forest stands. Allometric equations estimate biomass by regressing measured sample of biomass against tree variables that are easy to measure in the field (e.g., diameter at breast height, height).

2.7 Integration of Remote Sensing Methods for biomass Estimation

2.7.1 High spatial resolution of optical remote sensing

With growing demands for detailed forest information, high spatial resolution remote ensing has become a valuable source of information for assisting forest management (Culvenor, 2003). The term "high spatial resolution" is subjective depending on the context of application. Here, it is refer to both airborne (digital aerial photograph) and space-borne such as IKONOS and QuickBird with spatial resolution less than 10 m (Wulder, 1998).

Fine or high spatial resolution remote sensing data are frequently used for modelling tree parameters or forest canopy structures (Lévesque and King, 2003). Many approaches have been used to extract biophysical parameters from this type of data as summarized by (Culvenor, 2003), which are bottom - up algorithm (valley-following and directional texture), a top-down algorithm (multi- scale edge segments, threshold-based spatial clustering, a double-aspect method, and vision expert system), and template matching (Lu, 2006).

The advent of aerial photography catered to the basic requirement of location capabilities and is one of the most widely used forms of remote sensing of forest cover. The applications of aerial photography are the simplest and the oldest forms of aerial sensors used for remote sensing of the earth's surface features. Cameras can be of different types, namely single lens mapping, multiple lens mapping, panoramic and digital. The spatial resolution of camera lenses is more important than spectral information (Rosillo-Calle et al., 2007).

2.7.2 Medium resolution of optical multi-spectral remote sensing

Optical remote sensing using visible and near- infrared reflectance from the earth, which forms the basis for most of current global scale mapping. Optical measurements have been widely used in studies that link AGB measurement from the field to satellite observation that based on the sensitivity of the optical reflectance to variations in the canopy structure. But these measurements have not proven to be consistent over large areas because surface conditions may change more rapidly than the repeat time of the cloud free satellite observations and producing artefacts in the derived maps (Scott et al., 2009).

Optical remote sensing makes use of visible, near infrared and short wave infrared sensors to form images of the earth's surface by detecting the solar radiation reflected from targets on the ground. Different materials reflect and absorb differently at different wavelengths. Thus, the targets can be differentiated by their spectral reflectance signatures in the remotely sensed images.

2.7.2.1 **Vegetation Indices for biomass estimation**

According to Njoku. (2013) Vegetation Indices (VIs) are a mathematical combination of spectral bands that highlight the spectral properties of green plants so they can be distinguished from other features, it is calculated by combining the red spectral band (Chlorophyll absorbent) with the Near-infrared band (non-absorbent) some indices also include short- wave infrared band. "The computation is done by rationing, differencing, rationing differences and sums by forming a linear combination of band" (Zhang and Ni-meister, 2014). Studies such as Dong et al., 2016; Sibanda et al. (2017) have used VIs in estimating crop biomass. In forestry application, research such as Gunlu et al. (2014); Anderson et al. 1993, used the indices to estimate forest biomass either by using statistical techniques such as simple, multi-linear regression, neural network and k-nearest neighbor algorism models to come up with a predicted biomass. The accuracy of the prediction varied depending on how strong the correlation was between the AGB estimated from the field data with the indices. However, the major challenge of using the VIs is the saturation problems which affect the accuracy of the estimation leading to uncertainties (Lu et al., 2014).

Zhao et al. (2016) demonstrated how the use of stratification based on vegetation types and topography improves AGB estimation by reducing the saturation effect on Landsat Thematic Mapper (TM).The study compared the AGB estimation of the study area with stratification against the one with no stratification. The findings revealed that the Root Mean Square Error (RMSE) reduced from 29.3 to 24.5 Mg/ha by using stratification. Moreover, studies as Fernández-Manso et al. (2016); Guo et al. (2017); Padilla et al. (2017) have also shown that the red-edge VIs reduces saturation especially in complex structure Vegetation

2.7.3 **Microwave remote sensing for above ground biomass estimation**

2.7.3.1 **Application of radar remote sensing for biomass assessment**

Radar (radio detection and ranging) is an active system which emits radio waves and illuminates the surface of the earth and records the energy backscattered from the terrain. 'Side-looking airborne radar' (SLAR), can obtain images over vast regions to the left or right of the aircraft, two types of which being used, 'real aperture radar (RAR)', and currently the 'synthetic aperture radar (SAR)' based on whether the antenna being used is of fixed or variable length, respectively (Rosillo-Calle et al., 2007). The most commonly used wavelengths in imaging radar are K (1.19–1.67 cm), C (3.9–7.5 cm), S (7.5–15.0 cm), L (23.5, 24.0, 25.0 cm) and P (30.0–100 cm).

The radar backscatter models can be divided into three groups - physical, empirical and semi – empirical models (Hoekman, 1990). The physical models provide an insight into the relationship of backscatter and structure parameter of the forest which is supportive for other models. The empirical models have been restricted by the lack of physical understanding of the backscatter mechanism. Therefore, semi empirical models seem to be a promising approach to model the above ground biomass. Among these, the classical regression modelling is unbiased in explaining the relation of observed forest biophysical parameters and response value from remote sensing data (Lu, 2006).

Radar plays a major role for vegetation studies for two reasons: (1) the unique property of microwave remote sensing systems to function almost unrestricted by adverse atmospheric conditions (which prevent the use of optical systems) and (2) the property of (coherent) microwaves to enable measurement of certain object parameters which cannot be assessed through other remote sensing systems (Hoekman, 1990).

SAR data are acquired in X, C, L and P bands. Each of these bands has their own characteristics in re lating to forest stand parameters. The X band is scattered by leaves and canopy cover surface so it is suitable to extract information about the surface layer of the trees. The C band penetrates through lea ves and scatters by small branches and under layer elements. The L band penetrates through the surfa ce layers and is scattered by the trunk and main branches. The P band has the most penetration into t he canopy cover and the major part of P band backscattering is caused by trunk and the trunk-ground reflectance. So the backscatters of the P and L band are the most related to the biophysical pa rameters of the trees.

The next important parameter of SAR data is the polarization of the signals. The polarization is the direction of electric field in the electromagnetic waves and is the main factor into the interacti on between signals and the reflectors. Most of the microwave sensors emit the signals in horizontal (H) or vertical (V) polarizations. The SAR data may have four polarizations: 1) HH: the emitted and b ackscattered signals have horizontal polarization. 2) HV: the emitted signal has horizontal and the ba ckscattered signal has vertical polarization. 3) VH: the emitted signal has vertical and the backscatter ed signal has horizontal polarization. 4) VV: both emitted and reflected signals have vertical polari zation. The C, L and P bands are used in the biomass estimation. The past studies have shown the lo nger wavelengths (L and P band) and the HV polarization have the most sensitivity to the AGB (Luc kman et al. 1997; Kurvonen et al. 1999; Sun et al. 2002). It was found that the copolarized data (HH and VV) at the longer wavelengths, especially Pband, was sensitive to changing surface conditions. Crosspolarized (HV and VH) backscattering mainly originates from multiple scattering within the tre e canopy and is less influenced by the surface condition (Ranson et al.1994).

The AGB estimation using C band data has been achieved to good results in vegetation covers with l ower biomass. Radar backscattering at longer wavelengths (L and P bands) is lower than that from C band for low biomass sites, such as grassland, bogs, clear cuttings, areas of forest regeneration, and y oung plantations. Ground surfaces covered with grass, brush, or young trees have very low backsca ttering at P band since the scattering elements of grass and small trees are small compared wit h the Pwavelength (68 cm) to give significant backscattering. The same surfaces, however, will be very rough at C band so strong backscattering may occur (Ranson et al. 1994; Sun et al.1992).

The main scattering component for the C band, are the leaves and small branches, and it saturates us ually at 10 kg/m 2. In the tropical forests with a complex structure and mixed vegetation species, the L and P band saturates usually at 100 t/ha. In the areas with simple structure and one or two domin ant species the saturation level is about 250 t/ha. The best bands for biomass estimation in coniferous forests are C and L band with HV polarization. For deciduous forests a combination of the L and C band with the HH and HV polarization are the most sui table (Ranson et al. 1994; Sun et al.1992). The backscattering of the L band is more related to the tru nk and main branches and less sensitive to the environmental conditions so it is valuable in the biomass estimation (Sader 1987, Luckman et al. 1997; Kurvonen et al. 1999; Sun et al. 2002). Usi ng a combination of C and L band has shown better results than using of one band (Hoekman et al., 1 997).

2.7.4 Constraints and difficulties for remote sensing application in biomass assessment

Remote sensing has developed into an important tool for monitoring and evaluation, and as a subsequent decision-making tool for various bioenergy and carbon sequestration projects. The feasibility of the use of remote sensing for monitoring of carbon stocks and flows in a project has been assessed by (Vine et al., 1999).

Finding an optimum combination of accuracy of measurements and the cost of the technology is often a major challenge in projects using remote sensing for estimating forest or plantation biomass and carbon sequestration. Among the remote sensing techniques available, estimation of biomass and detection of biomass change can be best achieved using SAR data. Studies have shown that SAR data can detect the half of the tree trunks removed by selective logging. Modelling biomass production or carbon sequestration, however, needs both optical and SAR data to be combined. Changes in land use can be obtained only by optical data (Scott *et al.*, 2009). No single sensor or any satellite mission, whether radar, lidar or optical, can be expected to provide consistently infallible estimation of biomass but use of these measurements in a synergistic fashion can potentially overcome the limitation of each

(whether radar saturation, lidar sampling modes or optical temporal matches). Quantification of the uncertainties associated with biomass calculations and optimization of remote sensing techniques to reduce uncertainties is required. Considerations of issues of accessibility and affordability of data should be addressed at global and particularly project scale.

Chapter 3 Materials and Methods

3.1 Description of the study area

3.1.1 Location

Yayu District is located in Illubabor Zone of Oromia Regional State, at about 550 km west of Addis Ababa on the major road from Addis Ababa to Metu Town. The geographic location of the study area is between 8°4′ 56.05″– 8° 24′ 40.46″ N latitude and 35° 44′53.85″– 36° 5′12.23″ E longitude covering a total area of 808.17 km^2 (Fig 3.1). Yayu is bordered from the south by the Southern Nations, Nationalities and Peoples Region, on the west by Metu, on the north by Supena Sodo, on the east by Chora, with particular emphasis on the forest landscape along Geba, Dogi and Sese rivers. Towns in Yayu include Elemo and Yayu. Coffee is an important cash crop in the woreda. The largest share of the Yayu Forest Biosphere Reservation, a project of the Ethiopian Coffee Forest Forum, lies in this woreda.

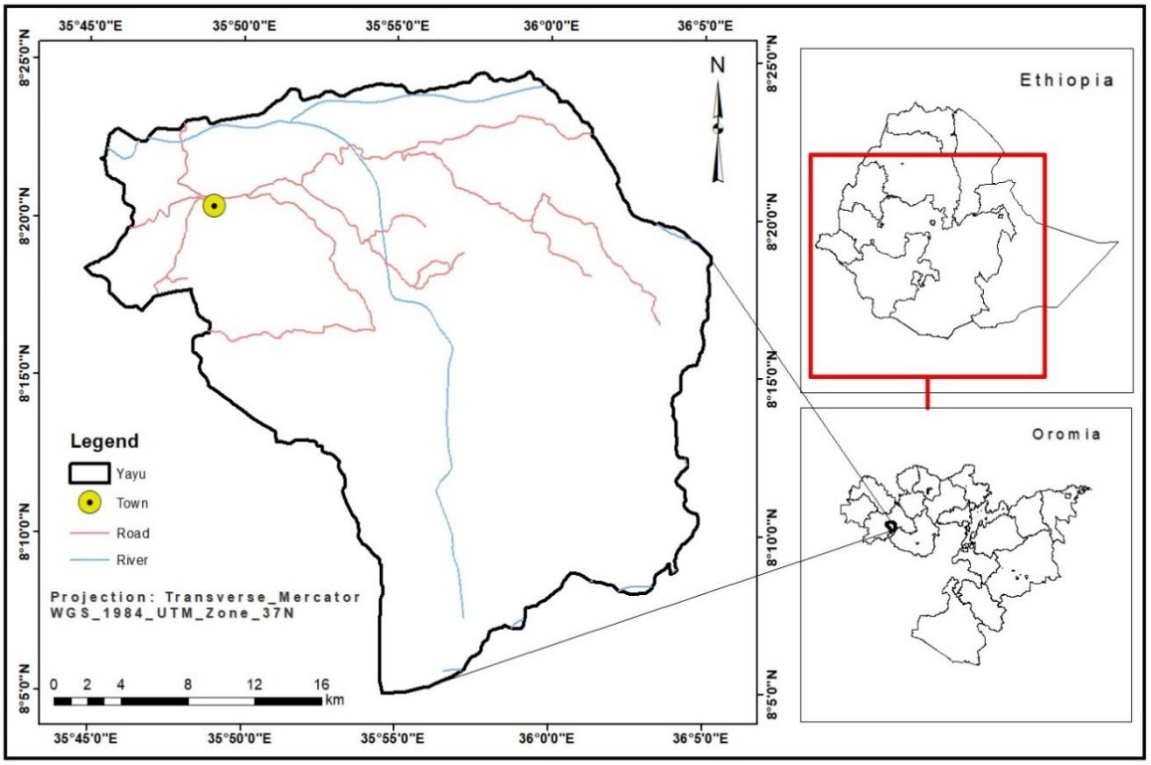

Figure 3.1: Location map of the study area

3.1.2 Topography and Drainage Systems

The forest area is characterized by a rolling topography, and is highly dissected by small streams and three major rivers, Geba, Dogi and Sese (Fig.3.2). The study area receives drainage from a huge area through Geba and Dogi rivers. The landform frequently changes from flat surfaces on the top of plateaus to very steep slopes and valley bottoms within short distances. The altitude ranges from 1217 at valley bottom to 2583 masl at the north-eastern higher elevation).

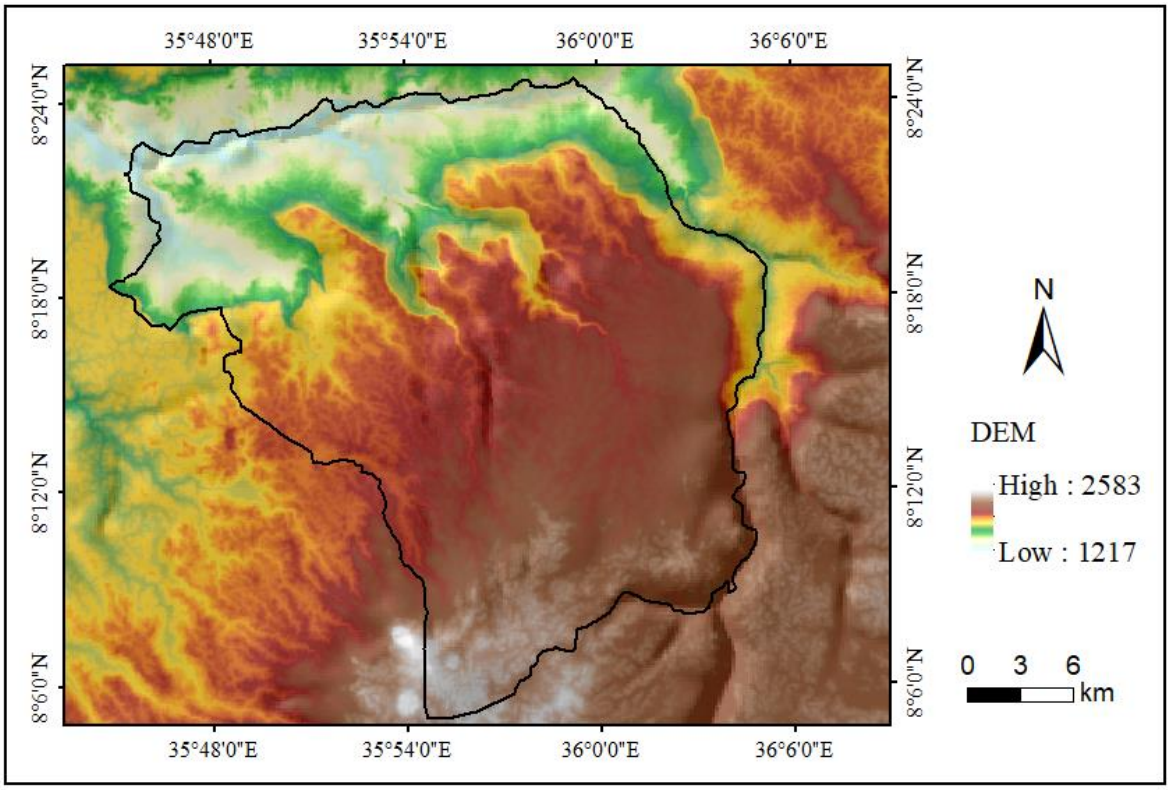

Figure 3.2: Topography of the study area

3.1.3 Climate

According to the data obtained from Ethiopian Meteorological Agency, which was recorded at Nopa Station, climatically the areas is hot and humid with mean minimum and mean maximum temperature of 14.01 and 28.24^{o}C, respectively and mean annual rainfall of 1770 mm with the minimum and maximum being 1238 and 3445 mm respectively (Fig.3.3). The hottest months are January, February, March and April while the coldest ones are August September and October. The rainfall pattern is uni-modal, with low rainfall in January and February, gradually

increasing to the peak period between May and October, and then decreasing in November and December (Fig.3.4). The highest rainfall is received in the period between June and August.

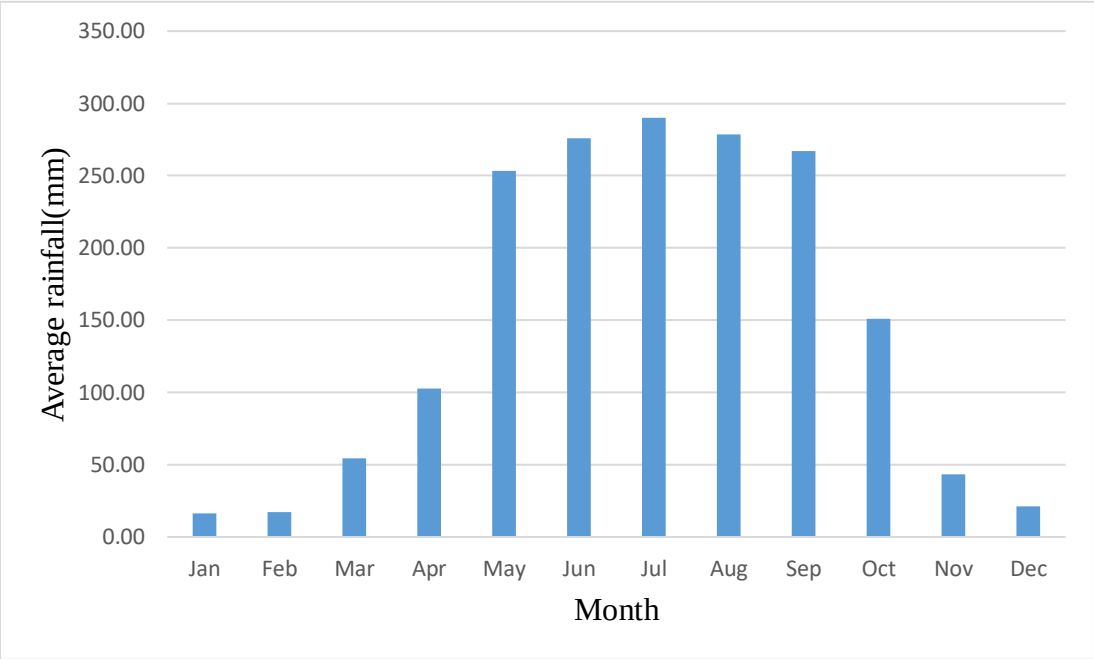

Figure 3.3: Average mean annual rainfall

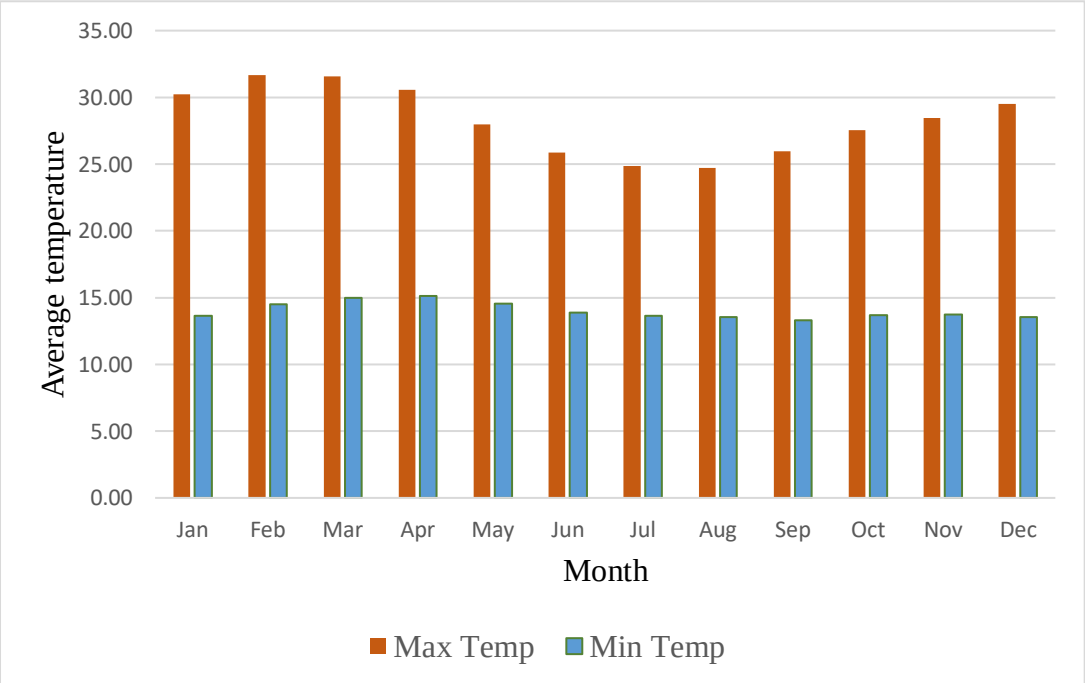

Figure 3.4: Maximum and minimum mean annual temperature

3.1.4 Land-use/land-cover

Five major land-use types are observed in Yayu District according to LU/LC classified from landsat 8 image of 2018; forest (61.8%), agriculture and settlement (30.2%), shrub land (2.9%), wetland (2.3%), and urban (2.7%) (Fig.3.5). Yayu District has the highest percentage forest cover compared to other districts in Ethiopia, which by far above the percent forest cover for the SW part of Ethiopia (18%) and that of the country as a whole (2.7%). Most forest areas are demarcated as National Forest Priority areas. However, the local community heavily depends on the forest mainly for coffee, spices and honey production. The main food crops are maize, sorghum and teff. Coffee is the major cash crop growing in the area.

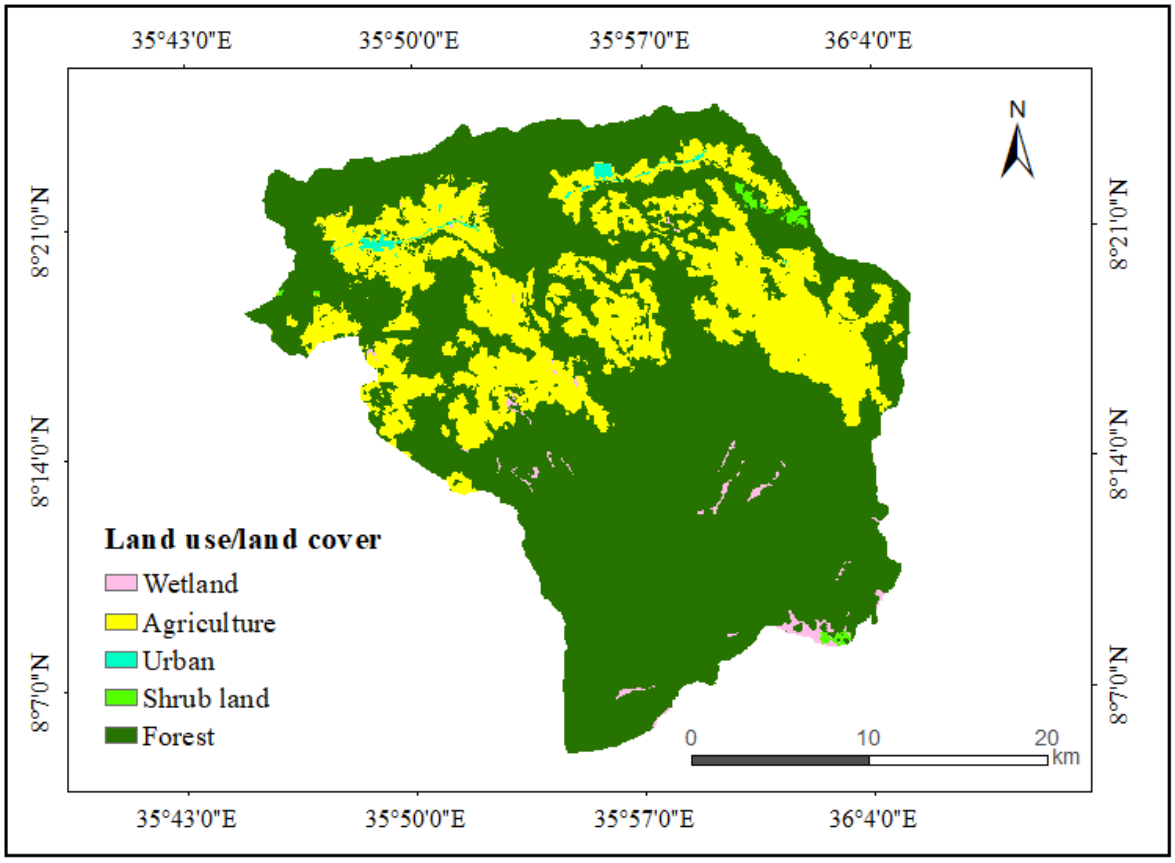

Figure 3.5: Land-use/land-cover map

3.1.5 Biodiversity

Yayu forest is one of the most diverse forests in Ethiopia with respect to plant species diversity. With about 220 plant species, Yayu forest excels other similar rain forests like the Harrena forest, in SE Ethiopia (128 species), and the Bonga forest in SW Ethiopia (154 species). The number of plant species in Yayu forest is also higher than most of the dryAfromontane forests of Ethiopia; for example, Chilimo forest (90 species); Jibat forest (54 species); Dakata Valley forest (202 species). Wild coffee has been identified as one of the most dominant under storey species in Yayu forest (Tadesse 2003).

3.1.6 Socio-economic Information

The major occupation in the area is agriculture, which employs over 90% of the labor force. The agricultural practice in the region is mainly smallholder subsistence farming. For more than 60% of the population, coffee production, processing and marketing are the major sources of employment (Tadesse, 2003).

3.2 Materials

3.2.1 Data and Source

The primary data (satellite imagery) were downloaded from European Space Agency data hub and secondary data specifically forest stand parameter such as DBH and tree height were obtained from office of Ethiopian coffee forest forum.

Table 3-1: List of data with their purpose and source.

Data	Purpose	Source
Sentinel-1 SAR image	For extracting texture characteristics and backscatter information using grey level co-occurrence matrix and resampling the result.	ESA(European Space Agency)
Sentinel-2 MSI image	For driving multispectral band, biophysical variable and vegetation indices	ESA(European Space Agency)
Forest DBH and Height	For calculating field AGB	ECFF (Ethiopian Coffee Forest Forum)
SRTM 3Sec	For geometric correction of sentinel image	Auto downloaded on SNAP software
Coordinate points (latitude, longitude and elevation)	For Navigation	Co-ordinate created on ArcMap

3.2.2 Software and tools

Table 3- **List of software and tools**

Software and tools	Purpose
SNAP	For sentinel 1 image processing and driving grey level co-occurrence matrix
ArcGIS	For image resampling**,** Extracting pixel value and producing maps
SPSS	For statistical analysis
QGIS	For preprocessing sentinel 2 image and extracting vegetation indices and land use classification
GPS	Field Data collection and navigation
Measuring tape and diameter tape	Forest DBH and height measurement and outline the plot

3.3 Methods

Field data and information from remote sensing data particularly sentinel imagery were used for computing and mapping Forest Above Ground Biomass. Sentinel 1 and Sentinel 2 imagery were downloaded from European Space Agency (ESA) and preprocessed for use on SNAP software. Texture analysis using grey level co-occurrence matrix were applied to extract texture and back scatter information such as contrast, dissimilarity, angular second momentum, entropy, correlation, and energy from sentinel 1 GRD SAR data by using SNAP software.

Vegetation indices such as Normalized Difference Vegetation Index (NDVI), Inverted Red-Edge Chlorophyll (EREC), Transformed Normalized Difference Vegetation Index (TNDVI) and vegetation biophysical variable such as Leaf Area Index (LAI), Fraction of Vegetation Cover (FVC), Fraction of Absorbed Photosynthetically Active Radiation (FPAR), Chlorophyll content in the leaf (Cab)) were derived from combination of different bands of sentinel 2 data. Land use land cover map were produced from Landsat-8 to extract forest cover in the study area. Selected sentinel 2 bands were also used as predictor variable. Digital elevation model (3sec) were auto downloaded and used while processing sentinel imagery which improve its accuracy.

Then field above ground biomass and information gained from both sentinel 1 and sentinel 2 imagery will be correlated statistically and regression analysis were applied on SPSS. To get the important variable from the above data, correlation were applied using SPSS statistical software. The variable with high coefficient of determination (r^2) and low root mean square error (RMS) will become the final above ground predictor (Fig 3.6.). Finally, a model was developed by considering coefficient of selected variables and constant values from multi linear regression analysis.

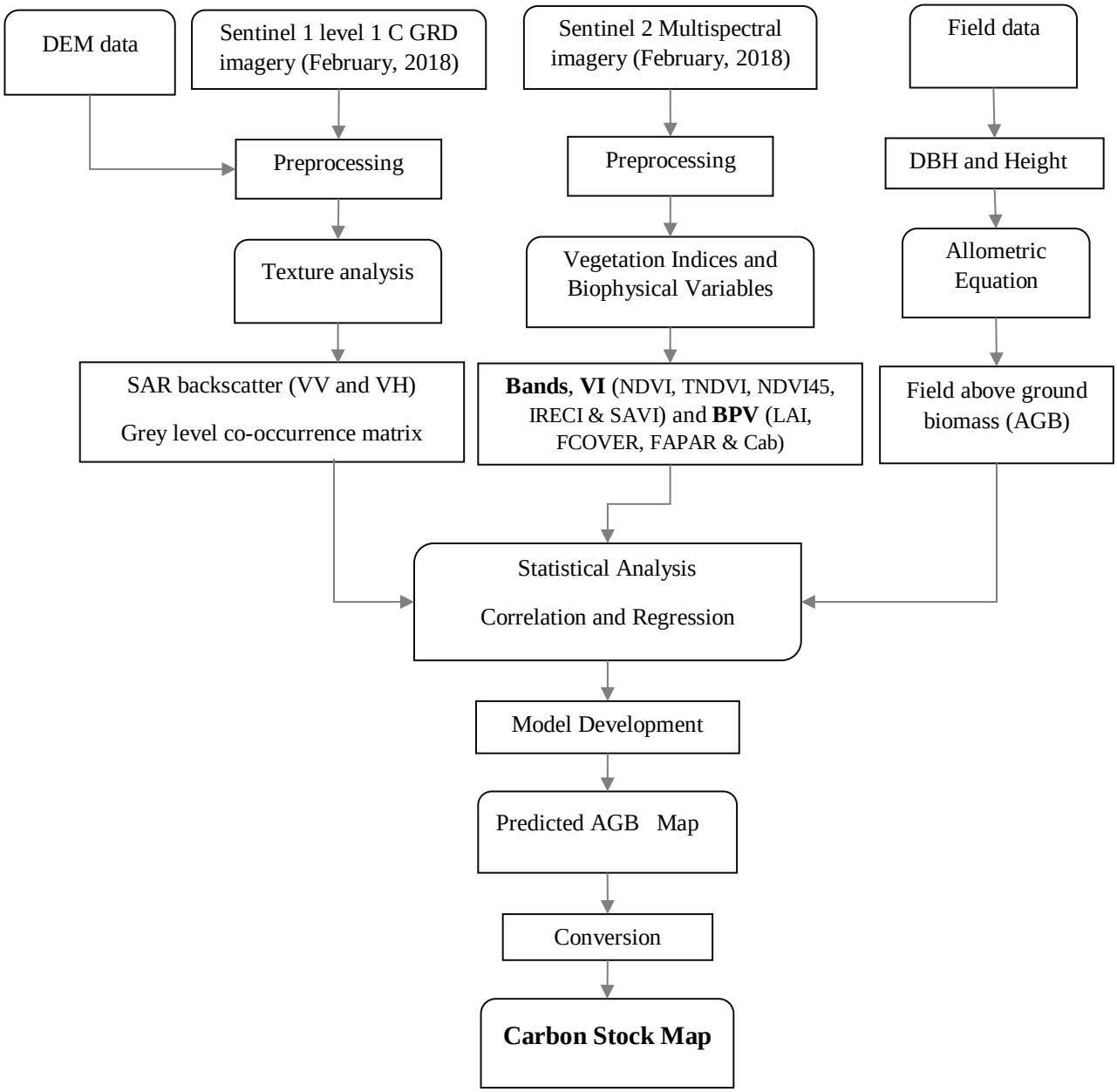

Figure 3.6: Flow chart of the methodology

where; NDVI is Normalized Difference Vegetation Indices), IRECI is Inverted Red-Edge Chlorophyll Index, TNDVI is Transformed Normalized Difference Vegetation Index, LAI is Leaf Area Index, FCOVER is Fraction of Vegetation Cover, FAPAR is Fraction of Absorbed Photosynthetically Active Radiation, RE NDVI is Red-Edge Normalized Difference Vegetation Index, Cab is Capability of chlorophyll content, VI is Vegetation Indices and BPV is Biophysical variables.

3.4 Analysis

3.4.1 Field Aboveground Biomass

The field data is taken from Ethiopian Coffee Forest Forum which works on forest and coffee resources that was collected in February, 2016. The purpose of fieldwork phase was to measure the aboveground biomass from the study area. This data later will be used as the ground truth data for both of estimation and validation work of modelling biomass. However, in executing a forest inventory, we need to establish a relationship between directly measurable tree or stand characteristics (e.g. DBH, height) and other forest stand parameters such as volume or biomass which is impossible to be measured directly (Husch *et al.*, 2003). The stand parameters of tropical forest will actually be measured from the field and then used for biomass calculation by allometric equations.

3.4.1.1 **Plot size**

The field sample plots used for this study were 20 in number, rectangular shape and 20 × 20 ($400m^2$) m size. From the sample data (plot) with different sample size i.e 20 × 20 m, 60 × 60 m and 100 × 100 m only those with 20 × 20 m which are part of 60 × 60m carbon plot were selected for this study. The data was collected using randomly taken plot generated on ArcGIS. The plot coordinate location were taken by considering the three different zone of yayu forest i.e Transitional, Buffer and Core zones. All trees with diameter greater than 10cm which found within $400m^2$ (0.04 ha) area of each plot were recorded. The parameter collected were species type, diameter at breast height and height of trees.

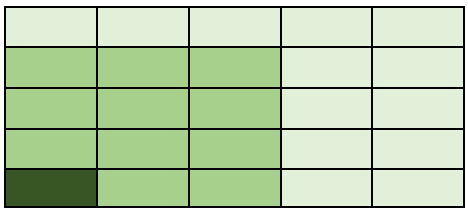

Where,

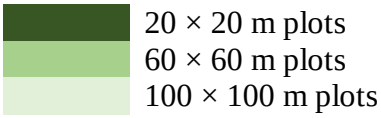

Figure 3.7: Chart showing size and shape of field plot samples

3.4.1.2 Calculation of AGB and Carbon stock

The AGB and carbon stock was computed based on large trees on the study area which excluded small trees. An allometric equation was used to calculate the AGB by using the forest stand parameters: DBH, Height and density (Table 3.3). The allometric equation which was used in this research was formulated by (Chave et al., 2014). It was found to be the best model for biomass estimation in tropical forest. It is also suitable for Yayu forest type and bioclimatic conditions the wood density values used was species specific (Gisel et al., 1992).

Equation 3-1: Forest above ground formula

$$\mathbf{AGB = 0.0673 \times (\rho D^2 H)^{0.976}} \qquad 3.1$$

where, AGB is Above-ground biomass.

ρ is Specific wood density (g/cm^3), D^2 is Diameter at breast height (DBH) (cm); H is Height of tree (m).

The above-ground biomass was then be converted into carbon using the (CF) factor 0.47 formulated by IPCC, (2006).

Equation 3-2: Carbon stock formula

$$C = AGB \times CF \qquad 3.2$$

Where,

C: Carbon stock (Mg C),

AGB: Above ground biomass and

CF: Fraction of above ground biomass (0.47)

Above ground biomass for the other 19 plots were computed on the same way as W_3 using allometric equation (Table3.2).

Table 3-2: Computed AGB using allometric equation for W3 (plot code)

Plot Code	Fam	Genus	Species	Diameter (cm)	Height (m)	Height (cm)	Density(g/cm^3)	AGB(g)	AGB(kg)
W_3	Fabaceae	Acacia	abyssinica	33.9	18	1800	0.826	81486.07	81.48607
	Fabaceae	Acacia	abyssinica	79.7	17	1700	0.826	408839.1	408.8391
	Boraginaceae	Cordia	africana	21.1	16	1600	0.482	17017.25	17.01725
	Boraginaceae	Cordia	africana	34.5	15	1500	0.482	41721.21	41.72121
	Melianthaceae	Bersama	abyssinica	14.7	14	1400	0.671	10188.74	10.18874
	Capparidaceae	Ritchiea	albersii	43.3	18	1800	0.5	80497.08	80.49708
	Boraginaceae	Cordia	africana	54.3	17	1700	0.482	114265.8	114.2658
	Total								**754.015**

3.4.2 Sentinel 1 image processing

Sentinel 1 Ground Range Detected (GRD) is downloaded from European Space Agency (ESA) data hub and preprocessing has made on SNAP software. Steps included were application of orbit file to provide accurate satellite altitude and velocity information, radiometric calibration for backscatter representation of the reflecting object (conversion from DN values to sigma nought values), speckle filtering for speckle suppression using Refined Lee adaptive filter, terrain-correction using SRTM 3 sec grid to correct for SAR geometric distortions, and re-projection from WGS84 to UTM Zone 37N. The result is resampled to 20 m to fit with field plot size. Before creating texture analysis using GLCM both polarization (Sigma0_VV and Sigma0_VH) have changed to decibel (dB) in order to represent the correct backscatter information. Conversion of sigma0 value to decibel help us to gain the correct backscatter values of the scene **(Getu Tesema, 2017).**

3.4.2.1 **Texture analysis**

Texture parameters are commonly used to measure the spatial distribution of image tone variance which can be used to estimate forest AGB (Moskal and Franklin, 2001). Here in image tone refers to the variation of grey scales of resolution cells in an image (Mather and Koch, 2011). Variation in image tone can result from changes in stem density, species type, or crown closure (Franklin et al., 2001).

3.4.2.2 **Grey-level co-occurrence matrix (GLCM)**

The most popular statistical methods used to measure the textural information of images is the '*Gray Level Co-occurrence Matrix'* (GLCM). The GLCM method gives reasonable texture information of an image that can be obtained only from two pixels. Grey level co-occurrence matrices introduced by Haralick. (1973) attempt to describe texture by statistically sampling how certain grey levels occur in relation to other grey levels. Suppose an image to be analyzed is rectangular and has Nx rows and Ny columns. Assume that the gray level appearing at each pixel is quantized to Ng levels. Let Lx= {1,2,…,Nx} be the horizontal spatial domain, Ly= {1,2,…,Ny} be the vertical spatial domain, and G= {0,1,2,…,Ng-1} be the set of Ng quantized gray levels. The set Lx×Ly is the set of pixels of the image ordered by their row-column designations. Then the image which can be represented as a function of co-occurrence matrix that assigns some gray level in Lx×Ly; I: Lx×Ly→G. The gray level transitions are calculated based on the parameters, displacement (d) and angular orientation (θ). By using a distance of one pixel and angles quantized to 45^0 intervals, four matrices of horizontal, first diagonal, vertical, and second diagonal (0, 45, 90 and 135 degrees) are used.

.Even though Haralick extracted 24 parameters from co-occurrence matrix, only seven are commonly used such as energy, entropy, contrast, local homogeneity, correlation, cluster shade and cluster and is stored in feature database. In addition, the first order statistical features (i.e., mean and standard deviation (StdDev) are used to describe the characteristics of image

The GLCM used for this study were variance, mean, contrast, homogeneity, correlation, entropy, dissimilarity, energy and second moment. Entropy measures the randomness of intensity distribution, low values for smooth images than for a coarse image. Energy measures the number of repeated pairs and also measures uniformity of the normalized matrix. The contrast feature is a difference moment of the P matrix and is a standard measurement of the

amount of local variations present in an image. The higher the value of contrast are, the sharper the structural variations in the image. Homogeneity measures the closeness of the distribution of elements in the GLCM to the GLCM diagonal. The converse of homogeneity results in the statement of contrast. (Table 3.3) shows the GLCM variables and their corresponding formula. Variables from texture analysis of sigma0_VH and sigma0_VV using grey level co-occurrence matrix were generated on SNAP software. Variables extracted from texture analysis of sentinel 1 using grey level co-occurrence matrix VH and VV were shown on Fig.3.8 and 3.9 respectively.

Table 3-3: GLCM texture measures

Parameters	GLCM variable formula	Description
Contrast	$\sum_{i,j=0}^{N-1} -\ln(i-j)2$	Calculates the level of local variation within a window (Yuan et al., 1991)
Correlation	$\sum_{i,j=0}^{N-1} Pij\frac{(i-\mu)(j-\mu)}{\sigma 2}$	Measures the grey-level linear dependency within an image (Kayitakire et al., 2006)
Dissimilarity	$\sum_{i,j=0}^{N-1} Pij\lvert i-j\rvert$	Is a measure of the local variation (Rubner et al., 2001).
Homogeneity	$\sum_{i.j=0}^{N-1} \frac{Pij}{1+(i-j)2}$	Measures the smoothness of image texture (Tuttle et al., 2006)
Mean	$\sum_{i,j=0}^{N-1} i(Pij)$	Average grey-level in the small neighborhood (Materka and Strzelecki, 1998)
Second Momentum	$\sum_{i,j=0}^{N-1} Pij^2$	Second moment is an indicator of local homogeneity (Yuan et al.,1991)
Variance	$\sigma 2\mathrm{i} = \sum_{i,j=0}^{N-1} Pij(i-\mu)^2$ $\sigma 2\mathrm{j} = \sum_{i,j=0}^{N-1} Pij(i-\mu i)^2$	Variability of the spectral response of pixels (Materka and Strzelecki, 1998).
Entropy	$\sum_{i,j=0}^{N-1} -\ln(Pij)pij$	A statistical measure of uncertainty (Yuan et al., 1991)
Energy	$\sum_{i,j=0}^{N-1} -\ln(Pij)2$	

where, N is the number of gray levels in the image and P(i,j) is the pixel value in position (i,j) of the texture image or normalized co-occurrence matrix where the sum of (i,j = 0, N-1) (P (i, j))=1.

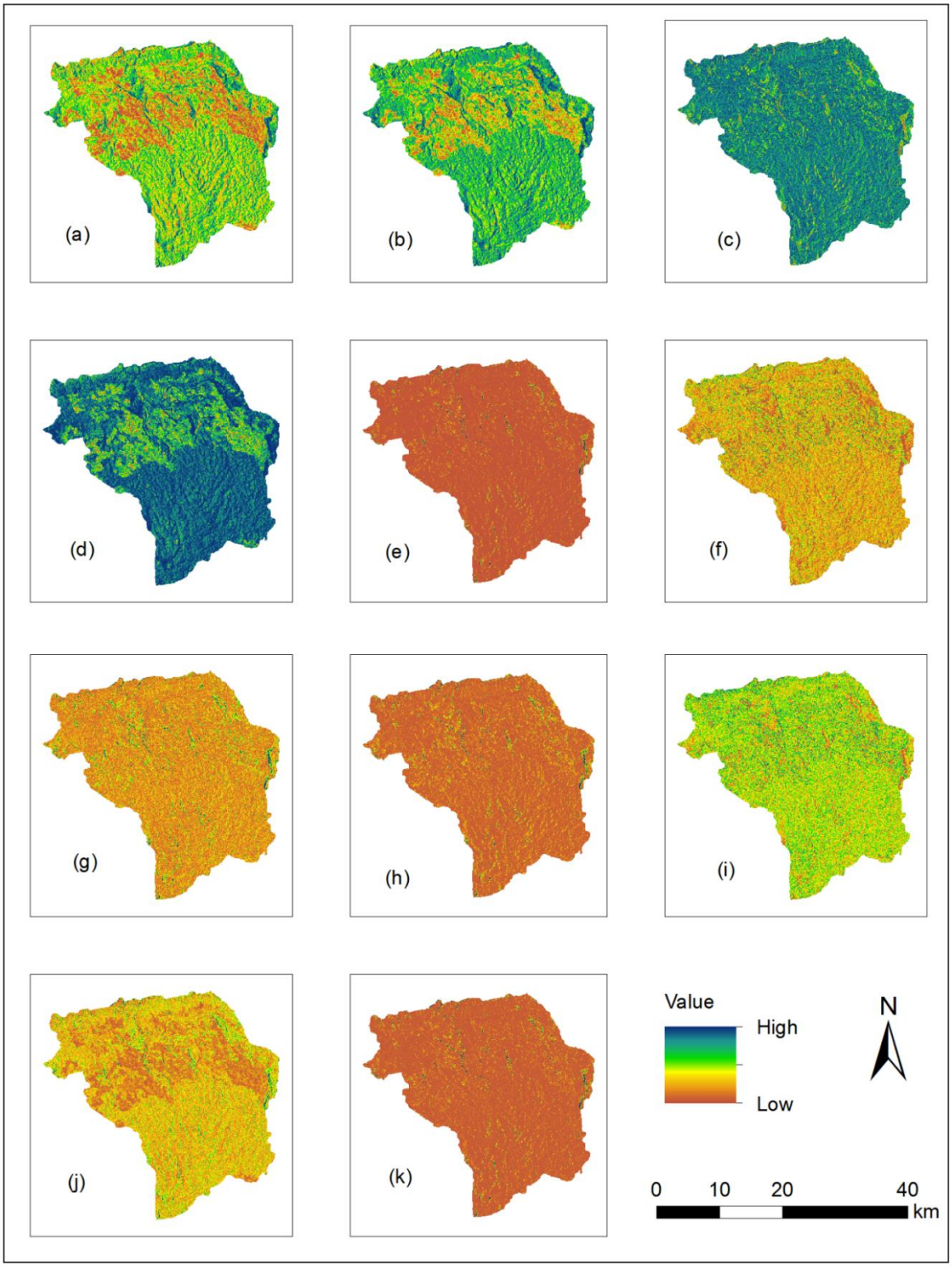

Figure 3.8: Grey level co-occurrence matrix generated from sigma0_VH polarization

where, a is Sigma0_VH_GLCMVariance,b is Sigma0_VH_GLCMMean, c is Sigma0_VH_Entropy, d is Sigma0_VH_GLCMCorrelation, e is Sigma0_VH_ASM f isSigma0_VH_Contrast, g is Sigma0_VH_Homogeneity, h is Sigma0_VH_Energy, i is Sigma0_VH_Dissimilarity, j is Sigma0_VH and k = Sigma0_VH_MAX .

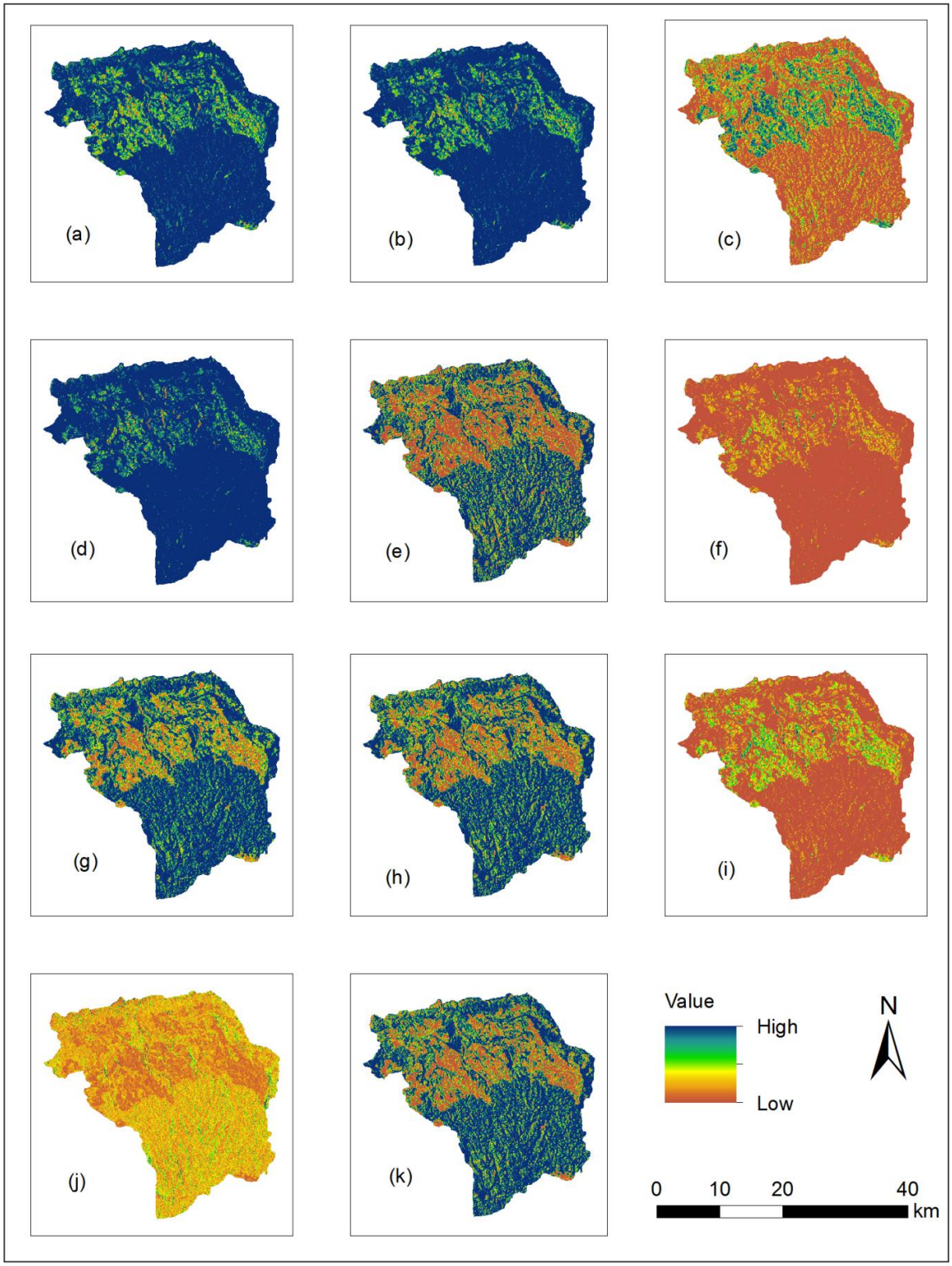

Figure 3.9: Grey level co-occurrence matrix generated from sigma0_VV polarization

Where a is Sigma0_VV_GLCMVariance, b = Sigma0_VV_GLCMMean, c is Sigma0_VV_Entropy, d is Sigma0_VV_GLCMCorrelation, e is Sigma0_VV_ASM, f is Sigma0_VV_Contrast, g is Sigma0_VV_Homogeneity, h = Sigma0_VV_Energy, i is Sigma0_VV_Dissimilarity j is Sigma0_VV, k = Sigma0_VV_MAX

3.4.3 Sentinel 2 image processing

Sentinel 2 Multispectral instrument (MSI) with swath width of 290 km and which is Ortho-rectified to UTM/WGS84 projection was downloaded from European Space Agency (ESA) data hub. Radiometric correction was done to improve the quality of the image. The main purpose of radiometric correction is to reduce atmospheric and sun angle effects (Baillarin et al., 2012). The image was transformed from radiance to surface reflectance, by applying the Dark Object Subtraction (DOS) method using the semi-automatic classification plugin (SCP) in QGIS software. The DOS method works by removing the darkest pixel in each band that might be affected by atmospheric scattering (Chavez, 1988). The blue, green, red and near infrared bands which were of 10m resolution resampled into a 20m resolution using ArcGIS software. This was done because the field data plots in which the results going to correlated has 20 × 20 m spatial resolution

3.4.3.1 **Vegetation Index**

Vegetation indices from satellite measurements have emerged as an important tool in monitoring, mapping and resource management of the terrestrial vegetation as they provide the radiometric measures of the amount, structure and condition of vegetation and thereby serve as useful indicators of seasonal and inter-annual variations. They also have a biophysical significance as they act as intermediaries in the assessment of leaf area index (LAI) and green leaf area index (GLAI), percent green cover or fractional green cover and fraction of absorbed photosynthetically active radiation

A **Vegetation Index** (**VI**) is a spectral transformation of two or more bands designed to enhance the contribution of vegetation properties and allow reliable spatial and temporal inter-comparisons of terrestrial photosynthetic activity and canopy structural variations (Huete *et al*). There are many Vegetation Indices (VIs), with many being functionally equivalent. Many of the indices make use of the inverse relationship between red and near-infrared reflectance associated with healthy green vegetation. Since the 1960s scientists have used satellite remote sensing to monitor fluctuation in vegetation at the Earth's surface. Measurements of vegetation attributes include leaf area index (LAI), percent green cover, chlorophyll content, green biomass and absorbed photosynthetically active radiation (APAR).

According to Bannari et al., (1995) vegetation Indices (VIs) have been historically classified based on a range of attributes, including the number of spectral bands (2 or greater than 2); the method of calculations (ratio or orthogonal), depending on the required objective; or by their historical development (classified as first generation VIs or second generation VIs). For the sake of comparison of the effectiveness of different Vis. Yuan et al. (1998) classified 7 VIs based on their computation methods (Subtraction, Division or Rational Transform). Due to advances in hyperspectral remote sensing technology, high-resolution reflectance spectrums are now available, which can be used with traditional multispectral VIs. In addition, VIs have been developed to be used specifically with hyperspectral data, such as the use of Narrow Band Vegetation Indices.

3.4.3.2 **Biophysical variable**

Surface biophysical or canopy properties provide an understanding of the physics of the interactions between solar radiation and vegetation elements thereby acting as a key input parameter for decoding the global climate change dynamics (Asrar et al., 1989). Surface parameter retrieval from satellite remote sensing data had been one of the major sources to obtain these parameters because it relates the vegetation characteristics to its spectral signature or reflectance thereby providing reasonable estimates of vegetation properties across various spectral, spatial and temporal scales (Asrar et al, 1989). According to Widlowski et al. (2004) biophysical variables describe the spatial distribution of vegetation state and dynamics, thus, are useful for biomass estimation. LAI, Fraction of absorbed photosynthetically active radiation (FAPAR), and FVC Capability of chlorophyll content were the main variables computed by the SNAP toolbox using biophysical variable processor.

3.4.3.3 **Bands, Vegetation Indices and biophysical variable derived from Sentinel-2 optical satellite image**

The vegetation indices and biophysical variable were computed on ArcGIS and SNAP software. The indices were selected based on its performance in biomass estimation in previous studies (Table 3.4). The vegetation indices for this study were produced on QGIS and ArcMap (Fig 10 and 11).

Table 3-4: Shows all the selected bands, derived VIs and biophysical variables.

Multispectral bands	**Description**
B2	Blue, 490 nm(10m)_Resampled to 20m
B3	Green, 560 nm(10m)_Resampled to 20m
B4	Red, 665 nm(10m)_Resampled to 20m
B5	Red edge, 705 nm(20m)
B6	Red edge, 749 nm(20m)
B7	Red edge, 783 nm(20m)
B8	Near Infrared, 842 nm(10m))_Resampled to 20m
B8a	Near Infrared, 865 nm(20m)
B11	Short Wave IR, 1610 nm(20m)
B12	Short Wave IR, 2190 nm(20m)
Vegetation Indices	
NDVI	(Band 8 - Band 4)/(Band 8 + Band 4)
NDI45	(Band 5 - Band 4)/(Band 5 + Band 4)
IRICI	(Band 7 - Band 4)/(Band 5/Band 6)
TNDVI	$[(\text{Band 8} - \text{Band 4})/(\text{Band 8} + \text{Band 4}) + 0.5]^{1/2}$
SAVI	(Band 8- Band 4/Band 8 + Band 4 + 0.5)*1.5
Vegetation biophysical variables	
LAI	Leaf Area Index
FVC	Fraction of Vegetation Cover
FPAR	Fraction of Absorbed Photosynthetically Active Radiation
Cab	Chlorophyll content in the leaf

Where; NDVI = Normalized Difference Vegetation Index, $NDVI_{red\ edge}$ = Red Edge Normalized Difference Vegetation Index, EVI_2 = Enhanced Vegetation Index 2, NDI45 = Normalized Difference Vegetation Index with band 4 and 5, IRICI = Inverted Red-Edge Chlorophyll Index, TNDVI = Transformed Normalized Difference Vegetation Index, LAI=Leaf Area Index, FVC = Fraction of Vegetation Cover, FPAR = Fraction of Absorbed Photosynthetically Active Radiation.

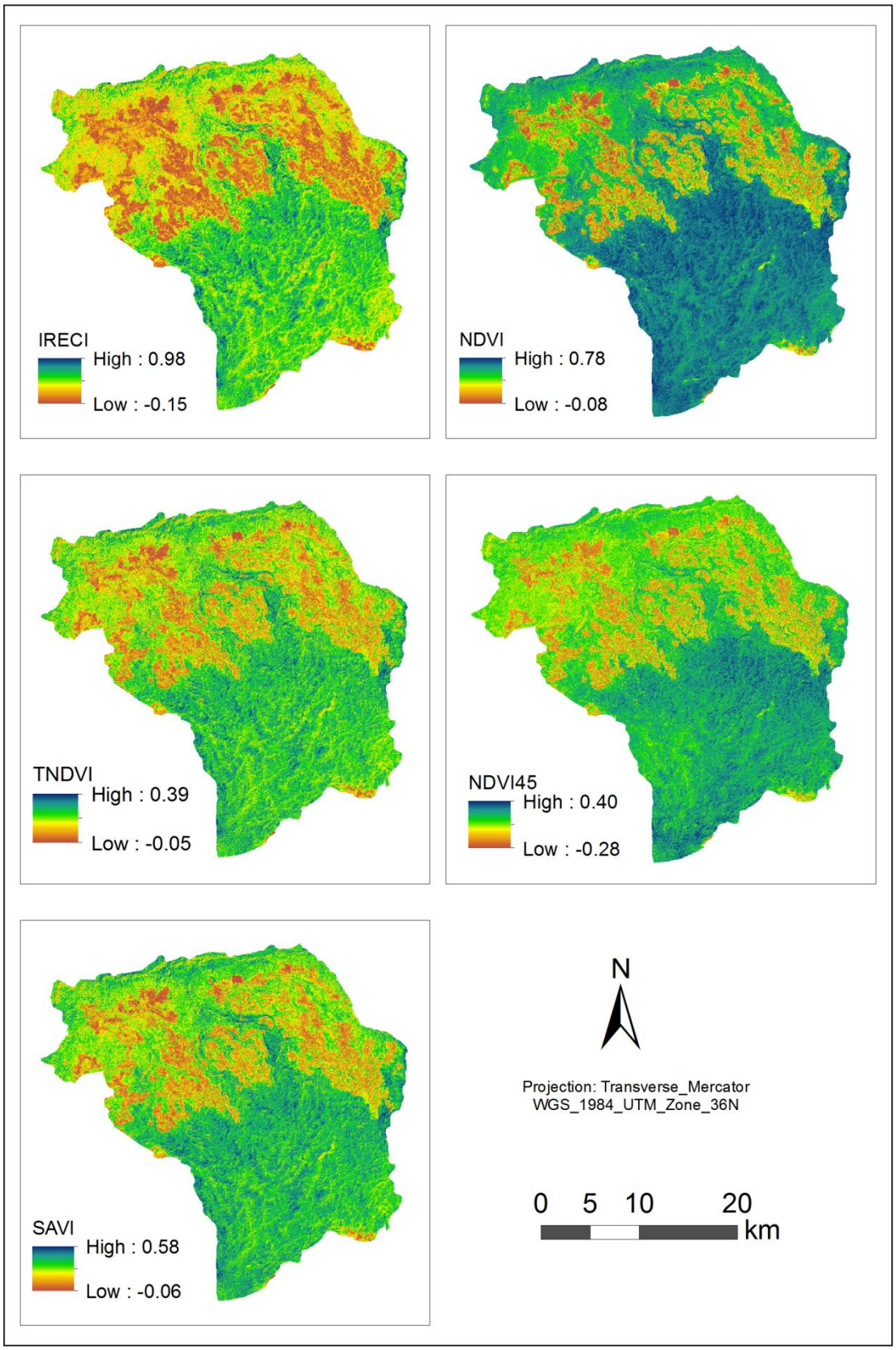

Figure 3.10: Vegetation indices

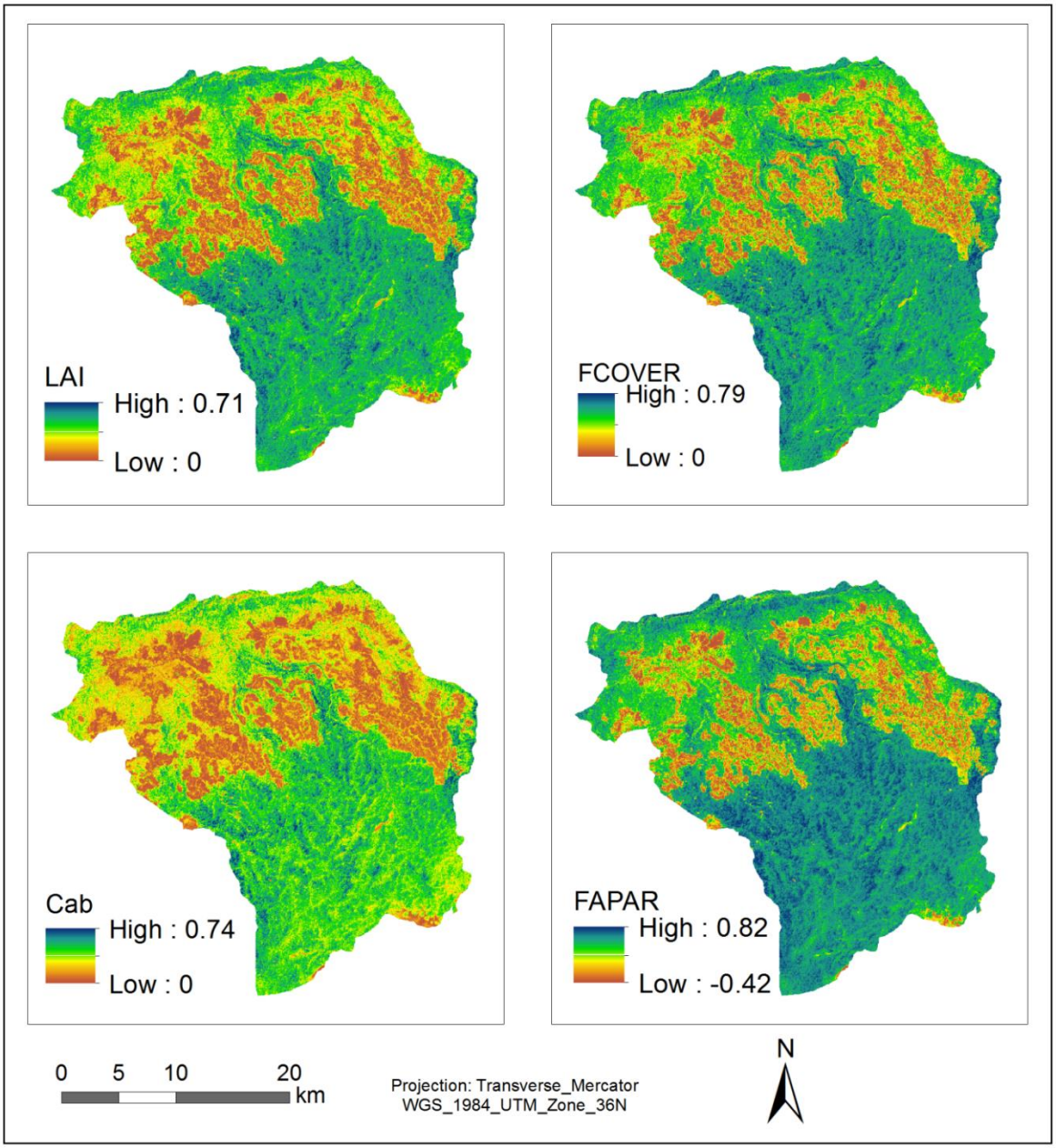

Figure 3.11: Vegetation biophysical variable

3.4.3 **Extracted pixel values of predictor variable**

The pixel values for each variable from both sentinel 1 and sentinel 2 were extracted using zonal statistics on ArcGIS, using field plot location (latitude, longitude) as a reference, and exported in csv format.

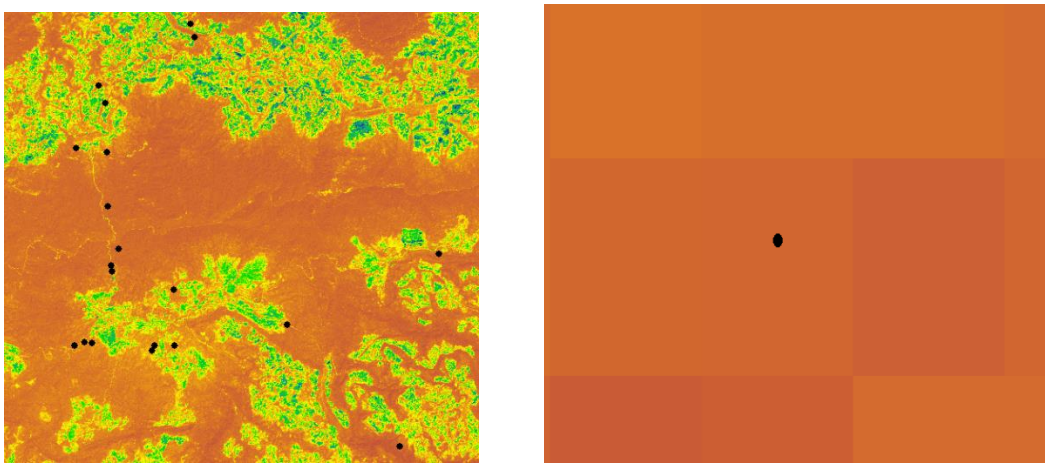

a) Field sample plot distributed over the study area b) Field sample plot overlaid on a pixel

Figure 3.12: Pixel value extraction (a and b)

3.4.3.1 **Sentinel 1 variables**

All texture analysis result from grey level co-occurrence matrix of sentinel 1 data was used in the extraction of pixel values. A total of 22 variables were used from sentinel 1 ground range detected (GRD) image including VV (vertical transmit and vertical receive) and VH (vertical transmit and horizontal receive). Twenty pixel values were extracted from each variable and totally 440 were used from sentinel 1 image (appendix C and D).

3.4.3.2 **Sentinel 2 variables**

Bands, vegetation indices and biophysical variables were used in extracting pixel values. A total of 19 predictor variables (10 bands, 5 vegetation indices and 4 biophysical variables) were used. The number of pixel value extracted from sentinel 2 multispectral instruments (MSI) were 138 (appendix E and F).

3.4.4 **Statistical Analysis**

Statistical analysis was carried out using Microsoft Excel and SPSS software. Correlation analysis were made prior to model development in order to know the relation between predictor variables and AGB. Thus it was carried out for both sentinel 1 and sentinel 2 images. To determine the relationship a scatter plot diagram was made. Linear regression models were used on SPSS to assess the relationship between each VIs, biophysical variable, backscatter information and observed AGB. Linear Regression refers to a group of techniques for fitting

and studying the straight-line relationship between two variables. Linear regression estimates the regression coefficients a and b in the equation **y** = a + bxj + ε_0, where x is the independent variable, Y is the dependent variable, a is the y intercept is the slope, and ε is the error.

A total of 20 pixel were used for each variable, having an average of four pixels (resampled to 20m) and which have same location with field plot. The model was evaluated based on the Root Mean Square Error (RMSE) and coefficient of determination (r^2). The best model was developed by integrating those variables with high r^2 and a low RMSE. The equation obtained from the regression model was then used to estimate AGB. The r^2 was preferred since it has a standard measure with values ranging from 0 to 1. The r^2 also shows the percentage of the variability explained by the model. Thus, making it easy to understand the relationship between the independent and dependent variable (Peters, 2007). The equation obtained from the regression model was then used to estimate AGB.

Equation 3-3: Root mean square error formula

$$RMSE=\sqrt{\frac{\sum_{i=1}^{n}(AGBo-AGBp)2}{n}} \quad \text{..... (3.4)}$$

where, AGB_o is Observed AGB Value (Dependent Variable),

AGB_p is Predicted AGB Value (Independent Variable),

n is Number of samples

3.4.5 Model development using regression analysis

The objective of regression analysis is to quantify the relationship between dependent variable and one or more independent variables. Regression implies a cause and effect relationship in which a change in the value of an independent variable will result in an expected average change in the dependent variable. The quantitative relationship is expressed by an equation and its graphic representation (Husch *et al.*, 2003). The square value of the correlation coefficient (r^2) is called the coefficient of determination. It can be interpreted as indicating the percentage of variation in one variable that is associated with other variable (Husch *et al.*, 2003).

Chapter 4 Results and Discussion

4.1 Results

4.1.1 Field Above ground biomass

The above ground biomass from field forest parameter were computed using allometric equation for 20 sample plot. Above ground biomass for each plots were converted from kg to tone in order to correlate with variables extracted from sentinel imagery. The highest above ground biomass were found in WA_2 (13^{th} plot) which contains dense and large trees, second and third were $B1_3$ (2^{nd} plot) and (6^{th} plot) respectively. The least AGB is found in BD_4 (5^{th} plot) which had relatively short of trees.

Table 4-1: Forest above ground biomass computed from field data

No	Plot code	Latitude	Longitude	Area	AGB(kg)	AGB(tone)
1	B8	147368	931779	400	196.66	0.19666
2	B13	145903	932027	400	975.2	0.9752
3	B15	147329	934143	400	489.16	0.48916
4	B16	147023	934962	400	237.39	0.23739
5	BD4	150452	925206	400	104.46	0.10446
6	FC1	147389	929212	400	927.31	0.92731
7	FC2	147854	927192	400	859.69	0.85969
8	GC4	155815	923434	400	807.59	0.80759
9	H3	150437	922525	400	194.95	0.19495
10	H6	149495	922560	400	403.98	0.40398
11	H7	149358	922303	400	617.37	0.61737
12	W2	151628	937211	400	390.43	0.39043
13	WA2	147518	926112	400	1104.14	1.10414
14	WA3	147484	926386	400	618.4	0.6184
15	WA6	145704	922617	400	481.18	0.48118
16	WA7	146176	922736	400	461.42	0.46142
17	WA8	146521	922727	400	383.69	0.38369
18	WE2	163083	926702	400	337.88	0.33788
19	B19	822091	917444	400	686.18	0.68618
20	W3	151444	937851	400	754.02	0.75402

4.1.2 Correlation between AGB and sentinel predictor variable

All computed information from image and field plot are organized in one spreadsheet .csv format and correlation was done on excel to see which variable is more correlated with the field above ground biomass.

4.1.2.1 Correlation of Sentinel 1 variable with field AGB

Moderate correlation were seen between observed AGB and sentinel 1 predictor variables with correlation coefficient (r) ranging from -0.34 to 0.48). Among predictors, VV_ASM (r = 0.48), VV_MAX (r =0.4), VV_ENE (r = 0.40), VV_HOM (r = 0.34) and VV_Polarization (r =0.33) were significantly correlated with AGB. Even though all relationships were not significant, vertical transmit and vertical receive angular second moment (Sigma0_VV_ASM) is more correlated (0.48) compared to other predictor's variables from sentinel 1 variables. From the 22 variables extracted, nine of them have negative and 13 variables have positive linear relationship with observed AGB. Texture analysis variables from grey level co-occurrence matrix of VV polarized including itself have a good correlation than VH polarized with field AGB in the study area (Figure 4.1, 4.2 and 4.3).

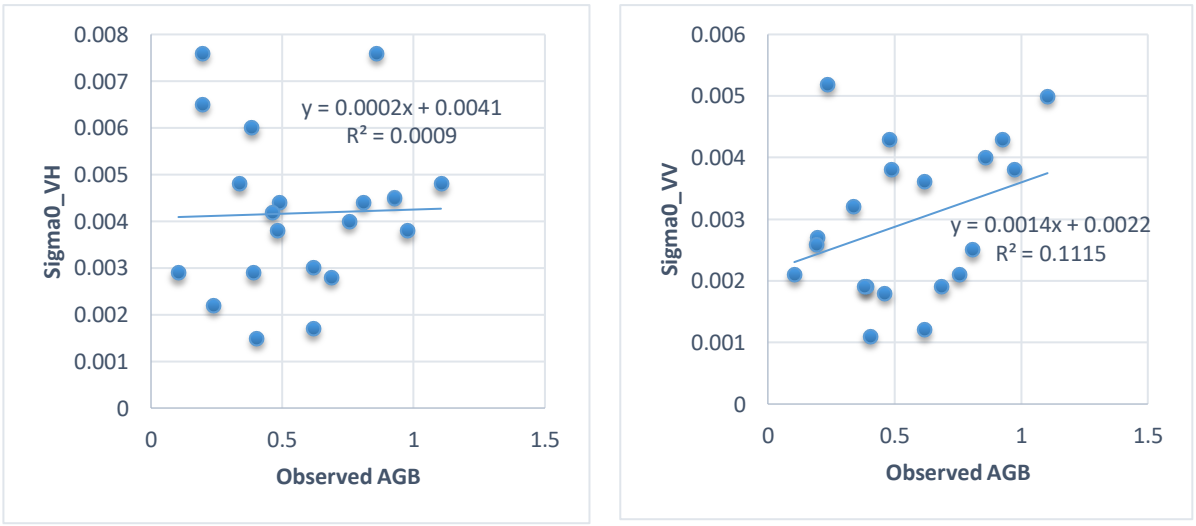

Figure 4.1: Scatter plot showing linear relationship of observed AGB with backscatter values of VV and VH polarization

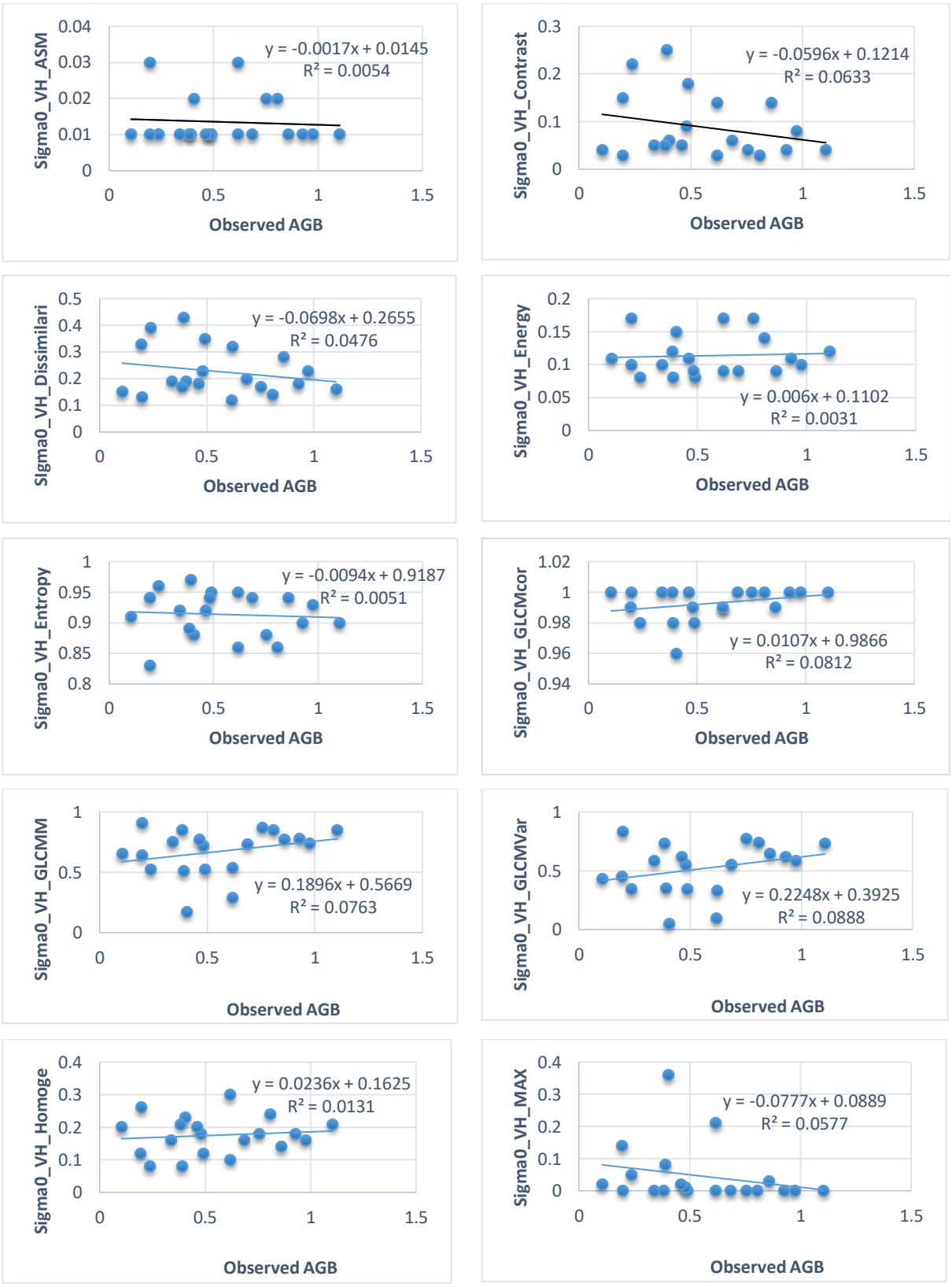

Figure 4.2: Scatter plot showing linear relationship between variables extracted from texture analysis of Sigma0_VH using grey level co-occurrence matrix and Observed AGB

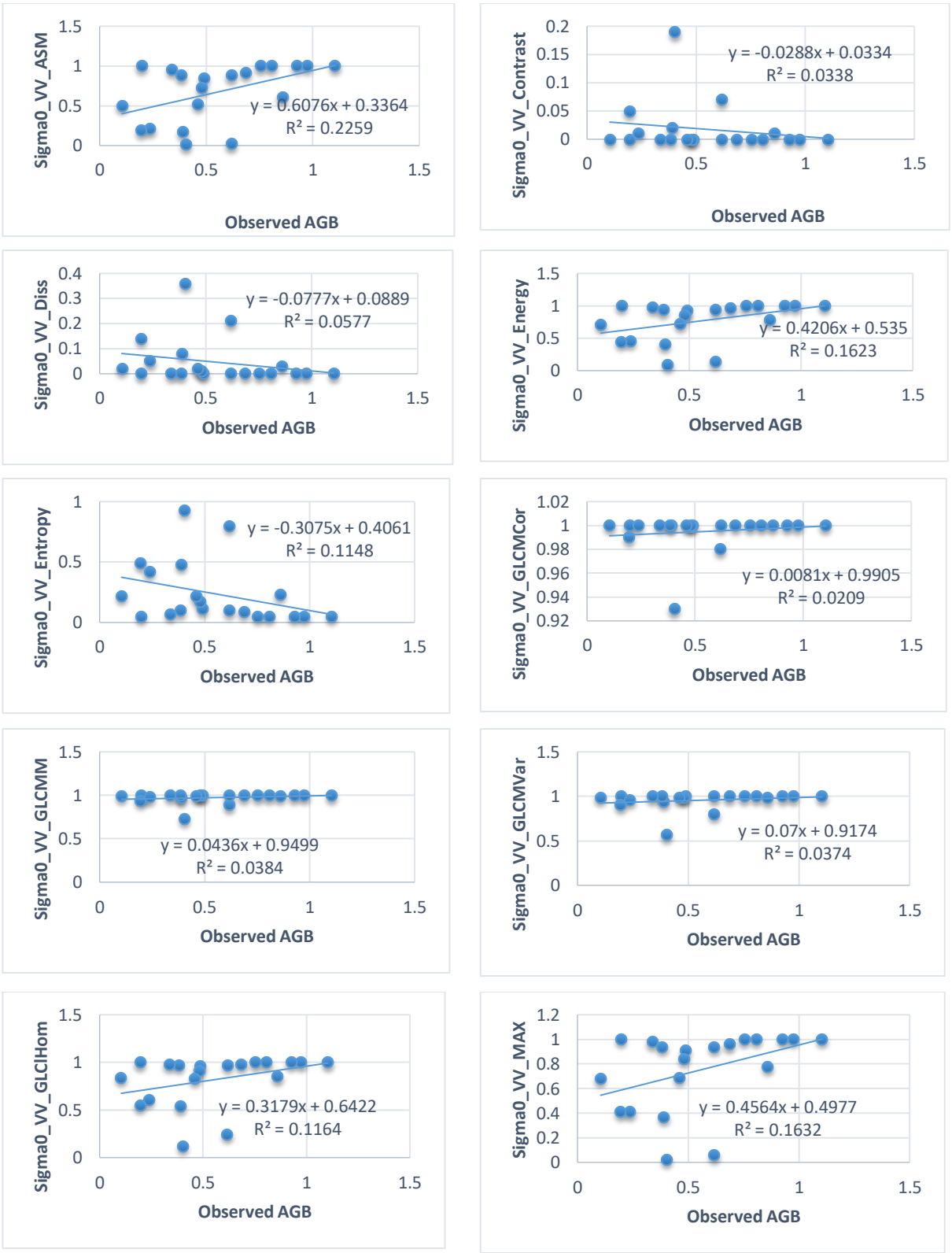

Figure 4.3: Scatter plot showing linear relationship between variables extracted from texture analysis of Sigma0_VV using grey level co-occurrence matrix and Observed AGB

4.1.2.2 Correlation of Sentinel 2 variable with field AGB

Good to strong correlation was observed between field AGB and predictor variables having a coefficient of determination (r) value from 0.13 to 0.74. Among predictors, NDVI(r = 0.36), IRECI (r =0.5), NDVI (r = 0.40), LAI (r = 0.74), FAPAR (r = 0.7), FCOVER (r = 0.64) and Cab (r =0.69) were strongly correlated with AGB. From vegetation indices IRECI and from biophysical variable LAI were best correlated with observed AGB. Among the overall variables, biophysical variables correlated strongly (0.65-0.74) with aboveground biomass. Figure 4.4 show that there is a good linear relationship between biomass and vegetation indices (r^2 = 0.017 −0.27) and Figure 4.5 show that there is a strong linear relationship between biomass and biophysical variables (r^2 = 0.42 - 0.54). Band 4 performed better than other sentinel 2 bands (r = -0.45 and r^2 = 0.2) and also more than vegetation indices followed by IRECI, which is included in developing AGB predictive model.

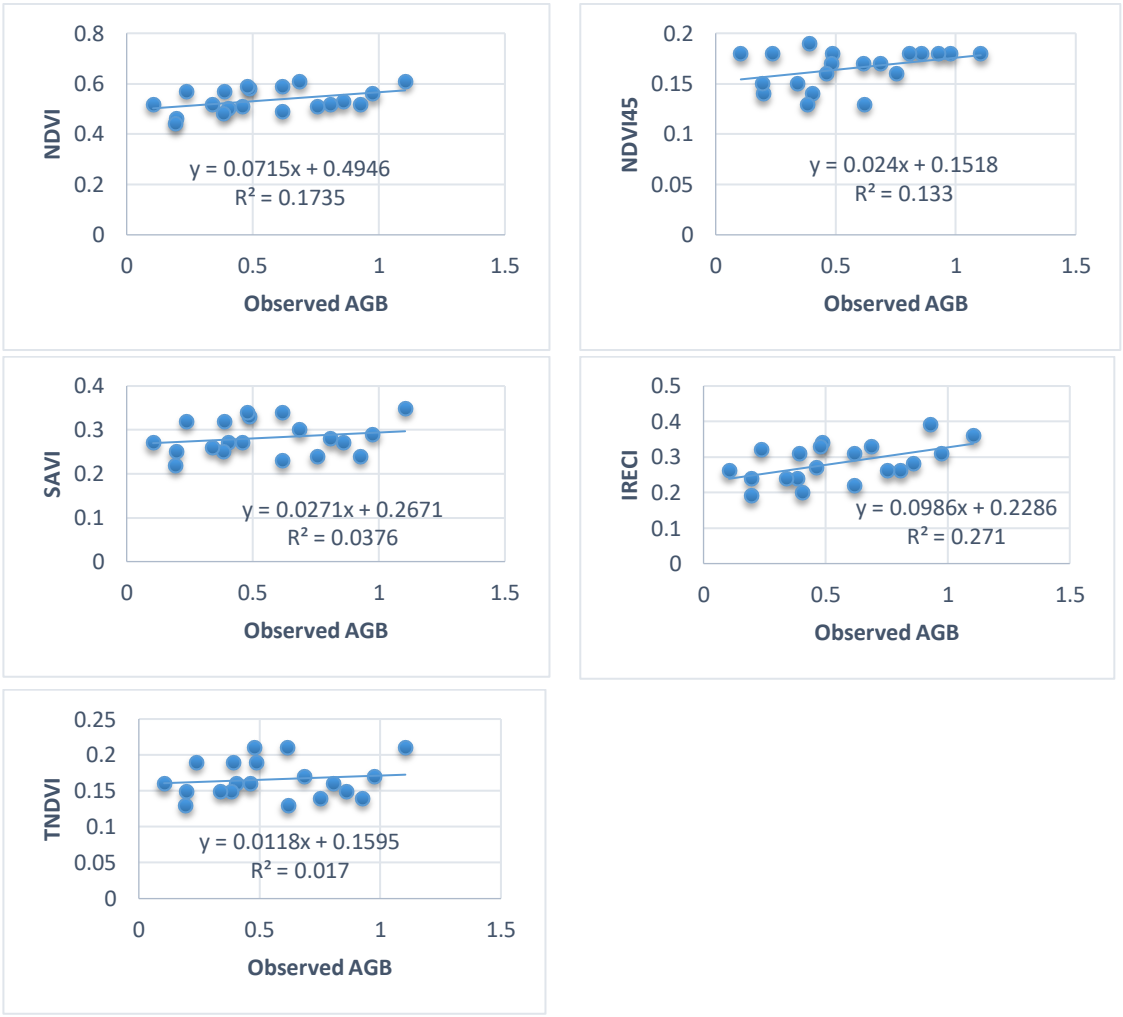

Figure 4.4: Linear relationship between Observed AGB and Vegetation Indices extracted from sentinel 2 MSI

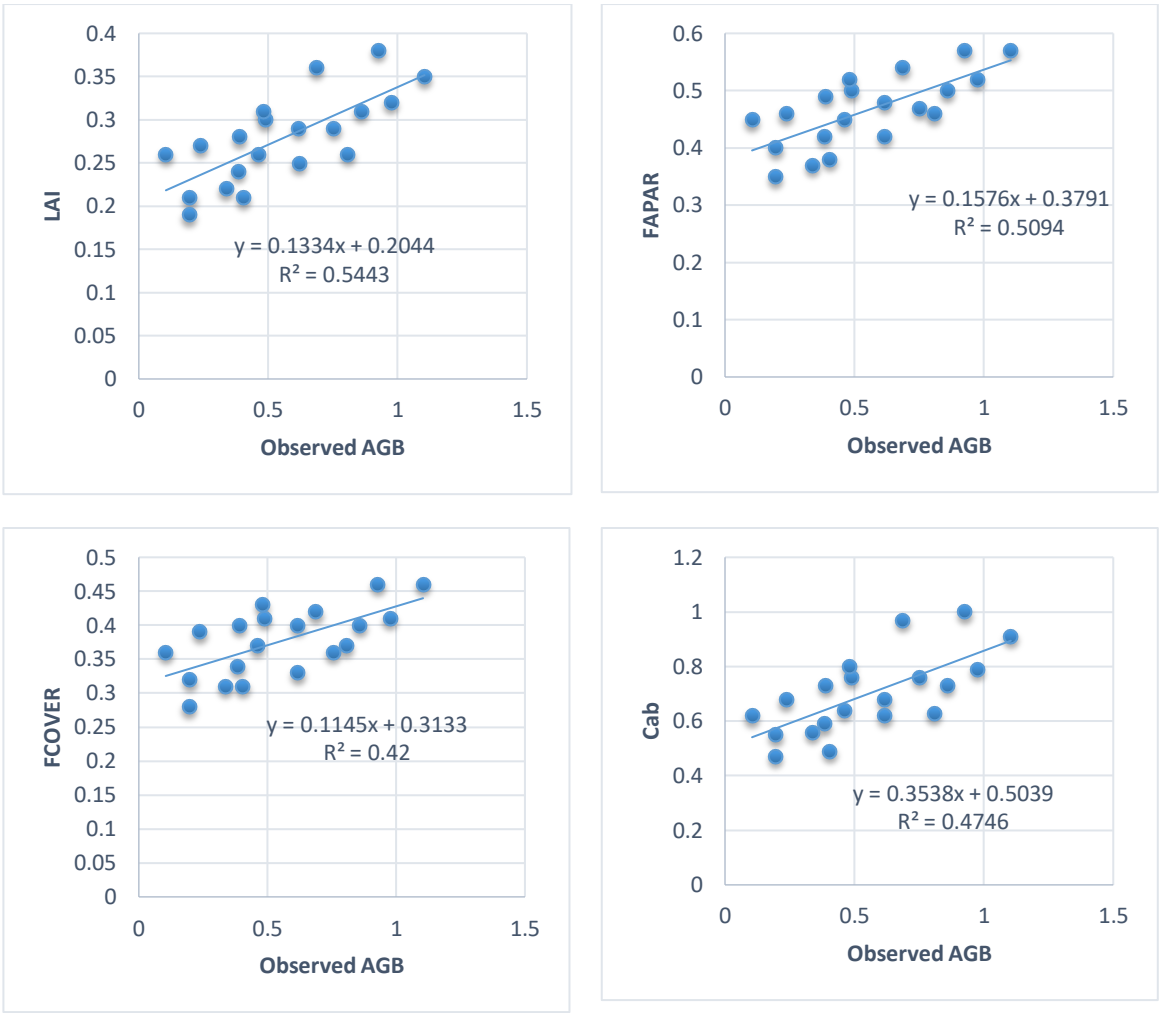

Figure 4.5: Linear relationship between Observed AGB and Vegetation Biophysical Variables extracted from sentinel 2 MSI

4.1.3 **Model development for AGB prediction**

The model was developed on SPSS statistical software based on variables which have good correlation with the field above ground biomass using multi linear regression analysis. Only five variables were selected to develop the model and others were excluded because of their less coefficient of determination values and multicollinearity. Three variables from biophysical variable, one from vegetation indices and one from bands were selected. The selected variables were LAI, FCOVER, FAPAR, IRECI and Band 4.Generally biophysical variable has performed better in developing the model.

Table 4-2: Linear regression result of Observed AGB with selected predictor variables

Model Summary				
Model	R	R Square	Adjusted R Square	Std. Error of the Estimate
1	.856[a]	.733	.638	.1714926
a. Predictors: (Constant), B4, FCOVER, IRECI, LAI, FAPAR				

Coefficients[a]						
Model		Unstandardized Coefficients		Standardized Coefficients	t	Sig.
		B	Std. Error	Beta		
1	(Constant)	-2.282	.905		-2.522	.024
	IRECI	-6.307	3.138	-1.195	-2.010	.064
	LAI	13.452	6.069	2.433	2.217	.044
	FAPAR	-6.180	7.340	-1.364	-.842	.414
	FCOVER	6.633	7.471	1.172	.888	.390
	B4	20.176	12.105	.507	1.667	.118
a. Dependent Variable: AGB_T						

Finally, equation were developed to predict above ground biomass using sentinel extracted variables.

Equation 4-1: Developed AGB predictive formula

Predicted AGB = (20.176 * ***B4***) + (6.633 * ***FCOVER***) – (6.180 * ***FAPAR***) + (13.452 * ***LAI***) - (6.307 * ***IRECI***) - 2.282

Where B4 = Band 4,

LAI=Leaf area index,

IRECI= Inverted Red-Edge Chlorophyll Index,

FCOVER = Fraction of vegetation cover,

FAPAR= Fraction of Absorbed Photosynthetically Active Radiation

4.1.4 Correlation of Observed and predicted above ground biomass

Predicted above ground biomass (AGB) for 20 pixels were calculated at sample plots location and correlated with field above ground biomass for 20 plot (Table 4.3). The dependent (field AGB) and independent (predicted AGB) variables have a good correlation with coefficient of determination (r^2) 0.73 (Fig.4.6). Since they have a good correlation it was selected to map the final AGB and carbon stock

Table 4-3: Observed and predicted above ground biomass

Plot Code	Latitude	Longitude	Observed AGB(tone/plot)	Predicted AGB(tone/pixel)
B8	147368	931779	0.20	0.29
B13	145903	932027	0.98	0.78
B15	147329	934143	0.49	0.45
B16	147023	934962	0.24	0.29
BD4	150452	925206	0.10	0.39
FC1	147389	929212	0.93	0.91
FC2	147854	927192	0.86	0.90
GC4	155815	923434	0.81	0.60
H3	150437	922525	0.19	0.18
H6	149495	922560	0.40	0.40
H7	149358	922303	0.62	0.56
W2	151628	937211	0.39	0.36
WA2	147518	926112	1.10	0.89
WA3	147484	926386	0.62	0.50
WA6	145704	922617	0.48	0.66
WA7	146176	922736	0.46	0.60
WA8	146521	922727	0.38	0.50
WE2	163083	926702	0.34	0.14
B19	822091	917445	0.69	0.94
W3	151445	937852	0.75	0.67

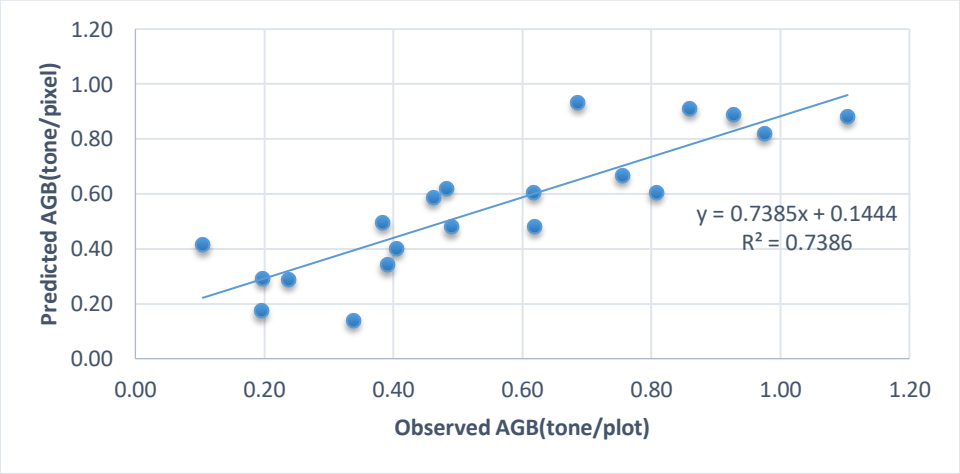

Figure 4.6: Scatter plot showing model validation of observed and predicted above ground biomass

4.1.5 Mapping Forest above ground biomass and carbon stock

The model was validated by considering coefficient of determination ($r^2 = 0.74$) and Root mean square error of 0.16 ton/pixel. Predicted above ground biomass map was produced by the developed equation on ArcGIS software using raster calculator. The forest area were extracted considering LULC of the Yayu forest. The result of AGB estimation for yayu forest in the study area was shown in Figure 4.7. From the map of AGB, it can be seen that over the area the amount of AGB was mostly from 6 up to 10 ton per pixel (150 up to 250 t/ha). In parts of the area which are close to road and other land cover types, it decreased to less than 6 ton per pixel, especially near the agricultural lands, because of anthropogenic activity. Only a minor area has AGB value higher than 10 ton per pixel (250 t/ha) which was found in the core zone of the forest and far from the anthropogenic activities, less degraded and difficult in accessibility.

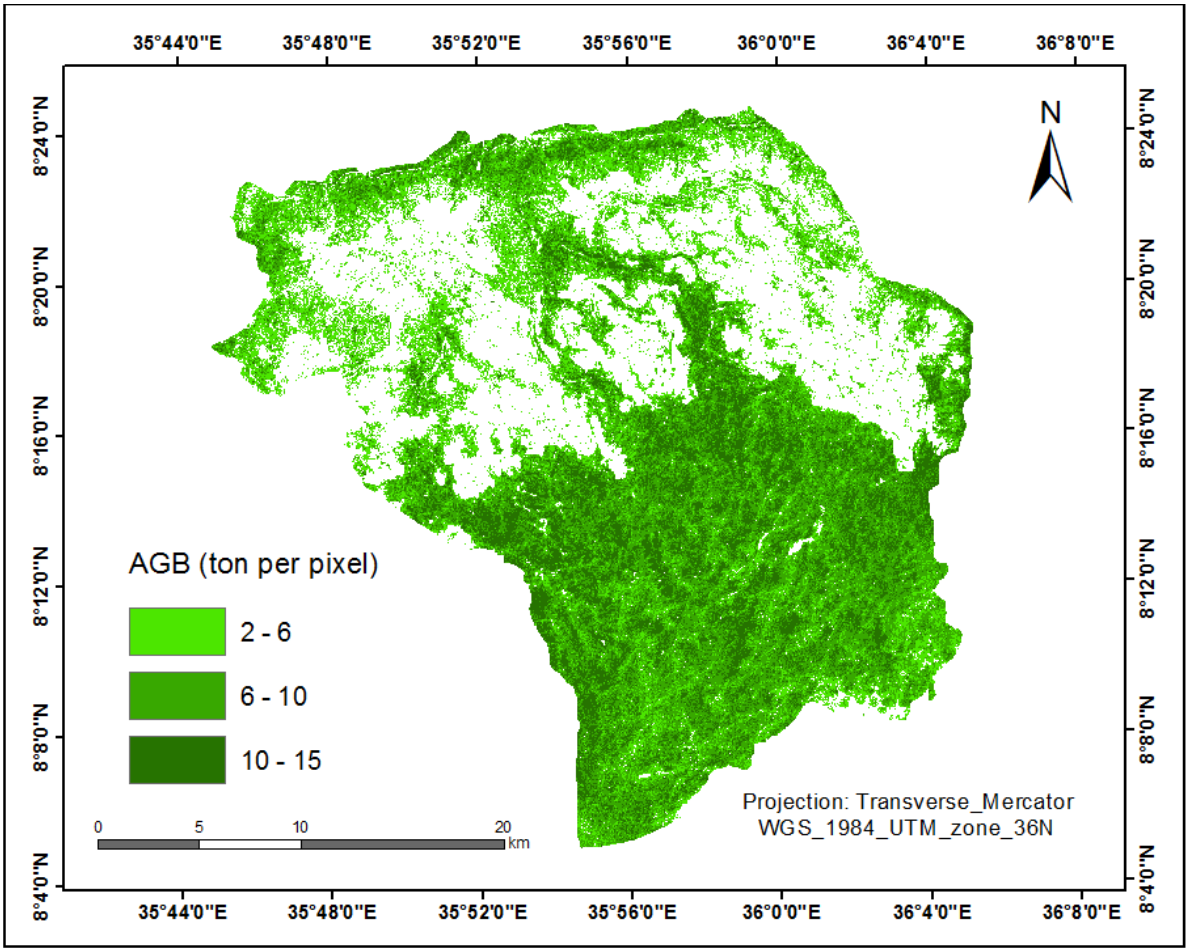

Figure 4.7: Forest above ground map of Yayu district

Finally carbon stock map was produced by multiplying above ground biomass with carbon conversion factor. Figure 4.8 presented the map of carbon stocks in natural forest calculated from AGB map. Because this map was produced based on above ground biomass, it has a similar trend in the carbon stocks distribution. The area that has difficulties in accessibility was the largest carbon stocks with the amount higher than 7.05 ton per pixel (176.25 t/ha). The carbon stocks with the amount less than 2.82 ton per pixel or (70.5 t/ha) was found in the easy accessible area that was near the road and other land cove types.

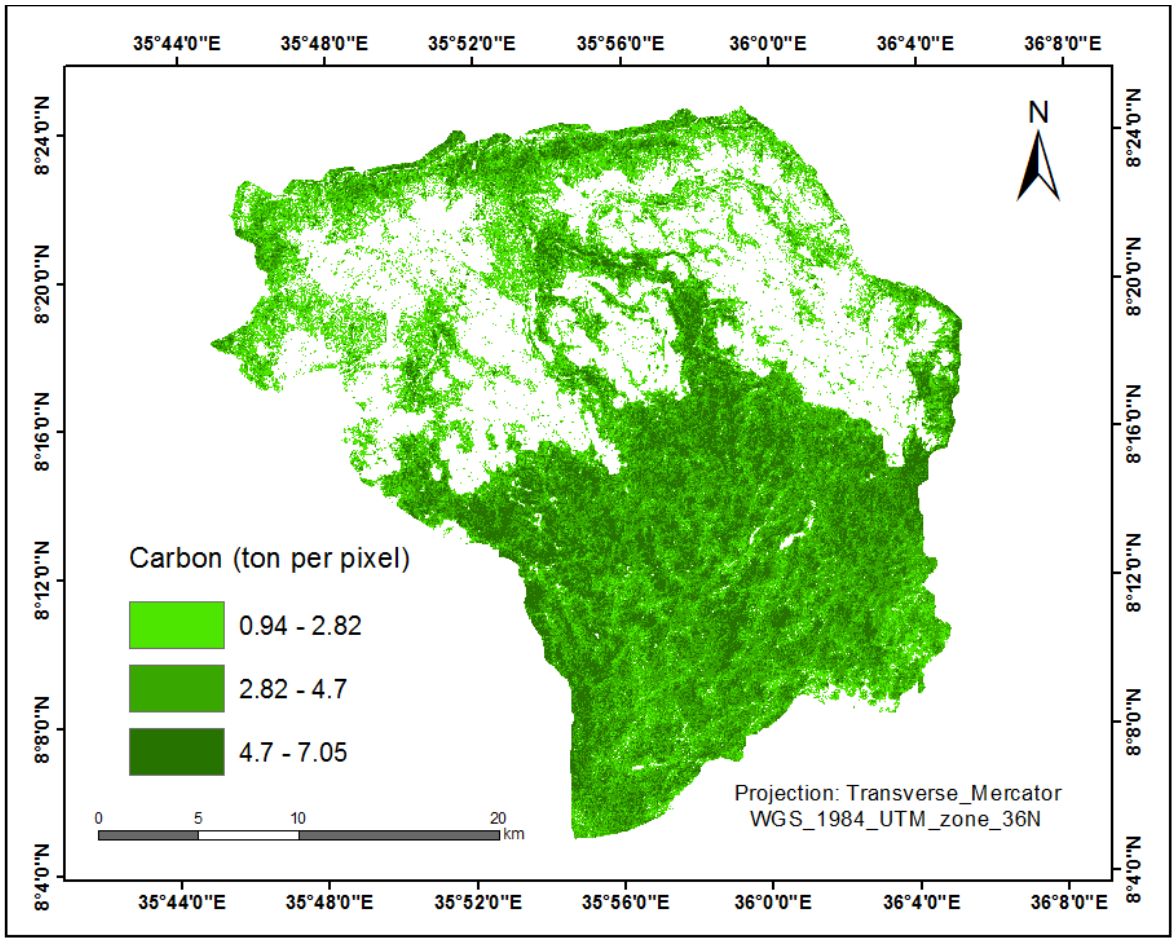

Figure 4.8: Forest carbon stock map of Yayu district

4.2 Discussion

4.2.1 Correlation of measured forest above ground biomass and sentinel 1 extracted variables

According to Saatchi and Moghaddam, 2000 Synthetic Aperture Radar (SAR) sensors are active instruments, sending a pulse of microwave radiation and detecting the radiation scattered back (backscatter, referred to as sigma0 [s0]) by the surface and the 3-dimensional structures on it. When longer wavelength microwaves are used (>20 cm) the detected radiation is mostly due to backscattering from the branching elements and stems of the trees, and thus radar should respond in a characteristic way to forest volume and biomass. As a result, long wavelength SAR has a stronger and more universal relationship than optical or short wavelength microwave sensors which are sensitive to leaf characteristics, where relationships with the woody component of vegetation are indirect and thus highly site and season specific. The saturation point is different for different forest type due to the competing mechanisms of scattering and attenuation (absorption) of microwave energy in the canopy of the vegetation, and is highly dependent on the canopy density, stem density, tree species, and vegetation and soil moisture conditions, as well as the characteristics of the radar data used (Brown, 1997). Studies have been made on the use of shorter wavelengths (e.g., C-band, 3.75 cm to 7.5 cm) for forest mapping especially in tropical forests since higher attenuation is observed for volumetric objects where energy propagated is absorbed (Argamos et al., 2018).

In the present study sentinel-1 C-band synthetic aperture radar image was used. Backscatter information from both polarization (HV and VV) has relatively a weak to moderate correlation with above ground biomass. Since the energy propagated by C-band SAR (3.75 to 7.5 cm wavelength) is attenuated by forest canopies due to its short wavelength and the information gathered is mainly on the leaves and small branches, the cost of obtaining an acceptable r^2 is to extract several statistical features will aid in modelling the AGB values (Argamos et al., 2018). Texture analysis using grey level co-occurrence matrix responds significant but relatively moderate relationship to AGB in the study area. These are partly because C-band SAR ground range detected does not respond directly to AGB, but to aspects of vegetation structure (Saatchi and Moghaddam, 2000) partially due to spatial variability in structure (Saatchi et al., 2009), and partially due to radar calibration and orthorectification (van Zyl, 1990)and field estimation errors propagating through the analysis (Chave et al., 2004). Another research also showed the capability of SAR image in discriminating various types of forest (Wu, 1990; Van der Sanden, 1997). According to Hoekman, 1990, the relationship between X- and C- band backscatter and stand parameters is quite poor. In addition backscatter responds

differently to differing soil and vegetation moisture conditions, and the surface topography, adding to observed prediction errors (Mitchard et al.2009).

As a general there is a good relationship between grey level co-occurrence matrix and field above ground biomass with correlation coefficient (r = between -0.34 - 0.48) Sigma0_VV_ASM performed better with the highest correlation values (r = 0.47).

4.2.2 Correlation of measured forest above ground biomass and sentinel 1 extracted variables

According to Pandit et al. (2018) the potential of Sentinel-2 for estimating forest AGB using random forest algorithm is high. They found that the 20 important top spectral variables derived from the Sentinel-2 satellite data could explain AGB with high accuracy (R^2=0.81 and RMSE=25.32Mgha−1). In the present study, biophysical variables showed strong relationship with the forest AGB. The top variables mostly comprised of SWIR and red-edge band based variables. This highlights the utility of Sentinel-2 data having better spectral, with additional SWIR and red-edge bands, and spatial resolutions among the available medium resolution sensors.

General speaking, strongest correlation was found between field biomass and all vegetation biophysical variables extracted from sentinel 2. Vegetation indices performed less (r = 0.13-0.52) compared to biophysical variables (r = 0.65 - 0.74).The selected bands have perfect negative (-0.65) to positive (0.33) relationship with AGB in the study site. According to Chen et al. (2018) texture characteristics of Sentinel-1 and the vegetation biophysical variables of Sentinel-2 were the most relative and important predictors for explaining the observed variability of AGB. The Sentinel-2A product has comparatively large spatial coverage and high resolution to perform efficiently for estimation of biomass than other open source sensors data products (Anwar et al., 2018). Although SAR C band and optical multispectral techniques have few advantages for detecting the sensibility of forest AGB compared to SAR P band or LiDAR, the available free Sentinel series at a relatively high spatial resolution with full coverage is indeed useful information for applications in global forest AGB estimation (Chen L.et al., 2018).

Chapter 5 Conclusion and Recommendations

5.1 Conclusion

This study demonstrates estimating and mapping Above Ground Biomass (AGB) and carbon stocks for tropical Yayu forest using Sentinel 1 SAR and sentinel 2 optical data. To achieve this, texture analysis using grey level co-occurrence matrix was used to extract variables from sentinel 1 SAR image and different vegetation indices and vegetation biophysical formulas were used to extract variables from Sentinel 2 optical image.

Correlation analysis was used to assess the relation of AGB with radar backscatter extracted from C- band VV and VH polarization, and variable from optical image including bands. Variables which have more influence on AGB were selected based on their coefficient of determination (r2). After that, a multi linear regression was established with the chosen inputs from previous correlation analysis to produce predictive model for above ground biomass.

The values of correlation coefficient between Sentinel 1 analysis result and above ground biomass ranges from -0.34 to 0.48 and VV polarization of Angular second moment has significant relationship (r = 0.48) with AGB. Correlation coefficient ranges from 0.31 to 0.74 between Sentinel 2 variables and above ground biomass and, the most significant and strongest correlation was seen with vegetation biophysical variables (r = 0.65 - 0.74).

Above ground biomass predictive model was developed by using LAI, FCOVER, FAPAR, IRECI and Band 4 as a predictor variables which have a strong correlation with field plot data. The model was validated considering correlation coefficient (0.738) and root mean square error (0.16) seen between observed and predicted above ground biomass.

Generally, in the study area Sentinel-2 derived variables shows a potential in biomass estimation compared to results achieved with Sentinel 1 extracted variables. Sentinel 1 variables have a good relationship with AGB even though not as much as sentinel 2 variables.

5.2 Recommendation

Nevertheless, the study still had some limitations the following points were recommended by the researcher.

- It is recommended that larger field data needs to be collected from the field in all three types of the forest zone (core, buffer and transition).
- Larger dataset of radar image with L and P bands in multi-temporal and multi – polarization could be helpful to improve the correlation with AGB and estimate carbon sequestration.
- High resolution Sentinel 2 image has a strong relationship with AGB and it is recommended to use it in different forest type.
- It is recommended to integrate allometric method and remote sensing imagery to obtain accurate and timely information of above ground biomass and carbon stock.
- The developed model might be modified in the future by using many field sample data and high spatial resolution imagery as well as longer wavelength bands such as L and P bands which have strong relationship to forest stand parameter.

References

Ahern, F.J., Erdle, T., Maclean, D.A. and Kneppeck, D. (1991). A quantitative relationship between forest growth rates and Thematic Mapper reflectance measurements. *International Journal of Remote Sensing* **12**: 387-400.

Akama, R., and Cescatti, A. (2016). Biophysical climate impacts of recent changes in global forest cover. *Science*.**351**: American Association for the Advancement of Science. Retrieved from http://science.sciencemag.org/content/351/6273/600 on 15.03.2019.

Alexandrov, G.A., Yamagata, Y. (2002). Net biome production of managed forests in Japan. *Science in China (Series C)* **45**:109-115.

Ali, A., Ullah, S., Bushra, S., Ahmad N., Ali A. and Khan, M. (2018). Quantifying forest carbon stocks by integrating satellite images and forest inventory data. *Australia journal of forest science.***135**.93-117

Anderson, G. L., Hanson, J. D. and Haas, R. H. (1993). Evaluating landsat thematic mapper derived vegetation indices for estimating above-ground biomass on semiarid rangelands. *Remote Sensing of Environment*. **45.**165–175.

Argamosa, R.J, Blanco A, Baloloy, A.B., Candido, C.G., Dumalag J.B., Dimapilis L.L.C., and Paringit E.C. (2018). Modelling above ground biomass of mangrove forest using sentinel-1 imagery. *ISPRS Annals of the Photogrammetry, Remote Sensing and Spatial Information Sciences*.**3**:1-8

Aschbacher, J. (2012). The European Earth monitoring (GMES) programme: Status and perspectives. *Remote sensing of environment*.120:3−8.

Asrar, G., Myneni, R. and Kanemasu, T. (1989). Measuring and modeling spectral characteristics of a tallgrass prairie. Remote Sensing of Environment **27**:143-155

Attema, E., Bargellini, P., Edwards, P., Levrini, G., Lokas, S., Moeller, L., Rosich-Tell, B., Secchi, P., Torres, R., Davidson, M. and Snoeij, P. (2007). Sentinel 1 - The Radar Missions for GMES Operational Land and Sea Services. *ESA Bulletin* 131.

Baillarin, S. J., Meygret, A., Dechoz, C., Petrucci, B., Lacherade, S., Tremas, T. and Spoto, F. (2012). Sentinel-2 level 1 products and image processing performances. *International Geoscience and Remote Sensing Symposium (IGARSS)*. **39**(B1):197-202.

Bannari, A., Morin, D., Bonn, F. and Huete, A. R. (1995). A review of vegetation indices. *Remote Sensing Reviews*. **13** (1–2): 95–120.

Bekele-Tessema, Birnie A. and Tengnas, B. (1993). Useful trees and Shrubs for Ethiopia. In: Rimmerfors P. *SIDA's Regional Soil Conservation Unit, Nairobi*.**4**:22−26.

Brown, S. (1997). Estimating biomass and biomass change of tropical forests, FAO For. Pap. 134, Food and Agric. Organ. of the U. N., Rome.

CHAVE J., CONDIT R., and AGUILAR S. *et al*. (2004). "Error propagation and scaling for tropical forest biomass estimates", *Philosophical Transactions of the Royal Society of London, Series B: Biological Sciences*.**359**:409–420.

Chave, J., Andalo, C., Brown, S., Cairns, M., Chambers, J., Eamus, D., Fölster, H., Fromard, F., Higuchi, N., Kira, T., Lescure, J. P., Nelson, B., Ogawa, H., Puig, H., Riéra, B. and Yamakura, T. (2005). Tree allometry and improved estimation of carbon stocks and balance in tropical forests. *Oecologia*.**145**: 87-99.

Chave, J., R. Condit, S. Aguilar, A. Hernandez, S. Lao, and R. Perez (2004), Error propagation and scaling for tropical forest biomass estimates. *Philos. Trans. R. Soc. London, Ser.* **359**(1443):409– 420

Chavez, P. S. (1988). An improved dark-object subtraction technique for atmospheric scatter correction of multispectral data An Improved Dark-Object Subtraction Technique for Atmospheric cattering Correction of Multispectral Data. *Remote Sensing of Environment*, **24**(3), 459–479.

Chen, L., Ren C., Zhang, B., Wang, Z., and Xi, Y. (2018). Estimation of Forest Above-Ground Biomass by Geographically Weighted Regression and Machine Learning with Sentinel Imagery. *Forests*.**9**:1-20

CLOUDBRIGE nature reserve. (2016). Tropical Rainforest. Retrieved from http://www.cloudbridge.org/the-project/about-tropical-forests/ on 28.03.2019

Collins, M. (2015). Quantifying environmental indicators and assessing performance in tropical forest management. PhD. Thesis. London School of Economics and Political Science (University of London), 245 PP. Retrieved from http://etheses.lse.ac.uk/3073/ on 21.03.2019.

Culvenor, D. S. (2003). Extracting individual tree information: a survey on techniques for high spatial resolution imagery. *Boston, Kluwer Academic*.

Dixon, R.K., Houghton, R.A., Solomon, A.M., Trexler M.C., and Wisniewski J. (1994). Carbon pools and flux of global forest ecosystems. *Science* **263**: 185-190.

Dong, J., Kaufmann, R.K., Myneni, R.B., Tucker, C.J., Kauppi, P.E., Liski, J., Buermann, W., Alexeyev, V. and Hughes, M.K. (2003). Remote Sensing estimates of boreal and temperate forest woody biomass: Carbon pools, sources, and sinks. *Remote Sens. Environ*. **84**:393–410.

Dong, T., Liu, J., Qian, B., Zhao, T., Jing, Q., Geng, X., Shang, J. (2016). Estimating winter wheat biomass by assimilating leaf area index derived from fusion of Landsat-8 and MODIS data. *International Journal of Applied Earth Observation and Geoinformation*. **49**: 63–74. doi.org/10.1016/j.jag.2016.02.001

Dube, T. and Mutanga, O. (2015). Evaluating the utility of the medium-spatial resolution Landsat 8 multi-spectral sensor in quantifying aboveground biomass in Umgeni catchment, South Africa, *ISPRS J. Photogrammetry. Remote Sens.* **101**:36–46.

Fernández-Manso, A., Fernández-Manso, O., & Quintano, C. (2016). Sentinel-2A red-edge spectral indices suitability for discriminating burn severity. *International Journal of Applied Earth Observation and Geoinformation*. **50**:170–175.

Foody, G. M., Boyd, D. S., & Cutler, M. E. J. (2003). Predictive relations of tropical forest biomass from Landsat TM data and their transferability between regions. *Remote Sensing of Environment*. **85:**463-474.

Forkuor, G., Dimobe, K., Serme, I. and Tondoh, J. (2017). Landsat-8 vs. Sentinel-2: Examining the added value of Sentinel-2's red-edge bands to land-use and land cover mapping in Burkina Faso. *GISci. Remote Sens*.**2**:1–24.

Franklin, S.E., Wulder, M.A. and Gerylo, G.R., (2001). Texture analysis of IKONOS panchromatic data for Douglas-fir forest age class separability in British Columbia. *Int. J. Remote Sens.* **22** (13):2627–2632.

Getu Tesema (2017). Flood detection and mapping using microwave remote sensing on Lake Koka cachment, Awash River basin. Unpublished MSc Thesis, Addis Ababa University, Addis Ababa, Ethiopia, 88 pp.

Gibbs, H.K., Brown, S., Niles, J.O. and Foley, J.A. (2007). Monitoring and estimating tropical forest carbon stocks: making REDD a reality. *Environmental Research Letter* **2:** 4.

Gisel, R., Sandra, B., Jonathan Chapman, and Ariel, E. (1992). *Wood Densities of Tropical Tree Species*. New Orleans,Louisiana. Retrieved from https://www.srs.fs.usda.gov/pubs/gtr/gtr_so088.pdf on 28.03.2019

GLOBAL CLIMATE OBSERVING SYSTEM (GCOS). (2006). Systematic observation requirements for satellite-based products for climate, Supplemental details to the satellite-based component of the Implemention plan for the Global Observing System for Climate in support of the UNFCCC, GCOS **107**:1338.

Gómez, M. (2017).Joint Use of Sentinel-1 and Sentinel-2 for Land Cover Classification: A Machine Learning Approach. Master's. Thesis, Lund University, Lund, Sweden.

Gunlu, A., Ercanli, Baskent, E. Z. and Cakir, G. (2014). Estimating aboveground biomass using landsat TM imagery: A case study of Anatolian Crimean pine forests in Turkey. *Annals of Forest Research*. **57**: 289–298.

Guo, B. Bin, Qi, S. L., Heng, Y. R., Duan, J. Z., Zhang, H. Y., Wu, Y. P., … Zhu, Y. J. (2017). Remotely assessing leaf N uptake in winter wheat based on canopy hyperspectral red-edge absorption. *European Journal of Agronomy*. **82**: 113–124.

Haralick, M., Shanmugan, K. and Dinstein, I. (1973).Texture features for image classification. *IEEE transactions on systems, man and cybernetics*.**6**:610-621

Hoekman, D. H. (1990). Radar remote sensing data for applications in forestry, Wageningen Agricultural University: 279

Hoekman, D. H. (1990). Radar remote sensing data for applications in forestry, Wageningen Agricultural University: 279 pp.

Hoekman, D. H. (1997), Land Cover Type and Forest Biomass Assessment in the Colombian Amazon. *Geoscience and Remote Sensing*.**11**:172−173.

Hua, H., Ryosuke, S. and Elgene, O.B. (1996). Generation of Global Terrestrial Biomass Map by Integrating Satellite Data and Carbon Dynamics Model. *GIS development proceedings.*

Huete, A.; Didan K., Miura T., Rodriquez E. P., Gao X. and Ferreria L. G. (2000). "Overview of the radiometric and biophysical performance of the MODIS vegetation indices". *Remote Sensing of Environment*. **83** (5): 195–213.

Hunt, C., (2009). Carbon Sinks and Climate Change: Forests in the Fight against Global Warming. *Edward Elgar Publishing*.

Husch, B., Beers, T. W. and Kershaw, J. A. (2003). Forest mensuration 4th ed. Hoboken, Wiley and Sons, Inc., Inc, Newyork, 443 pp.

Hussin, Y., Gilani, H., Van Leeuwen, L., Murthy, M., Shah, R., Baral, S., Tsendbazar, N., Shrestha, S., Shah, S. and Qamer, F. (2014). Evaluation of object-based image analysis techniques on very high-resolution satellite image for biomass estimation in a watershed of hilly forest of Nepal. *Appl. Geomatics*. **6**:59–68.

IPCC. (1996). LUCF Sector for good practice guidance., Good Practice Guidance for Land Use, Land-Use Change and Forestry. *Institute for Global Environmental Strategies (IGES), Kanagawa Japan.*PP.11–22. Retrieved from http://www.ipccnggip.iges.or.jp/public/gpglulucf/gpglulucf_files/Chp3/Chp3_1_Introduction.pdf on 02.01.2019

Kayitakire, F., Hamel, C. and Defourny, P. (2006). Retrieving forest structure variables based on image texture analysis and IKONOS-2 imagery. *Remote Sens. Environ*. **102** (3–4):390–401.

Kurvonen, L., Pulliainen, J. and Hallikainen, M. (1999). Retrieval of biomass in boreal forests from multitemporal ERS-1 and JERS-1 SAR images. *IEEE Transaction on geosience and remote sensing.* **37***:* 198−205.

Kurvonen, L., Pulliainen, J., & Hallikainen, M. (1999), Retrieval of Biomass in Boreal Forests from Multitempotal ERS1 and JERS1 SAR Images. *Geoscience and Remote Sensing.* **37**:198−205.

Kushwaha, S.P.S., Nandy, S., Gupta, M., (2014). Growing stock and woody biomass assessment in Asola-Bhatti Wildlife Sanctuary, Delhi, India. *Environ. Monit. Assess*. **186:**5911–5920.

Lemma A. (2005) Site action plan for the conservation and sustainable use of the Lake Awassa biodiversity. Institute of Biodiversity Conservation, Addis Ababa.

Lévesque, J. and King, D. J. (2003). Spatial analysis of radiometric fractions from high-resolution multispectral imagery for modelling individual tree crown and forest canopy structure and health. Remote Sensing of Environment. **84**: 589-602.

Lu, D. (2006). The potential and challenge of remote sensing-based biomass estimation. *International Journal of Remote Sensing*. **27**: 1297−1328.

Lu, D. (2006). The potential and challenge of remote sensing-based biomass estimation. International Journal of Remote Sensing. **27**: 1297 - 1328.

Lu, D., Chen, Q., Wang, G., Liu, L., Li, G. and Moran, E. (2014). A survey of remote sensing-based aboveground biomass estimation methods in forest ecosystems. *International Journal of Digital Earth*. **9**:63-105.

Luckman A. J., F. A. (1997), Texture in airborne SAR imagery of tropical forest and its relationship to forest regeneration stage. *International Journal of Remote Sensing*. **18**: 133−139.

Luckman, A., Baker, J., Kuplich, T. M., da Costa Freitas Yanasse, C. and Frery, A. C. (1997). A study of the relationship between radar backscatter and regenerating tropical forest biomass for spaceborne SAR instruments. Remote Sensing of Environment. **60**: 1−13.

Luong, N., Tateishi, R., Hoan, N. and Tu, T., (2015). Forest change and its effect on biomass in Yok Don National Park in central highlands of Vietnam using ground data and geospatial techniques. *Adv. Remote Sens*. **4 (02)**:108.

Lyon, J. (1998). A change detection experiment using vegetation indices. Photogrammetric Engineering and Remote Sensing: **3:**143–150.

Materka, A., and Strzelecki, M. (1998). Texture Analysis Methods–a Review. Technical university of lodz, institute of electronics, COST B11 report, Brussels.9–11 pp.

Mather, P.M. and Koch, M. (2011). Computer Processing of Remotely-sensed Images: an Introduction. Wiley-Blackwell, Chichester, West Sussex, UK; Hoboken, NJ.

Matthews, R. and Rtoberston, K. (2002). Answers to ten frequently asked questions about bioenergy, carbon sinks and their role in global climate change. *IEA Bioenergy Task* Graz, Austria**.38***:*21-29

Mauya, E. W., Hansen, E., Gobakken, T., Bollandsås, M., Malimbwi, E., and Næsset, E. (2015). Effects of field plot size on prediction accuracy of aboveground biomass airborne laser scanning- assisted inventories in tropical rain forests of Tanzania. *Carbon Balance and Management*.10:1−14.

McRoberts, R.E., Næsset, E. and Gobakken, T. (2013). Inference for lidar-assisted estimation of forest growing stock volume. *Remote Sens. Environ*. **128**: 268–275.

Mermoz, S., Bouvet, A., Le Toan, T. and Mathieu, R. (2015). UNDER-estimation of biomass loss with REDD+ standard reporting method, In 2015 *IEEE International Geoscience and Remote Sensing Symposium (IGARSS)*.14:3882–3885. Retrieved from doi.org/10.1109/IGARSS.2015.7326672 on 26.03.2019.

Michael, G. (2001). Rainforest Biomes. Retrieved from http://www.blueplanetbiomes.org/rainforest.htm on 30.03.2019

Mitchard, E. T., Saatchi, S. S., Woodhouse, I. H., Nangend, G., Ribeiro, N.S.,Williams, M., Ryan, C.M., Lewis, S. L. and Feldpausch, T. R.5 and Meir P. Using satellite radar backscatter to predict above-ground woody biomass: A consistent relationship across four different Africanlandscapes. *Geospatial research letter*.**36**:1-6.

Moskal, L.M. and Franklin, S.E. (2001). Classifying multilayer forest structure and composition using high resolution, compact airborne spectrographic imager image texture. Paper Presented at the ASPRS Proceedings.

Nandy, S., Ghosh, S., Kushwaha, S. and Kumar, A. (2019). Remote sensing-based forest biomass assessment in northwest Himalayan landscape. In: Navalgund, R., Senthil Kumar, A., Nandy, S. (Eds.), Remote Sensing of Northwest Himalayan Ecosystems. *Springer, Singapore*.**22**:285–311.

Nandy, S., Ghosh, S., Kushwaha, S.P.S. and Kumar, A.S., 2019. Remote sensing-based forest biomass assessment in northwest Himalayan landscape. In: Navalgund, R.R., Senthil Kumar, A., Nandy, S. (Eds.), *Remote Sensing of Northwest Himalayan Ecosystems. Springer, Singapore*.285–311.

NASA, 2016. Climate Change: Vital Signs of the Planet: Causes. Retrieved from http://climate.nasa.gov/causes/ on 15.03.2019.

Nelson, R.F., Kimes, D.S., Salas, W.A., Routhier, M., (2000). Secondary forest age and tropical forest biomass estimation using Thematic Mapper imagery. Bio geosciences Graham LC: Synthetic interferometer radar for topographic mapping. *Proc IEEE 1974*. **62**:763–768.

Njoku, E. G. (2013). Encyclopedia of Remote Sensing. *Journal of Chemical Information and Modeling*.***53*** **(9):** 1689-1699.Retrieved from http://staff.washington.edu/dushaw/epubs/Tomography_ on 30.3.2019

Padilla, F. M., Pe, M. T., Gallardo, M., & Thompson, R. B. (2017). Determination of sufficiency values of canopy reflectance vegetation indices for maximum growth and yield of cucumber. *European Journal of Agronomy*.**84**:1–15.

Pan, Y., Birdsey, R., Fang, J., Houghton, R., Kauppi, P., Kurz, W., Phillips, O.., Shvidenko, A., Lewis, S.L. and Canadell, J. et al. (2011). A large and persistent carbon sink in the world's forests. *Science*.**333**:988–993.

Pan, Y., Birdsey, R., Phillips, O. and Jackson, R.B. (2013). The structure, distribution, and biomass of the world's forests. *Annu. Rev. Ecol. Evol. Syst*. **44**:593–622.

Pandit, S., Tsuyuki, S., Dube, T., 2018. Estimating above-ground biomass in sub-tropical buffer zone community Forests, Nepal, using Sentinel 2 data. *Remote Sens*. **10** (4), 601.

Patenaude, G., Milne, R. and Dawson, T. (2005). Synthesis of remote sensing approaches for forest carbon estimation: reporting to the Kyoto Protocol. *Environmental Science and Policy*. **8**: 161-178.

Peters, A. J. (2007). Performance evaluation of spectral vegetation indices using a statistical sensitivity function. *Remote Sensing of Environment*.**106** (1): 59–65.

Ponce-Hernandez, R., Koohafkan, P. and Antoine, J. (2004). Assessing carbon stocks and modelling win–win scenarios of carbon sequestration through land-use changes. *FAO, Rome.*

Powell, S.L., Cohen, W.B., Healey, S.P., Kennedy, R.E., Moisen, G.G., Pierce, K.B. and Ohmann, J.L. (2010). Quantification of live aboveground forest biomass dynamics with Landsat time-series and field inventory data: A comparison of empirical modeling approaches. *Remote Sens. Environ*. **114**:1053–1068.

Ramoelo, A.; Cho, M., Mathieu, R. and Skidmore, A. (2015). Potential of Sentinel-2 spectral configuration to assess rangeland quality. *J. Appl. Remote Sens. Environ*. **124**: 516–533.

Ranson, K. J. and Sun, G. (1994). Mapping biomass of a northern forest using multifrequency SAR data. *Geoscience and Remote Sensing.* **32:** 388-396.

Rosillo-Calle, F., de Groot, P., Hemstock, S. L. and Woods, J. (2007). The Biomass Assessment Handbook. *London, Earthscan*.

Rubner, Y., Puzicha, J., Tomasi, C. and Buhmann, J.M. (2001). Empirical evaluation of dissimilarity measures for color and texture. *Comput. Vis. Image Underst*. **84** (1):25–43.

Saatchi, S. and Moghaddam M. (2000). Estimation of crown and stem water content and biomass of boreal forest using polarimetric SAR imagery. *IEEE Trans. Geosci. Remote Sens*. **38**(2):697 – 709.

Saatchi, S., M. Marlier, D. Clark, R. Chazdon, and A. Russell (2009), Impact of spatial variability of forest structure on radar estimation of aboveground biomass in tropical forests, *Remote Sens. Environ.*

SADER, S. (1987), Forest biomass, canopy structure, and species composition relationships with multipolarization L band synthetic aperture radar data. *Photogrammetric Engineering and Remote Sensing*.**55**:193–202.

Sales, M., Souza Jr., C., Kyriakidis, P., Roberts, D. and Vidal, E. (2007). Improving spatial distribution estimation of forest biomass with geostatistics: a case study for Rondônia, *Brazil. Ecol. Model*. **205**:221–230.

Scott, J. G., Baccini, A., Nadine T Laptorte, Tracy Johns, Wayne Walker, Josef Kellndorfer, Houghton,R. A. and Sun, M. (2009). Mapping and monitoring carbon stocks with sattelite observations: a comparison of methods. Carbon Balance and Management.

Shoko, C. and Mutanga, O. (2017) Examining the strength of the newly-launched Sentinel 2 MSI sensor in detecting and discriminating subtle differences between C3 and C4 grass species. *ISPRS J. Photogramm. Remote Sens*. **129**:32–40.

Shrestha, S. K. (2011). Carbon stock estimation using very high resolution satellite imagery and individual crown segmentation. (A case study of broadleaved and needle leaved forest of Dolakha, Nepal). (MSc) Faculty of Geoformation Science and Earth Observation (ITC) - University of Twente, Enschede.

Sibanda, M., Mutanga, O., & Rouget, M. (2017). Testing the capabilities of the new WorldView-3 space- borne sensor's red-edge spectral band in discriminating and mapping complex grassland management treatments. *International Journal of Remote Sensing*. ***38***: 1–22.

Somogyi, Z., Cienciala, E., Makipaa, R., Muukkonen, P., Lehtonen, A., Weiss, P. (2006). Indirect methods of large scale forest biomass estimation. *European Journal of Forest Research* **30***:100-110*.

Sun, G. R. (2002). Radiometric slope correction for forest biomass estimation from SAR data in the western Sayani Mountains, Siberia, Remote Sensing of Environment. **7:**279–287.

Tadesse Woldemariam. 2003. Vegetation of the Yayu Forest in SW Ethiopia: impacts of human use and implications for in situ conservation of wild coffee Arabica L. population. *Ecology and Development Series, Cuvillier Verlag.* **10**:28-32

Tuttle, E.M., Jensen, R.R., Formica, V.A. and Gonser, R.A. (2006). Using remote sensing imagetexture to study habitat use patterns: a case study using the polymorphic whitethroated sparrow (Zonotrichia albicollis). *Glob. Ecol. Biogeogr*. **15** (4):349–357.

Van der Sanden, J. (1997). Radar remote to support tropical forest management Wagenignen, University of Wagenignen.

van Zyl, J. (1990), Calibration of polarimetric radar images using only image parameters and trihedral corner reflector responses, IEEE Trans. Geosci. Remote Sens. **28**(3):337– 348

Vashum KT and Jayakumar, S. (2012). Methods to Estimate Above-Ground Biomass and Carbon Stock in Natural Forests. *J Ecosyst Ecogr.* **2**:116.

Vine, E., Sathaye, J. and Makundi, W. (1999). Guidelines for the Monitoring, Evaluation, Reporting, Verification, and Certification of Forestry Projects for Climate Change Mitigation, Lawrence Berkeley National Laboratory: Lawrence Berkeley National Laboratory. LBNL Paper LBNL- 41877. Retrieved from: http://www.escholarship.org/uc/item/20h2r692. on 25.02.2019

Widlowski, J.L., Pinty, B., Gobron, N., Verstraete, M.M., Diner, D.J, Davis, A.B., 2004. Canopy structure parameters derived from multi-angular remote sensing data for terrestrial carbon studies. *Climatic Change*. **67**(2-3):403-415.

Wu, S. T. (1990). Assessment of tropical forest stand characteristics with multipolarization SAR data acquired over a mountainous region in Costa Rica. IEEE Transactions on GeoScience and Remote Sensing **28**(4).

Wulder, M. (1998). Optical remote-sensing techniques for the assessment of forest inventory and biophysical parameters. Progress in Physical Geography. **22(4)**: 449-476.

Wulder, M.A., White, J.C., Fournier, R.A., Luther, J.E., and Magnussen, S. (2008). Spatially Explicit Large Area Biomass Estimation: Three Approaches Using Forest Inventory and Remotely Sensed Imagery in a GIS. *Sensors* **8**:529-560.

Yadav, B. and Nandy, S., 2015. Mapping aboveground woody biomass using forest inventory, remote sensing and geostatistical techniques. *Environ. Monit. Assess*. **187:**308.

Yuan, X., King, D. and Vlcek, J. (1991). Sugar maple decline assessment based on spectral and textural analysis of multispectral aerial videography. *Remote Sens. Environ*. **37** (1):47–54.

Zhang, X., & Ni-meister, W. (2014). Biophysical Applications of Satellite Remote Sensing. *Remote Sensing/Photogrammetry, Springer Heidelberg*. Retrieved from http://link.springer.com/book/10.1007/978-3-642-25047-7

Zhao, P., Lu, D., Wang, G., Wu, C., Huang, Y. and Yu, S. (2016). Examining Spectral Reflectance Saturation in Landsat Imagery and Corresponding Solutions to Improve Forest Aboveground Biomass Estimation. *Remote Sensing*. **8**:469−472.

Appendices

Appendix A: Rainfall and temperature data

	Jan	Feb	Mar	Apr	May	Jun	Jul	Aug	Sep	Oct	Nov	Dec
Average Rainfall	16.45	17.32	54.43	102.75	253.29	275.89	289.93	278.66	266.87	151.06	43.20	21.18
Max Temp	30.21	31.69	31.56	30.57	27.98	25.84	24.84	24.71	25.95	27.56	28.44	29.50
Min Temp	13.65	14.52	14.99	15.11	14.55	13.87	13.62	13.56	13.28	13.70	13.74	13.52

Appendix B: List of plot based forest parameter inventory data

Plot ID:**B8**		Date (d/m/y):1/06/16		Location (lat /long): 147368, 931779				
Subplot	Tag	Fam	Genus	Species	Diameter (cm)	POM	Height (m)	Density (g/cm^3)
1	204	Moraceae	Ficus	sur	37.7	1.3	14	0.441
1	205	Moraceae	Ficus	sur	35.7	1.3	14	0.441
1	206	Fabaceae	Millettia	ferruginea	23.8	1.3	14	0.738
1	207	Fabaceae	Millettia	ferruginea	20.1	1.3	16	0.738
1	209	Fabaceae	Albizia	grandibracteata	17.1	1.3	13	0.534
1	210	Euphorbiaceae	Bridelia	micrantha	30.3	1.3	14	0.54
1	211	Myrsinaceae	Maesa	lanceolata	12.6	1.3	8	0.676
1	212	Fabaceae	Millettia	ferruginea	17.3	1.3	15	0.738
1	213	Fabaceae	Albizia	grandibracteata	20	1.3	14	0.534
1	215	Boraginaceae	Ehretia	cymosa	26.5	1.3	11	0.56
1	216	Rubiaceae	Rothmannia	urcelliformis	12.1	1.3	2	0.642

Plot ID:**B15**		Date (d/m/y): 31/05/2016		Location (lat/long): 147329, 934143				
Subplot	Tag	Fam	Genus	Species	Diameter (cm)	POM	Height (m)	Density (g/cm^3)
1	440	Fabaceae	Albizia	schimperiana	64.2	1.3	24	0.53
1	441	Meliaceae	Ekebergia	capensis	12.3	1.3	8	0.58
1	442	Euphorbiaceae	Croton	macrostachyus	0	0	0	0.56
1	443	Asteraceae	Vernonia	amygdalina	14.8	1.3	7	0.413
1	444	Fabaceae	Albizia	schimperiana	27.2	1.3	20	0.53
1	445	Fabaceae	Albizia	schimperiana	33	1.3	21	0.53
1	446	Fabaceae	Albizia	schimperiana	34.7	1.3	20	0.53
1	447	Fabaceae	Albizia	schimperiana	22.1	1.3	16	0.53
1	448	Fabaceae	Albizia	schimperiana	25.7	1.3	22	0.53
1	449	Fabaceae	Albizia	schimperiana	22.3	1.3	18	0.53

Plot ID:**B13**		Date (d/m/y): 01/06/16		Location (lat/long): 145903, 932027				
Subplot	Tag	Fam	Genus	Species	Diameter (cm)	POM	Height (m)	Density (g/cm^3)
1	1779	Euphorbiaceae	Sapium	ellipticum	47.8	3.3	32	0.576
1	1780	Euphorbiaceae	Sapium	ellipticum	35.1	3.55	14	0.576
1	1781	Euphorbiaceae	Sapium	ellipticum	38.9	4.2	22	0.576
1	1782	Oleaceae	Olea	welwitschii	12.8	1.3	1.5	0.82
1	1783	Rubiaceae	Rothmannia	urcelliformis	13.9	1.75	10	0.642
1	1784	Rubiaceae	Rothmannia	urcelliformis	18.9	1.65	11	0.642
1	1785	Fabaceae	Millettia	ferruginea	28.3	1.65	27	0.738
1	1786	Fabaceae	Millettia	ferruginea	32.1	1.71	24	0.738
1	1787	Euphorbiaceae	Sapium	ellipticum	27.2	1.69	7	0.576
1	1788	Euphorbiaceae	Sapium	ellipticum	58.5	2.12	26	0.576
1	1789	Melianthaceae	Bersama	abyssinica	28.5	1.3	20	0.671
1	1790	Fabaceae	Millettia	ferruginea	21	1.7	14	0.738
1	1791	Meliaceae	Trichilia	dregeana	10.6	1.3	9	0.482
1	1792	Rutaceae	Vepris	dainellii	16.6	1.3	11	0.7
1	1793	Fabaceae	Millettia	ferruginea	10.6	1.5	5	0.738
1	1794	Fabaceae	Millettia	ferruginea	11	1.3	6	0.738
1	1795	Boraginaceae	Ehretia	cymosa	14	1.3	8	0.56
1	1796	Boraginaceae	Cordia	africana	20.4	1.3	15	0.41
1	1797	Boraginaceae	Ehretia	cymosa	27	1.6	6	0.56
1	1798	Boraginaceae	Ehretia	cymosa	11.7	1.3	6	0.56
1	1799	Boraginaceae	Ehretia	cymosa	11.8	1.3	7	0.56
1	1800	Fabaceae	Millettia	ferruginea	29.9	2.3	24	0.738

Plot ID:**B16**		Date (d/m/y): 31/05/16		Location (lat/long): 147023, 934962				
Subplot	Tag	Fam	Genus	Species	Diameter (cm)	POM	Height (m)	Density (g/cm^3)
1	1746	Euphorbiaceae	Bridelia	micrantha	15.5	1.3	9	0.54
1	1747	Euphorbiaceae	Sapium	ellipticum	18.4	1.3	28	0.576
1	1748	Euphorbiaceae	Sapium	ellipticum	16.5	1.3	10	0.576
1	1749	Euphorbiaceae	Macaranga	capensis	47.6	1.3	14	0.416
1	1750	Myrtaceae	Syzygium	guineense	19.9	1.3	2	0.712
1	1751	Fabaceae	Albizia	schimperiana	18.8	1.3	7	0.53
1	1752	Rhizophoraceae	Cassipourea	malosana	13.5	1.3	6	0.673
1	1753	Myrtaceae	Syzygium	guineense	13.5	1.3	8	0.712
1	1755	Myrtaceae	Syzygium	guineense	15.3	1.3	7	0.712
1	1756	Myrtaceae	Syzygium	guineense	16.7	2.1	8	0.712
1	1757	Euphorbiaceae	Sapium	ellipticum	13.2	1.3	5	0.576
1	1758	Euphorbiaceae	Sapium	ellipticum	16.3	1.3	10	0.576
1	1759	Euphorbiaceae	Sapium	ellipticum	24.7	1.3	10	0.576
1	1760	Euphorbiaceae	Sapium	ellipticum	16.9	1.3	12	0.576
1	1761	Euphorbiaceae	Sapium	ellipticum	28.5	1.3	16	0.576
1	1762	Euphorbiaceae	Sapium	ellipticum	23.3	1.3	14	0.576
1	1763	Euphorbiaceae	Sapium	ellipticum	18.8	1.6	5	0.576

Plot ID: **BD4**		Date (d/m/y): 1/06/16		Location (lat/long): **150452, 925206**				
Subplot	Tag	Fam	Genus	Species	Diameter	POM	Height	Density
1	683	Euphorbiaceae	Croton	macrostachyus	25.7	1.3	15	0.56
1	684	Euphorbiaceae	Sapium	ellipticum	22.7	1.3	9	0.576
1	685	Fabaceae	Albizia	grandibracteata	19.5	1.3	8	0.534
1	686	Fabaceae	Albizia	grandibracteata	13.6	1.3	6	0.534
1	687	Asteracceae	Vernonia	amygdalina	11.7	1.3	6	0.413
1	688	Asteracceae	Vernonia	amygdalina	28.2	1.3	4	0.413
1	689	Fabaceae	Albizia	schimperiana	20	1.3	15	0.53
1	690	Fabaceae	Albizia	grandibracteata	14.8	1.3	10	0.534
1	691	Euphorbiaceae	Sapium	ellipticum	31.6	1.3	15	0.576
1	692	Euphorbiaceae	Sapium	ellipticum	24.6	1.3	7	0.576
1	693	Euphorbiaceae	Sapium	ellipticum	16.2	1.3	4	0.576

Plot ID: **FC1**		Date (d/m/y):18/05/16		Location (lat/long): 147389, 929212				
Subplot	Tag	Fam	Genus	Species	Diameter	POM	Height	Density
1	1001	Icacinaceae	Apodytes	dimidiata	15.4	1.3	15.4	0.71
1	1002	Euphorbiaceae	Bridelia	micrantha	26.9	1.3	26.9	0.54
1	1003	Pittosporaceae	Pittosporum	viridiflorum	18.4	1.3	18.4	0.633
1	1004	Rubiaceae	Vangueria	apiculata	12.4	1.3	12.4	0.5
1	1005	Oleaceae	Olea	welwitschii	20.5	1.3	20.5	0.82
1	1006	Rubiaceae	Vangueria	apiculata	14.3	1.3	14.3	0.5
1	1007	Euphorbiaceae	Bridelia	micrantha	22.6	1.3	22.6	0.54
1	1008	Boraginaceae	Ehretia	cymosa	29.7	1.3	29.7	0.56
1	1009	Fabaceae	Albizia	grandibracteata	40.8	1.3	40.8	0.534
1	1010	Euphorbiaceae	Bridelia	micrantha	18.9	1.3	18.9	0.54
1	1011	Moraceae	Ficus	ovata	47.6	2.3	47.6	0.6
1	1012	Euphorbiaceae	Bridelia	micrantha	13	1.3	13	0.54
1	1013	Boraginaceae	Ehretia	cymosa	40.6	1.3	40.6	0.56
1	1016	Fabaceae	Albizia	grandibracteata	12.5	1.3	12.5	0.534
1	1017	Fabaceae	Albizia	grandibracteata	11.5	1.3	18.5	0.534
1	1018	Combretaceae	Combretum	paniculatum	18.5	1.3	17.5	0.56

Plot ID: **FC2**		Date (d/m/y): 21/5/2016		Location: 147854, 927192				
Subplot	Tag	Fam	Genus	Species	Diameter	POM	Height	Height in cm
1	3466	Fabaceae	Millettia	ferruginea	15.4	1.3	16	1600
1	3467	Moraceae	Trilepisium	madagascariense	26.9	1.3	16	1600
1	3468	Ulmaceae	Celtis	zenkeri	18.4	1.3	18	1800
1	3469	Rutaceae	Teclea	nobilis	12.4	1.3	11	1100
1	3470	Dracaenaceae	Dracaena	steudneri	20.5	1.3	9	900
1	3471	Rubiaceae	Psydrax	parviflora	14.3	1.3	18	1800
1	3472	Fabaceae	Millettia	ferruginea	22.6	1.3	20	2000
1	3473	Rubiaceae	Rothmannia	urcelliformis	29.7	1.3	16	1600
1	3474	Ulmaceae	Celtis	zenkeri	40.8	1.3	23	2300
1	3475	Ulmaceae	Celtis	zenkeri	18.9	1.95	28	2800
1	3476	Ulmaceae	Celtis	zenkeri	47.6	1.9	30	3000
1	3477	Moraceae	Trilepisium	madagascariense	13	1.3	25	2500
1	3478	Ulmaceae	Celtis	zenkeri	40.6	1.3	25	2500
1	3479	Ulmaceae	Celtis	zenkeri	21.9	1.3	28	2800
1	3480	Rubiaceae	Vangueria	apiculata	18	1.3	22	2200
1	3481	Ebenaceae	Diospyros	abyssinica	12.5	1.3	25	2500
1	3482	Moraceae	Trilepisium	madagascariense	11.5	1.5	11	1100
1	3483	Moraceae	Trilepisium	madagascariense	18.5	1.7	12	1200
1	3484	Moraceae	Trilepisium	madagascariense	17.5	1.7	13	1300
1	3485	Ebenaceae	Diospyros	abyssinica	29.9	1.7	26.4	2640
1	3486	Dracaenaceae	Dracaena	steudneri	11.7	1.3	26	2600
1	3487	Rubiaceae	Rothmannia	urcelliformis	14.9	1.3	18	1800
1	3488	Rubiaceae	Rothmannia	urcelliformis	22.9	1.3	16	1600

Plot ID: **GC4**		Date (d/m/y):02/06/16		Location(lat/long): 155815, 923434				
Subplot	Tag	Fam	Genus	Species	Diameter	POM	Height	Density
1	2385	Boraginaceae	Ehretia	cymosa	16.6	1.45	5	0.56
1	2386	Boraginaceae	Ehretia	cymosa	11.5	1.6	4	0.56
1	2387	Boraginaceae	Ehretia	cymosa	29.2	1.61	15	0.56
1	2388	Boraginaceae	Ehretia	cymosa	13.2	1.3	3	0.56
1	2389	Boraginaceae	Ehretia	cymosa	30	1.3	15	0.56
1	2390	Fabaceae	Albizia	schimperiana	27.6	1.3	15	0.53
1	2391	Fabaceae	Albizia	schimperiana	27.9	1.3	13	0.53
1	2392	Boraginaceae	Cordia	africana	26.2	1.3	12	0.482
1	2393	Boraginaceae	Cordia	africana	29.8	1.4	10	0.482
1	2394	Boraginaceae	Cordia	africana	37.6	1.6	20	0.482
1	2395	Fabaceae	Albizia	schimperiana	51.6	1.3	20	0.53
1	2396	Fabaceae	Albizia	schimperiana	51.4	1.3	20	0.53
1	2397	Fabaceae	Albizia	schimperiana	82.4	1.3	18	0.53
1	2398	Boraginaceae	Ehretia	cymosa	12.6	1.3	6	0.56

Plot ID:**H3**		Date (d/m/y):17/05/16		Location: 150437, 922525				
Subplot	Tag	Fam	Genus	Species	Diameter	POM	Height	Density
1	1901	Fabaceae	Albizia	grandibracteata	0	1.87	28	0.534
1	1902	Euphorbiaceae	Sapium	ellipticum	74.8	1.75	30	0.576
1	1903	Myrsinaceae	Maesa	lanceolata	17.8	1.3	16	0.676
1	1904	Rosaceae	Prunus	africana	92.1	1.98	34	0.85
1	1905	Fabaceae	Albizia	schimperiana	37.7	1.6	21	0.53
1	1906	Euphorbiaceae	Croton	macrostachyus	66	2.05	28	0.56

Plot ID:**H6**		Date (d/m/y): 17/05/16		Location: 149495, 922560				
Subplot	Tag	Fam	Genus	Species	Diameter	POM	Height	Density
1	369	Fabaceae	Acacia	abyssinica	0	1.3	23	0.826
1	370	Fabaceae	Albizia	schimperiana	29.3	1.3	20	0.53
1	371	Fabaceae	Albizia	schimperiana	66.9	1.3	33	0.53

Plot ID:**H7**		Date (d/m/y): 17/05/16		Location: 149358, 922303				
Subplot	Tag	Fam	Genus	Species	Diameter	POM	Height	Density
1	328	Fabaceae	Albizia	schimperiana	43	1.3	16	0.53
1	329	Boraginaceae	Cordia	africana	37.2	1.3	18	0.482
1	331	Fabaceae	Acacia	abyssinica	42	1.3	20	0.826
1	333	Boraginaceae	Cordia	africana	50.5	1.3	25	0.482
1	335	Boraginaceae	Ehretia	cymosa	13.5	1.3	6	0.56
1	336	Myrsinaceae	Maesa	lanceolata	37.6	1.3	2	0.676
1	337	Boraginaceae	Ehretia	cymosa	22.2	1.3	10	0.56
1	338	Flacourtiaceae	Oncoba	spinosa	28.4	1.3	18	0.647
1	339	Boraginaceae	Ehretia	cymosa	31.1	1.3	20	0.56
1	340	Boraginaceae	Ehretia	cymosa	25	1.3	28	0.56
1	341	Boraginaceae	Ehretia	cymosa	26	1.3	17	0.56

Plot ID:**W2**		Date (d/m/y): 19/05/16		Location:				
Subplot	Tag	Fam	Genus	Species	Diameter	POM	Height	Density
1	2586	Rubiaceae	Rothmannia	urcelliformis	16.8	1.3	7	0.642
1	2588	Oleaceae	Chionanthus	mildbraedii	10.5	1.3	4	0.33
1	2589	Rubiaceae	Vangueria	apiculata	27.5	1.3	12	0.5
1	2590	Oleaceae	Chionanthus	mildbraedii	21	1.3	9	0.33
1	2591	Fabaceae	Millettia	ferruginea	27.4	1.3	14	0.738
1	2592	Fabaceae	Millettia	ferruginea	17.9	1.4	9	0.738
1	2593	Oleaceae	Chionanthus	mildbraedii	10.2	1.3	5	0.33
1	2594	Oleaceae	Chionanthus	mildbraedii	15.7	0	0	0.33
1	2595	Ulmaceae	Celtis	zenkeri	21	1.3	16	0.59
1	2596	Rubiaceae	Rothmannia	urcelliformis	20.4	1.4	11	0.642
1	2598	Oleaceae	Chionanthus	mildbraedii	15.1	1.3	6	0.33
1	2599	Moraceae	Ficus	sur	34.3	1.3	13	0.441
1	2600	Moraceae	Ficus	sur	67.7	2	24	0.441
1	2601	Fabaceae	Millettia	ferruginea	13.1	1.4	14	0.738

Plot ID:**WA2**		Date (d/m/y) : 22/05/2016		Location: 147518, 926112				
Subplot	Tag	Fam	Genus	Species	Diameter	POM	Height	Density
1	101	Fabaceae	Albizia	grandibracteata	11.5	1.3	10	0.534
1	102	Fabaceae	Albizia	grandibracteata	18.1	1.3	17	0.534
1	103	Fabaceae	Albizia	grandibracteata	16	1.3	20	0.534
1	104	Fabaceae	Albizia	grandibracteata	51.1	1.5	10	0.534
1	105	Fabaceae	Albizia	grandibracteata	20	1.3	14	0.534
1	106	Fabaceae	Albizia	grandibracteata	69	1.9	26	0.534
1	107	Fabaceae	Albizia	grandibracteata	61.1	1.3	30	0.534
1	108	Moraceae	Trilepisium	madagascariense	33.7	1.95	20	0.499
1	109	Moraceae	Morus	mesozygia	19.9	1.3	24	0.722
1	110	Guttiferae	Garcinia	buchananii	23.5	2	27	0.5
1	111	Euphorbiaceae	Sapium	ellipticum	61.4	4	32	0.576

Plot ID:**WA6**		Date (d/m/y): 23/05/2016		Location: 145704, 922617				
Subplot	Tag	Fam	Genus	Species	Diameter	POM	Height	Density
1	2214	Fabaceae	Albizia	grandibracteata	26.4	1.3	9	0.534
1	2215	Boraginaceae	Cordia	africana	29	1.3	18	0.482
1	2216	Boraginaceae	Cordia	africana	15.3	1.3	14	0.482
1	2217	Boraginaceae	Cordia	africana	30.1	1.3	22	0.482
1	2218	Melianthaceae	Bersama	abyssinica	15	1.3	8	0.671
1	2219	Sapindaceae	Blighia	unijugata	19	1.3	12	0.564
1	2220	Fabaceae	Albizia	grandibracteata	42.9	1.3	24	0.534
1	2221	Moraceae	Ficus	sur	41	1.3	20	0.441
1	2222	Ebenaceae	Diospyros	abyssinica	12	1.3	18	0.79
1	2223	Fabaceae	Albizia	grandibracteata	36.4	1.3	23	0.534
1	2224	Fabaceae	Albizia	grandibracteata	32.1	1.3	22	0.534
1	2225	Ebenaceae	Diospyros	abyssinica	16.5	1.3	14	0.79
2	2228	Fabaceae	Albizia	schimperiana	19.1	1.3	13	0.53

Plot ID:**WA3**		Date (d/m/y): 23/05/2016		Location:147484, 926386				
Subplot	Tag	Fam	Genus	Species	Diameter	POM	Height	Density
1	1657	Araliaceae	Polyscias	fulva	36.6	1.3	22	0.44
1	1658	Meliaceae	Trichilia	dregeana	34.2	1.3	18	0.482
1	1659	Araliaceae	Polyscias	fulva	11.4	1.3	10	0.44
1	1660	Euphorbiaceae	Sapium	ellipticum	34	2.9	19	0.576
1	1661	Euphorbiaceae	Sapium	ellipticum	12.6	1.3	18	0.576
1	1662	Moraceae	Trilepisium	madagascariense	19.2	1.3	17	0.499
1	1663	Euphorbiaceae	Sapium	ellipticum	12.2	1.3	18	0.576
1	1664	Euphorbiaceae	Sapium	ellipticum	26.1	2.8	18	0.576
1	1665	Euphorbiaceae	Sapium	ellipticum	36.1	3.2	19	0.576
1	1667	Euphorbiaceae	Sapium	ellipticum	34.8	1.6	22	0.576
1	1668	Moraceae	Ficus	vasta	0	1.4	30	0.441
1	1669	Moraceae	Ficus	vasta	39.1	2.8	25	0.441
1	1670	Moraceae	Ficus	vasta	0	2.7	23	0.441
1	1671	Rubiaceae	Rothmannia	urcelliformis	13.5	1.3	0	0.642
1	1672	Rutaceae	Clausena	anisata	13.4	1.3	8	0.482
1	1673	Moraceae	Ficus	exasperata	54.9	1.8	26	0.377
1	1674	Meliaceae	Trichilia	dregeana	10.3	1.3	10	0.482
1	1675	Boraginaceae	Ehretia	cymosa	16	1.3	6	0.56
1	1676	Meliaceae	Trichilia	dregeana	14.4	1.3	11	0.482

Plot ID:**WA7**	Date (d/m/y): 23/05/2016		Location: 146176, 922736					
Subplot	Tag	Fam	Genus	Species	Diameter	POM	Height	density
1	601	Fabaceae	Albizia	grandbracteata	71.1	1.3	35	0.534
1	602	Fabaceae	Albizia	grandbracteata	19.4	1.3	10	0.534
1	603	Moraceae	Ficus	sur	53.7	2	3	0.441

Plot ID:**WA8**		Date (d/m/y): 23/05/2016		Location(lat/long): 146521, 922727				
Subplot	Tag	Fam	Genus	Species	Diameter	POM	Height	Density
1	2078	Euphorbiaceae	Croton	macrostachyus	29	1.3	20	0.518
1	2080	Moraceae	Ficus	sycomorus	16.3	1.3	10	0.422
1	2081	Moraceae	Ficus	sycomorus	70.2	2.74	32	0.422
1	2087	Meliaceae	Trichilia	dregeana	11.8	1.53	10	0.482
1	2088	Myrsinaceae	Maesa	lanceolata	17.7	1.3	8	0.676
1	2089	Myrsinaceae	Maesa	lanceolata	16.4	1.3	8	0.676
1	2090	Myrsinaceae	Maesa	lanceolata	18.4	1.3	8	0.676

Plot ID: **WE2**		Date (d/m/y): 20/05/16		Location(lat/long): 163083, 926702				
Subplot	Tag	Fam	Genus	Species	Diameter	POM	Height	density
1	839	Boraginaceae	Ehretia	cymosa	11.8	1.8	6	0.56
1	840	Boraginaceae	Ehretia	cymosa	23.1	1.8	12	0.56
1	841	Boraginaceae	Ehretia	cymosa	23.9	1.8	12	0.56
1	842	Boraginaceae	Cordia	africana	30.9	1.5	24	0.482
1	843	Boraginaceae	Cordia	africana	18.9	1.3	25	0.482
1	844	Boraginaceae	Cordia	africana	39.3	2.2	30	0.482
1	845	Boraginaceae	Cordia	africana	7.7	2.2	30	0.482
1	846	Boraginaceae	Ehretia	cymosa	17.4	1.3	10	0.56
1	847	Euphorbiaceae	Croton	macrostachyus	44.2	1.3	22	0.518

Plot ID:**B19**		Date (d/m/y): 31/05/2016		Location: 822091, 917444				
Subplot	Tag	Fam	Genus	Species	Diameter	POM	Height	Density
1	2719	Flacourtiaceae	Oncoba	spinosa	11.9	1.3	6	0.647
1	2720	Fabaceae	Acacia	abyssinica	41.1	1.3	18	0.826
1	2721	Flacourtiaceae	Oncoba	spinosa	10.4	1.3	10	0.647
1	2722	Euphorbiaceae	Croton	macrostachyus	15.8	1.3	8	0.518
1	2723	Fabaceae	Albizia	schimperiana	11.5	1.3	6	0.53
1	2724	Flacourtiaceae	Oncoba	spinosa	10.5	1.3	8	0.647
1	2725	Melianthaceae	Bersama	abyssinica	17.4	1.3	14	0.671
1	2726	Euphorbiaceae	Croton	macrostachyus	17.7	1.3	12	0.518
1	2727	Fabaceae	Albizia	schimperiana	20	1.3	12	0.53
1	2728	Euphorbiaceae	Croton	macrostachyus	20.3	1.3	14	0.518
1	2729	Flacourtiaceae	Oncoba	spinosa	11.6	1.3	8	0.647
1	2730	Anacardiaceae	Rhus	ruspolii	12.5	1.3	6	0.62
1	2731	Myrsinaceae	Maesa	lanceolata	15	1.3	6	0.676
1	2732	Euphorbiaceae	Croton	macrostachyus	14.9	1.3	8	0.518
1	2733	Euphorbiaceae	Croton	macrostachyus	16.2	1.3	18	0.518
1	2734	Anacardiaceae	Rhus	ruspolii	28.4	1.3	4	0.62
1	2735	Anacardiaceae	Rhus	ruspolii	12.6	1.3	4	0.62
1	2736	Anacardiaceae	Rhus	ruspolii	17	1.3	6	0.62
1	2737	Flacourtiaceae	Oncoba	spinosa	12	1.3	8	0.647
1	2738	Euphorbiaceae	Croton	macrostachyus	12.8	1.3	11	0.518
1	2739	Euphorbiaceae	Croton	macrostachyus	12.9	1.3	11	0.518
1	2740	Euphorbiaceae	Croton	macrostachyus	18	1.3	11	0.518
1	2741	Euphorbiaceae	Croton	macrostachyus	13.3	1.3	8	0.518
1	2742	Euphorbiaceae	Croton	macrostachyus	12.6	1.7	5	0.518
1	2743	Euphorbiaceae	Croton	macrostachyus	11.6	1.5	8	0.518
1	2745	Fabaceae	Albizia	schimperiana	12.8	1.3	12	0.534
1	2746	Euphorbiaceae	Croton	macrostachyus	14	1.3	14	0.518
1	2747	Fabaceae	Albizia	schimperiana	70.4	1.3	20	0.534
1	2749	Euphorbiaceae	Croton	macrostachyus	24.2	1.3	15	0.518

1	2750	Euphorbiaceae	Croton	macrostachyus	16	1.3	14	0.518
1	2751	Boraginaceae	Ehretia	cymosa	14.1	1.3	10	0.56
1	2752	Boraginaceae	Ehretia	cymosa	14.3	1.3	9	0.56
1	2753	Euphorbiaceae	Croton	macrostachyus	19	1.3	10	0.518
1	2754	Euphorbiaceae	Croton	macrostachyus	11.5	1.3	8	0.518
1	2755	Euphorbiaceae	Croton	macrostachyus	14.6	1.3	8	0.518
1	2756	Boraginaceae	Ehretia	cymosa	12.6	1.3	9	0.56
1	2758	Anacardiaceae	Rhus	ruspolii	22.2	1.3	9	0.62
1	2759	Euphorbiaceae	Croton	macrostachyus	14.8	1.3	16	0.518
1	2760	Oleaceae	Chionanthus	mildbraedii	27	1.3	14	0.705
1	2761	Myrsinaceae	Maesa	lanceolata	12.5	1.3	3	0.676
1	2762	Euphorbiaceae	Croton	macrostachyus	21.4	1.3	18	0.518
1	2763	Euphorbiaceae	Croton	macrostachyus	12	1.3	12	0.518
1	2764	Euphorbiaceae	Croton	macrostachyus	19	1.3	16	0.518

Plot ID:**W3**		Date (d/m/y):19/05/16		Location(lat/long): 151444,937851				
Subplot	Tag	Fam	Genus	Species	Diameter	POM	Height	density
1	3006	Fabaceae	Acacia	abyssinica	33.9	1.3	18	0.826
1	3007	Fabaceae	Acacia	abyssinica	79.7	1.3	17	0.826
1	3008	Boraginaceae	Cordia	africana	21.1	1.3	16	0.482
1	3009	Boraginaceae	Cordia	africana	34.5	2.15	15	0.482
1	3010	Melianthaceae	Bersama	abyssinica	14.7	1.5	14	0.671
1	3011	Capparidaceae	Ritchiea	albersii	43.3	1.3	18	0.5
1	3013	Boraginaceae	Cordia	africana	54.3	1.3	17	0.482

Appendix C: Pixel values extracted from texture analysis (grey level co-occurrence matrix) of sentinel 1 VH_ polarization

Plot	latitude	longitude	Area	AGB_T	Sigma0_VH_ASM	Sigma0_VH_Contrast	Sigma0_VH_Dissimilarity	Sigma0_VH_Energy	Sigma0_VH_Entropy	Sigma0_VH_GLCMCorrelation	Sigma0_VH_GLCMMean	Sigma0_VH_GLCMVariance	Sigma0_VH_Homogeneity	Sigma0_VH_MAX	Sigma0_VH
B8	147368	931779	400	0.19666	0.03	0.03	0.13	0.17	0.83	1	0.91	0.83	0.26	0.07	0.0076
B13	145903	932027	400	0.9752	0.01	0.08	0.23	0.1	0.93	1	0.74	0.58	0.16	0.03	0.0038
B15	147329	934143	400	0.48916	0.01	0.18	0.35	0.08	0.95	0.98	0.52	0.34	0.12	0.01	0.0044
B16	147023	934962	400	0.23739	0.01	0.22	0.39	0.08	0.96	0.98	0.52	0.34	0.08	0.01	0.0022
BD4	150452	925206	400	0.10446	0.01	0.04	0.15	0.11	0.91	1	0.65	0.43	0.2	0.03	0.0029
FC1	147389	929212	400	0.92731	0.01	0.04	0.18	0.11	0.9	1	0.78	0.62	0.18	0.04	0.0045
FC2	147854	927192	400	0.85969	0.01	0.14	0.28	0.09	0.94	0.99	0.77	0.64	0.14	0.02	0.0076
GC4	155815	923434	400	0.80759	0.02	0.03	0.14	0.14	0.86	1	0.85	0.74	0.24	0.05	0.0044
H3	150437	922525	400	0.19495	0.01	0.15	0.33	0.1	0.94	0.99	0.64	0.45	0.12	0.04	0.0065
H6	149495	922560	400	0.40398	0.02	0.06	0.19	0.15	0.88	0.96	0.17	0.05	0.23	0.09	0.0015
H7	149358	922303	400	0.61737	0.03	0.03	0.12	0.17	0.86	0.99	0.29	0.1	0.3	0.1	0.0017
W2	151628	937211	400	0.39043	0.01	0.25	0.43	0.08	0.97	0.98	0.51	0.35	0.08	0.02	0.0029
WA2	147518	926112	400	1.10414	0.01	0.04	0.16	0.12	0.9	1	0.85	0.73	0.21	0.04	0.0048
WA3	147484	926386	400	0.6184	0.01	0.14	0.32	0.09	0.95	0.99	0.54	0.33	0.1	0.03	0.003
WA6	145704	922617	400	0.48118	0.01	0.09	0.23	0.09	0.94	0.99	0.72	0.55	0.18	0.02	0.0038
WA7	146176	922736	400	0.46142	0.01	0.05	0.18	0.11	0.92	1	0.77	0.62	0.2	0.04	0.0042
WA8	146521	922727	400	0.38369	0.01	0.05	0.17	0.12	0.89	1	0.85	0.73	0.21	0.04	0.006
WE2	163083	926702	400	0.33788	0.01	0.05	0.19	0.1	0.92	1	0.75	0.58	0.16	0.04	0.0048
B19	822091	917444.6	400	0.68618	0.01	0.06	0.2	0.09	0.94	1	0.73	0.55	0.16	0.02	0.0028
W3	151444.9	937851.6	400	0.75402	0.02	0.04	0.17	0.13	0.88	1	0.87	0.77	0.18	0.04	0.004

Appendix D: Pixel values extracted from texture analysis (grey level co-occurrence matrix) of sentinel 1 VV_ polarization

Plot	latitude	longtude	Area	AGB_T	Sigma0_VV_ASM	Sigma0_VV_Contrast	Sigma0_VV_Dissimilarity	Sigma0_VV_Energy	Sigma0_VV_Entropy	Sigma0_VV_GLCMCorrelation	Sigma0_VV_GCMMean	Sigma0_VV_GLCMVariance	Sigma0_VV_GLCMHomogeneity	Sigma0_VV_MAX	Sigma0_VV
B8	147368	931779	400	0.19666	1	0	0	1	0.05	1	1	1	1	1	0.0027
B13	145903	932027	400	0.9752	1	0	0	1	0.05	1	1	1	1	1	0.0038
B15	147329	934143	400	0.48916	0.84	0	0	0.92	0.11	1	1	1	0.96	0.91	0.0038
B16	147023	934962	400	0.23739	0.21	0.01	0.05	0.46	0.42	1	0.98	0.96	0.61	0.41	0.0052
BD4	150452	925206	400	0.10446	0.5	0	0.02	0.71	0.22	1	0.99	0.99	0.84	0.68	0.0021
FC1	147389	929212	400	0.92731	1	0	0	1	0.05	1	1	1	1	1	0.0043
FC2	147854	927192	400	0.85969	0.61	0.01	0.03	0.78	0.23	1	0.99	0.98	0.85	0.78	0.004
GC4	155815	923434	400	0.80759	1	0	0	1	0.05	1	1	1	1	1	0.0025
H3	150437	922525	400	0.19495	0.19	0.05	0.14	0.44	0.49	0.99	0.94	0.9	0.55	0.41	0.0026
H6	149495	922560	400	0.40398	0.01	0.19	0.36	0.09	0.93	0.93	0.73	0.57	0.12	0.02	0.0011
H7	149358	922303	400	0.61737	0.02	0.07	0.21	0.14	0.8	0.98	0.89	0.8	0.24	0.06	0.0012
W2	151628	937211	400	0.39043	0.17	0.02	0.08	0.41	0.48	1	0.97	0.94	0.54	0.37	0.0019
WA2	147518	926112	400	1.10414	1	0	0	1	0.05	1	1	1	1	1	0.005
WA3	147484	926386	400	0.6184	0.88	0	0	0.94	0.1	1	1	1	0.97	0.94	0.0036
WA6	145704	922617	400	0.48118	0.72	0	0.01	0.85	0.17	1	1	0.99	0.91	0.84	0.0043
WA7	146176	922736	400	0.46142	0.52	0	0.02	0.72	0.22	1	0.99	0.99	0.83	0.69	0.0018
WA8	146521	922727	400	0.38369	0.88	0	0	0.94	0.1	1	1	1	0.97	0.94	0.0019
WE2	163083	926702	400	0.33788	0.96	0	0	0.98	0.07	1	1	1	0.98	0.98	0.0032
B19	822091	917444.6	400	0.68618	0.92	0	0	0.96	0.09	1	1	1	0.98	0.96	0.0019
W3	151444.9	937851.6	400	0.75402	1	0	0	1	0.05	1	1	1	1	1	0.0021

Appendix E: Pixel values extracted from vegetation indices of sentinel 2 image

Plot	latitude	longitude	Area	AGB(ton)	TNDVI	NDVI45	SAVI	IRECI	NDVI	LAI	FAPAR	FCOVER	Cab
B8	147368	931779	400	0.19666	0.15	0.14	0.25	0.24	0.46	0.21	0.4	0.32	0.55
B13	145903	932027	400	0.9752	0.17	0.18	0.29	0.31	0.56	0.32	0.52	0.41	0.79
B15	147329	934143	400	0.48916	0.19	0.18	0.33	0.34	0.58	0.3	0.5	0.41	0.76
B16	147023	934962	400	0.23739	0.19	0.18	0.32	0.32	0.57	0.27	0.46	0.39	0.68
BD4	150452	925206	400	0.10446	0.16	0.18	0.27	0.26	0.52	0.26	0.45	0.36	0.62
FC1	147389	929212	400	0.92731	0.14	0.18	0.24	0.39	0.52	0.38	0.57	0.46	1
FC2	147854	927192	400	0.85969	0.15	0.18	0.27	0.28	0.53	0.31	0.5	0.4	0.73
GC4	155815	923434	400	0.80759	0.16	0.18	0.28	0.26	0.52	0.26	0.46	0.37	0.63
H3	150437	922525	400	0.19495	0.13	0.15	0.22	0.19	0.44	0.19	0.35	0.28	0.47
H6	149495	922560	400	0.40398	0.16	0.14	0.27	0.2	0.5	0.21	0.38	0.31	0.49
H7	149358	922303	400	0.61737	0.21	0.17	0.34	0.31	0.59	0.29	0.48	0.4	0.68
W2	151628	937211	400	0.39043	0.19	0.19	0.32	0.31	0.57	0.28	0.49	0.4	0.73
WA2	147518	926112	400	1.10414	0.21	0.18	0.35	0.36	0.61	0.35	0.57	0.46	0.91
WA3	147484	926386	400	0.6184	0.13	0.13	0.23	0.22	0.49	0.25	0.42	0.33	0.62
WA6	145704	922617	400	0.48118	0.21	0.17	0.34	0.33	0.59	0.31	0.52	0.43	0.8
WA7	146176	922736	400	0.46142	0.16	0.16	0.27	0.27	0.51	0.26	0.45	0.37	0.64
WA8	146521	922727	400	0.38369	0.15	0.13	0.25	0.24	0.48	0.24	0.42	0.34	0.59
WE2	163083	926702	400	0.33788	0.15	0.15	0.26	0.24	0.52	0.22	0.37	0.31	0.56
B19	822091	917444.6	400	0.68618	0.17	0.17	0.3	0.33	0.61	0.36	0.54	0.42	0.97
W3	151444.9	937851.6	400	0.75402	0.14	0.16	0.24	0.26	0.51	0.29	0.47	0.36	0.76

Appendix F: Pixel values extracted from bands indices of sentinel 2 image

Plot	latitude	longtude	Area	AGB(ton)	B2	B3	B4	B5	B6	B7	B8	B8a	B11	B12
B8	147368	931779	400	0.19666	0.1	0.09	0.08	0.1	0.17	0.2	0.2	0.23	0.19	0.1
B13	145903	932027	400	0.9752	0.09	0.08	0.06	0.09	0.21	0.27	0.2	0.29	0.14	0.07
B15	147329	934143	400	0.48916	0.09	0.08	0.06	0.1	0.17	0.2	0.23	0.23	0.18	0.1
B16	147023	934962	400	0.23739	0.09	0.08	0.06	0.09	0.19	0.22	0.23	0.25	0.17	0.09
BD4	150452	925206	400	0.10446	0.09	0.08	0.06	0.09	0.17	0.2	0.2	0.24	0.16	0.09
FC1	147389	929212	400	0.92731	0.09	0.08	0.05	0.08	0.18	0.22	0.17	0.24	0.11	0.05
FC2	147854	927192	400	0.85969	0.09	0.08	0.06	0.08	0.17	0.2	0.19	0.23	0.13	0.06
GC4	155815	923434	400	0.80759	0.09	0.08	0.07	0.09	0.17	0.2	0.21	0.22	0.16	0.09
H3	150437	922525	400	0.19495	0.1	0.08	0.07	0.09	0.16	0.19	0.18	0.21	0.17	0.09
H6	149495	922560	400	0.40398	0.1	0.09	0.07	0.09	0.14	0.16	0.21	0.18	0.15	0.09
H7	149358	922303	400	0.61737	0.1	0.09	0.06	0.1	0.17	0.19	0.25	0.23	0.18	0.1
W2	151628	937211	400	0.39043	0.09	0.08	0.06	0.09	0.18	0.22	0.23	0.25	0.17	0.09
WA2	147518	926112	400	1.10414	0.09	0.08	0.06	0.09	0.18	0.22	0.25	0.24	0.14	0.07
WA3	147484	926386	400	0.6184	0.09	0.08	0.06	0.08	0.15	0.17	0.17	0.2	0.13	0.06
WA6	145704	922617	400	0.48118	0.1	0.09	0.06	0.09	0.18	0.23	0.25	0.25	0.15	0.08
WA7	146176	922736	400	0.46142	0.1	0.08	0.07	0.09	0.18	0.21	0.2	0.24	0.17	0.09
WA8	146521	922727	400	0.38369	0.1	0.09	0.07	0.09	0.17	0.21	0.2	0.23	0.16	0.08
WE2	163083	926702	400	0.33788	0.09	0.08	0.06	0.08	0.16	0.18	0.19	0.2	0.16	0.09
B19	822091	917444.6	400	0.68618	0.08	0.07	0.05	0.07	0.15	0.19	0.19	0.22	0.11	0.05
W3	151444.9	937851.6	400	0.75402	0.09	0.07	0.06	0.08	0.15	0.19	0.17	0.21	0.13	0.07

Appendix G: Multiple Regression analysis on SPSS

Variables Entered/Removed[a]			
Model	Variables Entered	Variables Removed	Method
1	B4, FCOVER, ireci, LAI, FAPAR[b]	.	Enter
a. Dependent Variable: AGB_T			
b. All requested variables entered.			

Model Summary				
Model	R	R Square	Adjusted R Square	Std. Error of the Estimate
1	.856[a]	.733	.638	.1714926
a. Predictors: (Constant), B4, FCOVER, ireci, LAI, FAPAR				

ANOVA[a]						
Model		Sum of Squares	df	Mean Square	F	Sig.
1	Regression	1.133	5	.227	7.705	.001[b]
	Residual	.412	14	.029		
	Total	1.545	19			
a. Dependent Variable: AGB_T						
b. Predictors: (Constant), B4, FCOVER, ireci, LAI, FAPAR						

Coefficients[a]						
Model		Unstandardized Coefficients		Standardized Coefficients	t	Sig.
		B	Std. Error	Beta		
1	(Constant)	-2.282	.905		-2.522	.024
	ireci	-6.307	3.138	-1.195	-2.010	.064
	LAI	13.452	6.069	2.433	2.217	.044
	FAPAR	-6.180	7.340	-1.364	-.842	.414
	FCOVER	6.633	7.471	1.172	.888	.390
	B4	20.176	12.105	.507	1.667	.118
a. Dependent Variable: AGB_T						

Appendix H: Pivot table for LU/LC accuracy assessment

	Forest	Shrub land	Agriculture	Wetland	Urban	Ground Truth	User Accuracy
Forest	29	0	1	0	0	30	96.67
Shrub land	0	26	2	1	1	30	86.67
Ariculture	0	1	28	1	0	30	93.33
Wetland	1	1	0	27	1	30	90.00
Urban	0	1	3	0	26	30	86.67
Total	30	29	34	29	28	150	
Producer Accuracy	96.67	89.66	82.35	93.10	92.86		
Overall Accuracy	90.67						
Kappa coefficient	0.88						

Appendix I: Thesis Originality Test Report

NO	**PARTICULARS**	**TEST I**		**TEST II**		**TEST III**		**TEST IV**		**AVERAGE**	**REMARK**
		Originality (%)	Plagiarism (%)	Originality (%)	Plagiarism (%)	Originality (%)	Plagiarism (%)	Originality (%)	Plagiarism (%)		
1	Abstract	100	-	-	-	-	-	-	-	100	
2	Introduction	100	-	-	-	-	-	-	-	100	
3	Literature review	98	1	99	2	100	-	-	-	98.66	
4	Methodology	100	-	100	-	100	-	-	-		
5	Result and Discussion	100	-	100	-	100	-	-	-		
6	Conclusion and Recommendation	100	-	100	-	100	-	-	-		
7	Overall Thesis									98.66	